UNIVERSIDAD
DE ALMERÍA

UNIVERSIDAD DE ALMERÍA
DEPARTAMENTO DE INGENIERÍA

TESIS DOCTORAL

Diseño y evaluación experimental de un mecanismo de fuerza constante para máquinas de acondicionamiento muscular. Aplicación al ejercicio de press de banca

AUTOR: Silvia Sánchez Salinas

DIRECTOR:
Prof. Dr. Javier López Martínez

Almería, Junio de 2022

Diseño y evaluación experimental de un mecanismo de fuerza constante para máquinas de acondicionamiento muscular. Aplicación al ejercicio de press de banca

Design and experimental evaluation of a constant force mechanism for bodybuilding machines. Application to the bench press exercise

AUTOR: Silvia Sánchez Salinas

DIRECTOR:
Prof. Dr. Javier López Martínez

Tesis Doctoral presentada dentro del Programa de Doctorado en Tecnología de Invernaderos e Ingeniería Industrial y Ambiental (RD 99/11), en la línea de investigación de Optimización Computacional, Calidad Eléctrica y Contadores Inteligentes e Ingeniería Industrial.

Agradecimientos

Una vez acabada mi Tesis Doctoral debo pararme a mirar atrás y pensar cómo he llegado hasta aquí, y dar las gracias a todas las personas que han ayudado a la consecución de este importante proyecto. Este trabajo no hubiera sido posible sin la ayuda de mi director de Tesis, Javier López Martínez. Desde que dirigió mi primer proyecto fin de carrera, ya van unos cuantos años trabajando juntos. Gracias por el tiempo dedicado y los conocimientos que me has brindado a lo largo de toda esta etapa. He recibido tu ayuda como alumna, como doctoranda y como compañera de trabajo, siempre has estado dispuesto a ayudarme y a ofrecerme todo tu conocimiento. Es muy fácil trabajar contigo. Gracias de todo corazón. También quiero brindar mi agradecimiento al resto de personas que han hecho posible esta tesis, como son los coautores de los artículos presentados en la misma. Gracias a Daniel García Vallejo, José M. Muyor, Celia Núñez Torres y Alfonso García Agúndez. No me puedo olvidar de mi familia, muchas gracias por toda la ayuda recibida durante este tiempo y, en especial, gracias a mi marido por su paciencia, ya que convivir con una doctoranda no debe ser una tarea fácil. Pero, sobre todo, gracias a mis tres hijos por el tiempo que me han concedido, un tiempo robado a su infancia. Sin vuestro apoyo, este trabajo nunca se habría escrito. A todos, muchas gracias.

Índice general

Preámbulo

Mediante la presente Tesis Doctoral se pone de manifiesto la investigación llevada a cabo sobre mecanismos de fuerza constante y su implementación en máquinas de musculación tipo Smith para la realización del ejercicio de press de banca.

Esta Tesis Doctoral se presenta por la modalidad de compendio de publicaciones. El trabajo de investigación llevado a cabo queda avalado mediante la publicación de tres artículos en revistas incluidas en el Journal Citation Reports (JCR) de la Web of Science (WOS), e incluidas en la categoría **A** de la escala de valoración de los resultados de investigación contenida en el Plan Propio de Investigación y Transferencia de la Universidad de Almería. Adicionalmente, a estas tres publicaciones científicas, la Tesis Doctoral incluye una cuarta aportación, recogida en formato de artículo, que será enviada al XV Congreso Iberoamericano de Ingeniería Mecánica.

Esta Tesis ha sido parcialmente desarrollada dentro del Proyecto UAL2020-CTS-A2100, financiado por el Programa Operativo FEDER 2014-2020 y la Consejería de Transformación Económica, Industria, Conocimiento y Universidades de la Junta de Andalucía.

Publicación científica 1

En el Capítulo 2 se presenta el artículo titulado "Validación experimental de un mecanismo de fuerza constante y análisis de su rendimiento mediante un modelo multicuerpo calibrado" (*Experimental validation of a constant-force mechanism and analysis of its performance with a calibrated multibody model*), publicado en la revista Mechanism and Machine Theory.

Este artículo se centra en la evaluación experimental y la modelización matemática de un mecanismo de fuerza constante. El diseño del mecanismo está basado en el uso de levas, rodillos y resortes, dispuestos de una particular manera, y consiguiendo un valor de fuerza constante sobre el eslabón de entrada para toda la carrera del mecanismo. La evaluación y validación del mecanismo se lleva a cabo mediante la realización de una serie de ensayos

en los que se obtiene las curvas de fuerza, en los que se pone de manifiesto la influencia de las fuerzas de fricción y del proceso de fabricación en el comportamiento del mecanismo. Además, en esta publicación, se desarrolla un modelo multicuerpo del mecanismo de fuerza constante que es calibrado con la ayuda de los resultados experimentales de los ensayos. Este modelo multicuerpo se basa en la suposición de rodadura sin deslizamiento entre las levas y los rodillos, lo que hace que el modelo incluya restricciones de velocidad. Mediante la calibración del modelo se persigue el desarrollo de una herramienta matemática para estudiar el comportamiento del mismo en condiciones diferentes a las presentadas en este artículo. Además, este modelo de CFM se utiliza para realizar un análisis de sensibilidad de algunos parámetros importantes en el diseño del mecanismo.

Publicación científica 2

En el Capítulo 3 se presenta el artículo titulado "Diseño y análisis de un press de banca de fuerza constante" (*Design and analysis of a constant-force bench press*), publicado en la revista Mechanism and Machine Theory.

En este trabajo se propone el uso de un mecanismo de fuerza constante como medio de carga en el ejercicio de musculación de press de banca. El sistema de carga propuesto permite de mantener una resistencia de fuerza sustancialmente constante, en contraposición al press de banca tradicional realizado con pesas (peso libre), en el que la presencia de elevadas fuerzas de inercia tienen una gran influencia en la fuerza que el atleta debe desarrollar durante el ejercicio. El sistema de carga propuesto se compara con el press de banca tradicional de peso libre. Para ello, se elabora un modelo matemático del ejercicio de press de banca realizado en una máquina tipo Smith. Se utilizan datos experimentales medidos en una sesión de prueba con el press de banca tradicional para, a partir del modelo matemático desarrollado, estimar tres variables relevantes en la realización del ejercicio: la fuerza vertical en el hombro, el momento articular neto en el hombro y la potencia muscular. Estos resultados, obtenidos para el peso libre, se comparan con los que se obtendrían asumiendo una resistencia de fuerza constante, encontrando diferencias significativas. El medio de carga basado en el mecanismo de fuerza constante da lugar a una curva de fuerza en el hombro menos fluctuante, a menores picos en la curva del momento articular en el hombro, y a una menor varianza entre las distintas repeticiones del ejercicio.

Publicación científica 3

En el Capítulo 4 se presenta el artículo titulado "Diseño de trayectorias y pares mediante optimización paramétrica para el ejercicio de press de banca en una máquina Smith" (*Design of trajectories and torques by parameter optimization for the bench press exercise on a Smith machine*), publicado en la revista Mechanism and Machine Theory.

El ejercicio de press de banca en máquina Smith, utilizado frecuentemente en los programas de entrenamiento, puede analizarse como un sistema biomecánico actuado de forma redundante. En trabajos anteriores, se ha modelado este ejercicio mediante un modelo matemático con un grado de libertad, actuado únicamente en el hombro. En este trabajo se incluye en el modelo un actuador en el par articular del codo. Debido a la redundancia que esto supone, se pueden encontrar muchas combinaciones diferentes de pares hombro-codo que conducen al mismo movimiento. En este trabajo se presenta un modelo de optimización paramétrica para el ejercicio de press de banca, y se estudian dos supuestos distintos: que el ejercicio se realiza con el fin de ganar resistencia, o que se busca realizarlo de la manera más segura, es decir, evitando sobrecargas. A partir de ensayos, en los que la cinemática del movimiento es recogida mediante un electrogoniómetro ubicado en el codo del deportista, se obtiene el movimiento de referencia para la optimización. Los resultados muestran que la forma óptima de realizar el ejercicio para cada supuesto conlleva la ejecución del ejercicio siguiendo distintos patrones de movimiento, lo que sugiere el potencial de esta metodología en el diseño de programas de entrenamiento en ejercicios deportivos o de rehabilitación.

Aportación científica 4

En el Capítulo 5 se presenta, en formato de artículo, la aportación titulada "Diseño y estudio experimental de una máquina de acondicionamiento muscular basada en un mecanismo de fuerza constante", que próximamente se enviará al XV Congreso Iberoamericano de Ingeniería Mecánica.

En el entrenamiento de la fuerza o la resistencia, se buscan patrones de movimiento de la carga y la activación que se adapten al objetivo del entrenamiento. Tradicionalmente, se emplean máquinas con masa móvil (pesas) como sistema de carga. Una característica de este tipo de máquinas es la aparición de fuerzas de inercia debidas a la aceleración de la masa móvil, lo que hace que la fuerza que ejerce el deportista pueda ser muy variable a lo largo del ejercicio.

En este trabajo se propone el empleo de un mecanismo de fuerza constante

como sistema de carga en una máquina de acondicionamiento muscular tipo Smith. El propósito de este nuevo sistema es el de reducir las fuerzas de inercia y conseguir una curva de fuerza más constante. En primer lugar, se lleva a cabo la fabricación de sendas unidades de mecanismos de fuerza constante y su incorporación a una máquina Smith. Para la caracterización del sistema se obtienen las curvas de fuerza-desplazamiento a velocidad constante. En segundo lugar, se llevan a cabo mediciones en el ejercicio de press de banca, realizado con el sistema tradicional de peso libre y con el nuevo sistema de carga propuesto. Los resultados muestran diferencias significativas en las curvas de fuerza para ambos sistemas de carga. Con el sistema de carga propuesto los picos de fuerza son menores y se reduce sustancialmente la caída de la fuerza en la fase de frenado.

Referencias de las publicaciones

Publicación científica 1

Título: *"Experimental validation of a constant-force mechanism and analysis of its performance with a calibrated multibody model"*

Autores: Silvia Sánchez Salinas, Alfonso García Agúndez, Javier López Martínez y Daniel García Vallejo.

Revista científica: Mechanism and Machine Theory

Volumen: 173

Artículo: 104819

Año: 2022

doi: 10.1016/j.mechmachtheory.2022.104819

Datos JCR (Journal Citation Reports):

Factor de impacto (2020): 3,866
Categoría: Mechanical Engineering
Ranking categoría: 29/133
Cuartil: Q1
Editor: Elsevier
País: England

Publicación científica 2

Título: "Design and analysis of a constant-force bench press"

Autores: Silvia Sánchez Salinas, Celia Núñez Torres, Javier López Martínez, Daniel García Vallejo y José M. Muyor.

Revista científica: Mechanism and Machine Theory

Volumen: 142

Artículo: 103612

Año: 2019

doi: 10.1016/j.mechmachtheory.2019.103612

Datos JCR (Journal Citation Reports):

Factor de impacto (2019):3.312
Categoría: Mechanical Engineering
Ranking categoría: 30/130
Cuartil: Q1
Editor: Elsevier
País: England

Publicación científica 3

Título: "Design of trajectories and torques by parameter optimization for the bench press exercise on a Smith machine"

Autores: Silvia Sánchez Salinas, Daniel García Vallejo, Javier López Martínez y José M. Muyor.

Revista científica: Mechanism and Machine Theory
Volumen: 155
Artículo: 1034089
Año: 2021
doi: 10.1016/j.mechmachtheory.2020.104089
Datos JCR (Journal Citation Reports):

Factor de impacto (2020): 3,866
Categoría: Mechanical Engineering
Ranking categoría: 29/133
Cuartil: Q1
Editor: Elservier
País: England

Aportación científica 4

La aportación científica 4, consiste en un trabajo que será enviado al XV Congreso Iberoamericano de Ingeniería Mecánica, a celebrar del 22 al 24 de noviembre de 2022 en la Universidad Politécnica de Madrid. Este trabajo llevará como título: "Diseño y estudio experimental de una máquina de acondicionamiento muscular basada en un mecanismo de fuerza constante", habiendo sido ya enviado el resumen del mismo y aceptado por el comité científico del congreso.

Resumen

En el entrenamiento de la fuerza y la resistencia, se buscan patrones de movimiento de la carga y la activación muscular que se adapten al objetivo del entrenamiento. Tradicionalmente, se emplean máquinas con masa móvil (pesas) como sistema de carga. Una característica de este tipo de máquinas es la aparición de fuerzas de inercia debidas a la aceleración de la masa móvil, lo que hace que la fuerza que ejerce el deportista pueda ser muy variable a lo largo del ejercicio.

En esta Tesis Doctoral se propone el diseño de una máquina de acondicionamiento muscular para la realización del ejercicio de press de banca en el que el patrón de fuerza que tenga que realizar el deportista sea lo más constante posible durante la ejecución del ejercicio, independientemente de la velocidad de ejecución del mismo, evitando en la medida de lo posible la presencia de fuerzas de inercia. Para ello se propone el uso de un mecanismo de fuerza constante como medio de carga en la máquina de musculación. Los mecanismos de fuerza constante están diseñados para mantener un valor de fuerza sensiblemente constante en el eslabón de entrada durante un amplio rango de la carrera del mecanismo. En este trabajo se desarrolla un mecanismo de fuerza constante patentado por la Universidad de Almería, el cual está basada en el uso de levas, resortes y rodillos, para conseguir la característica de fuerza constante. Partiendo del diseño conceptual descrito en la citada patente, se ha dimensionado, fabricado y evaluado experimentalmente un prototipo del mecanismo.

Una vez validado el prototipo, se han dimensionado y fabricado dos unidades del mecanismo de fuerza constante para su implementación en una máquina de acondicionamiento muscular tipo Smith. Esta máquina Smith modificada se ha empleado para evaluar y comparar el ejercicio de press de banca realizado con los dos sistemas de carga: con peso libre y con el mecanismo de fuerza constante. Los resultados muestran diferencias significativas en las curvas de fuerza entre ambos sistemas de carga. Con el sistema de carga propuesto, la curva de fuerza se mantiene más estable, reduciéndose sustancialmente la caída de la fuerza en la fase de frenado, a diferencia del

peso libre.

Para el estudio del ejercicio de press de banca se propone además un modelo matemático multicuerpo, con el cual se ha obtenido el valor de los parámetros más significativos del ejercicio, como son los pares articulares, la fuerza resultante ejercida por el deportista y la potencia requerida. Estos parámetros han sido comparados en la realización del ejercicio empleando el sistema de carga tradicional (peso libre) y empleando el nuevo sistema de carga propuesto. Para profundizar en el estudio del ejercicio de press de banca, se propone un modelo de optimización paramétrica que ha permitido conocer el reparto de pares articulares óptimo (hombro y codo) durante la ejecución del ejercicio y con base a unos requerimientos de ejecución determinados. En concreto, se han estudiado dos objetivos distintos en la realización del entrenamiento: ganar resistencia y realizar el ejercicio de la forma más segura posible, evitando sobrecargas.

PALABRAS CLAVE: máquina de acondicionamiento muscular, press de banca, mecanismo de fuerza constante, modelo multicuerpo, validación experimental

Abstract

In strength and endurance training, the patterns of load movement and muscle activation should be adapted to the training objective. Traditionally, machines with moving mass (weights) are used as loading systems. One of the characteristics of this type of machine is the presence of inertial forces due to the acceleration of the moving mass, which means that the force exerted by the athlete can be highly variable throughout the exercise.

This Doctoral Thesis proposes the design of a bench press bodybuilding machine so that the force pattern to be exerted by the athlete is as constant as possible during the execution of the exercise, regardless of the execution speed, avoiding the presence of high inertial forces. To this end, the use of a constant force mechanism as the loading device in the bodybuilding machine is proposed. Constant force mechanisms are designed to maintain a constant force value at the input link throughout a wide range of the mechanism stroke. This work details the development of a constant force mechanism patented by the University of Almería which is based on the use of cams, springs and rollers to achieve the constant force characteristic. A prototype of the mechanism has been designed, manufactured and experimentally evaluated on the basis of the conceptual design described in the referred patent.

Once the prototype was validated, two units of the constant force mechanism were sized and manufactured for implementation in a Smith-type bodybuilding machine. This modified Smith machine has been used to evaluate and compare the bench press exercise performed with the two loading systems: free weight and constant force mechanism. The results show significant differences in the force curves between both loading systems. With the proposed loading system, the force curve remains more constant than in the free weight system, substantially reducing the force drop in the braking phase.

For the study of the bench press exercise, a multibody model is also proposed, which provided the value of the most significant parameters of the exercise, such as the joint torques, the resultant force exerted by the athlete, and the required power. These parameters have been compared in the perfor-

mance of the exercise using the traditional loading system (free weight) and using the new proposed loading system. To further study the bench press exercise, a parametric optimization model was proposed in order to determine the optimal distribution of joint torques (shoulder and elbow) during the performance of the exercise together with the assumption of certain execution requirements. Specifically, this research focuses on two different training objectives: to gain resistance, and to perform the exercise in the safest possible way, avoiding overloads.

KEYWORDS: bodybuilding machine, bench press, constant force mechanism, multibody model, experimental validation.

Capítulo 1

Introducción

1.1. Antecedentes

En este apartado se exponen, de manera no exhaustiva, los antecedentes relacionados con la Tesis. Se comienza introduciendo los mecanismos de fuerza constante, las distintas soluciones constructivas y los usos encontrados. Posteriormente, se describen los distintos sistemas de carga empleados en máquinas de musculación y su influencia en el entrenamiento de la fuerza, centrándonos en el ejercicio de press de banca. Finalmente, se muestra la importancia de los modelos matemáticos para el análisis del movimiento humano y se mencionan los escasos modelos del ejercicio de press de banca encontrados en la literatura.

Mecanismos de fuerza constante

Los mecanismos de fuerza constante (CFM, por sus siglas en inglés, *Constant Force Mechanisms*) tienen como principal objetivo proporcionar un valor de fuerza constante sobre uno de los eslabones del mecanismo durante un cierto rango de la carrera del mecanismo, siendo diversas las aplicaciones encontradas hasta la fecha. En el diseño de los CFM se han utilizado dos enfoques distintos [92]. El primer enfoque se basa en el uso de mecanismos flexibles (*compliant mechanisms*), donde la movilidad del mecanismo se consigue mediante la deflexión de los elementos flexibles que lo forman [28, 35, 82]. Las componentes flexibles suelen diseñarse con geometrías relativamente complejas, consiguiendo la característica de fuerza constante en un determinado rango de movimiento del mecanismo. La geometría de los elementos flexibles se pueden obtener a partir de técnicas de optimización [19, 47, 56, 64, 84] o mediante el modelado de los elementos como cuerpos pseudo rígidos [14, 15, 43, 83, 84]. Los mecanismos de fuerza constante flexibles pueden ser

diseñados para conseguir una fuerza constante unidireccional [46, 50] o un par constante [29, 64]. Algunas propuestas de estos tipos de mecanismos se basan en la combinación de un elemento de rigidez positiva junto con un elemento de rigidez negativa, de forma que al actuar conjuntamente la curva fuerza-desplazamiento resultante presenta una región con pendiente nula o casi nula [42, 63, 83, 94, 98]. Una forma de conseguir una rigidez negativa es utilizar elementos de viga sometidos a pandeo, donde la rigidez de la viga puede conocerse a partir de la ecuación de Euler [48, 51, 54]. Los CFM flexibles son de especial interés en aplicaciones que no requieran grandes desplazamientos, tienen la ventaja de ser de construcción simple y compacta, pudiéndose diseñar de una única pieza. Además, no tienen pérdidas por fricción. Debido a la limitación en la amplitud del desplazamiento que suelen presentar en este tipo de mecanismos, algunos trabajos recientes se han centrado en aumentar la carrera de los mismos [54].

Dentro del segundo enfoque, están aquellos mecanismos de fuerza constante en cuyo diseño se combinan resortes junto con una transmisión no lineal. Este tipo de CFM pueden diseñarse para desplazamientos mayores que los CFM flexibles [46, 53] y el valor de la fuerza puede modificarse fácilmente cambiando, añadiendo o quitando, resortes [13, 46, 50, 53]. Por el contrario, como inconveniente, el diseño resulta compacto y la curva de fuerza se ve afectada por las fuerzas de fricción.

Según Bidgoly et al. [13], se pueden diferenciar dos grupos dentro de los CFM pertenecientes a este segundo enfoque. En el primer grupo, el resorte lineal presenta uno de sus extremos articulado, mientras que el otro extremo es traccionado por un cable que se enrolla en una leva o polea no circular, con una forma concreta. Combinando la característica del resorte lineal con la leva de radio variable, se consigue un par constante en el eje de rotación de la leva [20, 76]. En el segundo grupo, uno o ambos extremos del resorte se mueven siguiendo la superficie de una leva, donde se utilizan rodillos para seguir el perfil de la leva y reducir la fricción [40, 46, 50, 53, 97]. La geometría particular de la leva permite mantener un valor de fuerza constante en el eslabón de entrada del mecanismo. Algunas soluciones permiten modificar el valor de la fuerza prefijando la tensión inicial del muelle [50] o disponiendo varios resortes en paralelo [52, 53].

Una generalización de los CFM son los mecanismos con rigidez definida por el usuario. En lugar de diseñar el mecanismo para una rigidez nula (fuerza constante), se pueden aplicar los mismos métodos de diseño para obtener un resorte no lineal con una curva de rigidez específica [13, 71, 72].

Dentro de las aplicaciones de los CFM, están experimentando un considerable desarrollo en el campo de la robótica, donde se utilizan como mecanismos para compensar la fuerza de la gravedad [22], como sistemas de

seguridad frente a sobrecargas [63], o en la manipulación de objetos para limitar la fuerza de agarre [16, 45, 47, 98], evitando en este último caso el uso de complejos sistemas de control de fuerza. Los CFM han encontrado nuevas aplicaciones en campos como la cirugía, con el diseño de pinzas para controlar la fuerza de pinzado de las mismas [43, 44] o en catéteres de ablación cardíaca [85]; en exoesqueletos [49]; en micropinzas para la manipulación de células biológicas [93]; en entornos de baja gravedad [74] o en contactos eléctricos [95].

Se pueden encontrar algunas patentes que incluyen un mecanismo de fuerza constante como fuente de resistencia [36]. Orientado a entornos de baja gravedad, la NASA (National Aeronautics and Space Administration) patentó una unidad de resistencia basada en la combinación de muelles y levas [74]. La patente nº 4231568 [67] también utiliza una disposición de muelles y levas para generar la fuerza de resistencia en el ejercicio. Otras patentes relacionadas con los sistemas de carga en máquinas de musculación se basan en el uso de múltiples resortes paralelos antagonistas [17, 34], en resortes de gas y transmisiones no lineales [27], en cilindros de vacío [65], o en dispositivos neumáticos [39, 96]. A pesar del considerable número de patentes que incluyen un mecanismo de fuerza constante como sistema de carga en máquinas de musculación, cabe destacar que no se ha encontrado en la literatura ninguna máquina comercial o estudios experimentales que utilicen estos sistemas de carga.

Sistemas de carga en máquinas de musculación

Se pueden clasificar las máquinas de musculación en función del sistema de carga o medio que aporta resistencia al ejercicio. Frost et al. [26] establece la clasificación de las máquinas de musculación en: resistencia isoinercial o de peso libre, resistencia adaptativa (máquinas hidráulicas e isocinéticas), y de resistencia variable. Cada uno de los sistemas de carga presentan una respuesta resistente (oposición al movimiento) diferente, teniendo, por tanto, implicaciones distintas en el desarrollo muscular.

En los ejercicios de peso libre o resistencia isoinercial, que es el método tradicional y más extendido para mejorar la capacidad de fuerza y la potencia en el deporte [26], la fuerza que debe ejercer el deportista sobre la masa (pesas) para desplazarla dependerá del valor de la aceleración que adquiere en cada instante la masa [70]. En este sentido, durante una elevación isoinercial, la masa adquiere inicialmente aceleraciones positivas, partiendo de una velocidad nula al inicio hasta alcanzar una velocidad máxima en un tiempo intermedio de la fase concéntrica del ejercicio (aquella en la que el músculo se contrae y el movimiento va en contra de la gravedad), donde la aceleración se hace nula. Por ello, es necesario un esfuerzo máximo (un pi-

co de fuerza) al inicio del levantamiento concéntrico, mientras que luego el esfuerzo neuromuscular disminuye [69]. Posteriormente, se produce una fase de desaceleración para volver a velocidad nula al final de la fase concéntrica. En consecuencia, en el ejercicio de peso libre se produce una disminución de la fuerza que ejerce el deportista en la segunda parte de la fase concéntrica. Esta fase de desaceleración puede ser significativa para masas ligeras o medias, donde las velocidades de ejecución del ejercicio pueden ser mayores (entrenamiento a máxima potencia). En el caso de desaceleraciones altas, cuando la desaceleración de la masa supera a la aceleración de la gravedad, el deportista deberá ejercer fuerza en sentido opuesto al desplazamiento. De este modo, dentro de la fase concéntrica de un ejercicio de elevación puede identificarse una fase de propulsión y otra de frenado [38]. Cuanto más rápido se realiza el ejercicio, mayores son las aceleraciones y, por tanto, las variaciones en la fuerza que ejerce el deportista durante el ejercicio. Algunos estudios han encontrado que el deportista emplea hasta el 52 % del tiempo de contracción muscular en desacelerar la carga, compensando el impulso que tiene lugar al comienzo del ejercicio, lo que lleva a una disminución de la actividad muscular. El entrenamiento de esta forma puede tener implicaciones negativas cuando el ejercicio se realiza a alta velocidad y potencia [25]. Sánchez-Medina et al. [70] evidenció la importancia de considerar las fases de propulsión y frenado en la evaluación de la fuerza en el ejercicio de press de banca con peso libre. Otros estudios señalan una menor actividad de la musculatura agonista y sinérgica para fases de frenado amplias [58]. Frost et al. [25] advierten que se deben tener en cuenta todas estas consideraciones durante el entrenamiento con peso libre, ya que puede tener implicaciones negativas en deportes que se caracterizan por tener elevadas velocidades y potencia.

Una variante del ejercicio con peso libre son los movimientos balísticos, en los que se proyectan o lanzan las masas de manera libre. En esta modalidad el deportista no está limitado a la necesidad de tener que frenar las masas al final de la fase concéntrica y, consecuentemente, se puede emplear una mayor parte de esta fase en acelerar las masas, incrementando los valores medios y máximos de velocidad y potencia, en comparación con el ejercicio no balístico equivalente [25, 58].

Otros sistemas de carga persiguen solventar las limitaciones que presenta el peso libre. Los ejercicios realizados con máquinas isocinéticas permiten el desarrollo de la máxima fuerza muscular a lo largo de todo el movimiento del ejercicio. Sin embargo, presentan la limitación de que la velocidad de realización del ejercicio está retenida a un valor constante. Por otro lado, entre los sistemas de carga variable, en los que la resistencia varía a lo largo del ejercicio, se incluye el uso de bandas elásticas y cadenas, y las máquinas

basadas en levas y palancas. Estos sistemas buscan incrementar el nivel de carga para determinados ángulos articulares con la intención de conseguir y mantener la máxima fuerza muscular a lo largo de todo el recorrido de la fase concéntrica. Las resistencias elásticas y las cadenas se suelen incorporar al ejercicio peso libre para incrementar la carga en la segunda parte de la fase concéntrica, reduciendo así la variabilidad de la fuerza durante la misma [5, 6, 21]. Esta situación provoca, por otro lado, una mayor carga desde el comienzo de la fase descendente (excéntrica) [18, 69]. Los estudios que han comparado los efectos neuromusculares agudos del entrenamiento con peso libre (isoinerciales) con los de carga variable (gomas elásticas y cadenas) son muy dispares y sin conclusiones claras. Algunos estudios no han encontrado diferencias significativas entre ambos sistemas [4, 21, 69]; otros encuentran ventajosa la utilización de gomas elásticas/cadenas añadidas al peso libre [6], y otros encuentran diferentes resultados en diferentes fases del movimiento y en los diferentes músculos analizados [37, 77, 88].

Dentro de los sistemas de carga variable se pueden incluir también los sistemas de carga neumáticos [26]. El sistema neumático, originalmente patentado por Keiser en 1891 [39], se basa en un compresor de aire y un cilindro neumático que, en combinación con un dispositivo mecánico, produce una carga variable. Este sistema pretende, reduciendo las masas móviles de la máquina, solventar las limitaciones asociadas con las fuerzas de inercia en los ejercicios con peso libre. Frost et al.[25], evaluaron el ejercicio de press de banca para tres tipos de carga distintos: peso libre, peso libre con movimiento balístico, y el sistema neumático. Las curvas de velocidad, de fuerza y de potencia, obtenidas en cada sesión, presentaron diferencias significativas entre los tres tipos de carga. Los resultados mostraron una variación menor en las curvas de fuerza en el caso de la máquina neumática en comparación con el peso libre y el balístico; así como una mayor fuerza, potencia y actividad muscular durante el último 10-20 % de la fase concéntrica. La curva de fuerza obtenida con la carga neumática aún muestra variaciones significativas durante la fase concéntrica, llegando incluso a registrarse fuerzas negativas (fase de frenado) al final de esta fase para el caso de velocidades de ejecución altas. Otros estudios comparan los sistemas de carga de peso libre y neumático para el ejercicio de press de banca [8, 62], concluyendo que la selección del sistema de carga de la máquina de musculación debe hacerse en función del objetivo del entrenamiento.

Otros autores han centrado sus estudios en la comparación del efecto del uso de sistemas de resistencia isoinercial (peso libre) con sistemas de resistencia variable [5, 6, 33, 69, 88, 89, 90], o evaluado el uso de la resistencia adaptativa (isocinética) en diferentes ejercicios [7, 9, 11, 57, 59, 78]. Aunque los resultados de estos estudios son a veces contradictorios, la mayoría de

ellos concluyen que los patrones de movimiento de carga y las activaciones musculares pueden modificarse en función del tipo de resistencia (isoinercial, isocinética o variable) y que es necesario elegir los ejercicios en función del objetivo de entrenamiento [41].

El ejercicio de press de banca

El ejercicio de press de banca es muy usado como entrenamiento y/o modalidad terapéutica para mejorar el rendimiento neuromuscular [60]. Además, este ejercicio se considera la prueba más sencilla y adecuada para evaluar la fuerza del tren superior del cuerpo humano [87]. Tradicionalmente, el press de banca se basa en el levantamiento de una barra provista de pesas en ambos extremos. Para realizar el ejercicio, el usuario debe colocarse en posición decúbito supino sobre un banco, es decir, acostado hacia arriba. El ejercicio consta de dos fases: la ascendente y la descendente. Durante fase ascendente, conocida como fase concéntrica o positiva, el músculo se acorta y tiene lugar hasta el momento en el que se tienen los brazos casi completamente extendidos, momento en el que el pectoral se encuentra en su mayor fase de congestión. Durante la fase descendente, llamada también fase excéntrica o negativa, el pectoral se encuentra alargado.

El ejercicio de press de banca se puede realizar de forma guiada utilizando una máquina tipo Smith. La máquina de Smith, es un equipo de ejercicio en peso libre en el que una barra de pesas desliza sobre barras guía verticales [75]. La principal diferencia de la realización del ejercicio de press de banca en máquina de Smith frente a la realización sin ella, es que los requisitos de estabilidad son menores, lo que crea un patrón de movimiento unidimensional guiado [10]. En este sentido, un inconveniente podría ser que la trayectoria de la barra en el ejercicio realizado en la máquina de Smith no es natural, ya que obliga a los usuarios a mover la barra en una trayectoria lineal [55]. Sin embargo, la máquina Smith es más segura para los usuarios [60] porque limita los movimientos de la barra en las direcciones medio-lateral y anteroposterior, centrándose en la dirección vertical [75].

Modelos matemáticos en el análisis del movimiento humano

El análisis del movimiento humano mediante técnicas de mecánica computacional ha sido un área de investigación de gran interés desde hace muchos años [32]. Las técnicas de dinámica de sistemas multicuerpo (MSD, por sus siglas en inglés, *Multibody System Dynamics*) son muy potentes y hay muchas contribuciones de la comunidad MSD al problema de la simulación de la marcha [2, 3, 61, 68]. Entre otros enfoques, las técnicas de optimización de parámetros se han utilizado con frecuencia para síntesis de movimiento de

robots bípedos [12]. Estas técnicas han demostrado ser muy útiles en la investigación de la marcha humana en dos dimensiones, como se muestra en las referencias [1, 31]. En este enfoque, las fuerzas musculares y las coordenadas generalizadas se describen en términos de un conjunto específico de parámetros, cuyos valores óptimos se encuentran minimizando funciones de coste que incluyen una estimación del gasto energético y una medida de la desviación de los patrones de marcha normales. El método se basa principalmente en la dinámica inversa, ya que este tipo de dinámica se resuelve utilizando el movimiento como base a partir de los parámetros de diseño en cada iteración del algoritmo de optimización. La principal ventaja de esta metodología es la completa eliminación de las integraciones en tiempo real de las ecuaciones de movimiento, lo que reduce significativamente el coste computacional de la simulación. En la Ref. [30] se utilizó con éxito la optimización de parámetros para resolver un problema combinado de control óptimo y diseño óptimo, ya que al mismo tiempo se pudieron obtener las trayectorias, fuerzas musculares, etc., y los parámetros óptimos de un modelo de órtesis activa.

En los últimos años, la investigación sobre la predicción del movimiento humano ha experimentado un gran desarrollo gracias a la incorporación de técnicas computacionalmente eficientes, entre las que el uso de la diferenciación algorítmica ha hecho posible una importante reducción del tiempo de simulación mediante la optimización. Ejemplos notables se encuentran en la simulación tridimensional de la marcha humana en Falisse et al. [23, 24] o en la simulación de los movimientos de sentarse a estar de pie en Serrancolí et al. [73]. Además, la combinación de las herramientas computacionales proporcionadas por Matlab con las capacidades de modelado músculo-esquelético de OpenSim han sido utilizadas eficientemente por Lee y Umberger [86] para crear un marco de trabajo para generar simulaciones predictivas del movimiento músculo-esquelético basadas en técnicas de control óptimo de colocación directa.

Para el estudio de los ejercicios de musculación son útiles los modelos matemáticos. Dichos modelos permiten, además de evaluar una determinada ejecución del ejercicio, estudiar cómo influirían las variaciones de los distintos parámetros en el mismo. En el caso del ejercicio de press de banca únicamente se han encontrado en la literatura los modelos desarrollados por Wang y otros [91] y Rahmani y otros [66]. Wang y otros [91] estudian la distribución de la fuerza en el pectoral y en la musculatura de las extremidades superiores del cuerpo, según la abertura del agarre (separación entre manos) en el ejercicio del press de banca. Para ello construyen un modelo del cuerpo humano utilizando el software AnyBody [91]. Rahmani y otros [66] presentan un modelo matemático de 2 grados de libertad en el plano sagital para el ejercicio de press de banca. El modelo considera los brazos como segmentos rígidos,

sin masa, conectados por dos articulaciones de revolución (codo y hombro). Además, supone un par prismático de desplazamiento vertical del hombro.

1.2. Motivación y justificación

Los diseños conceptuales de mecanismos de fuerza constante presentados por López y otros [53] podrían ser implementados en las máquinas de musculación que disponen de pesas con movimiento guiado, como es el caso de las máquinas tipo Smith y las máquinas de poleas. Por lo tanto, serían aplicables a todos los tipos de ejercicios que dichas máquinas permiten. Cabe destacar que no se ha encontrado ninguna máquina de musculación que use mecanismos de fuerza constante como medio de carga, no existiendo, por tanto, estudios científicos sobre el rendimiento de estos sistemas de carga en los ejercicios de musculación. Si bien, la literatura consultada muestra el interés de la comunidad científica y del deporte en soluciones que permitan mantener un valor de fuerza constante a lo largo del ejercicio. Una mejor comprensión de las propiedades biomecánicas que gobernarán los sistemas de carga de fuerza constante, proporcionará al investigador, al clínico y al profesional de Ciencias de la Actividad Física y del Deporte, una apreciación mucho mayor de los beneficios y limitaciones asociados a este modo de entrenamiento de la fuerza.

1.3. Hipótesis

En este trabajo se pretende demostrar la aplicabilidad de los mecanismos de fuerza constante como sistema de carga en una máquina de acondicionamiento muscular tipo Smith. Posiblemente, se obtengan patrones de fuerza y potencia, sustancialmente distintos a los que se obtengan con peso libre (isoinercial) durante la realización del ejercicio de press de banca. Es esperable que la fuerza que ejerza el deportista durante la ejecución del ejercicio muestre variaciones sustancialmente menores.

1.4. Objetivos

El objetivo general de esta tesis es implementar un mecanismo de fuerza constante como sistema de carga en una máquina de acondicionamiento muscular tipo Smith. Evaluar y comparar la cinemática y cinética para los sistemas de carga con peso libre (isoinercial) y con mecanismo de fuerza cons-

tante en el ejercicio de press de banca.

Objetivos específicos:

- Fabricar y validar experimentalmente un prototipo de mecanismo de fuerza constante.
- Desarrollar un modelo matemático del ejercicio de musculación de press de banca realizado en máquinas tipo Smith.
- Implementar un mecanismo de fuerza constante como sistema de carga en una máquina de acondicionamiento muscular tipo Smith.
- Realizar un análisis comparativo del ejercicio de press de banca para los sistemas de carga con peso libre y con mecanismo de fuerza constante.
- Desarrollar un modelo de optimización paramétrica para el análisis de formas de realización óptimas del ejercicio.

1.5. Metodología

Para alcanzar los objetivos descritos anteriormente, en primer lugar, se ha llevado a cabo una revisión bibliográfica para tener un conocimiento global del estado del arte y conocer los últimos trabajos realizados en cada tema considerado.

Para el primer objetivo, *fabricar y validar experimentalmente un prototipo de mecanismo de fuerza constante*, partimos de un trabajo previo a esta tesis. El CFM a utilizar fue desarrollado conceptualmente por López y otros [53]. Dicho CFM está basado en la combinación de resortes, levas y rodillos, para obtener la característica de fuerza constante. Con este punto de partida, el primer paso es validar experimentalmente el diseño conceptual de CFM. Se realizará el diseño de detalle de un prototipo de CFM y se llevará a cabo su fabricación. Este prototipo se evaluará experimentalmente en laboratorio, realizando ensayos de carga con la máquina de tracción H5KS Hounsfield. Estos ensayos se realizarán bajo diversas condiciones (con diferentes resortes para modificar la carga, a distintas velocidades de desplazamiento, con distintos materiales de los rodillos para evaluar la fricción, etc.) Además, se elaborará un modelo multicuerpo del CFM para estudiar la influencia de distintas variables de diseño y funcionamiento. Para llevar a cabo las simulaciones se hará uso del software Matlab. El modelo multicuerpo será validado con los resultados experimentales.

Para la consecución del segundo objetivo, *desarrollar un modelo matemático del ejercicio de musculación de press de banca realizado en máquinas tipo Smith*, se parte del estudio de los modelos matemáticos existentes. El modelo del press de banca se realizará haciendo uso de las técnicas de dinámica de sistemas multicuerpo. En el modelo matemático se asumirá los miembros superiores del cuerpo humano como sólidos rígidos y las fuerzas musculares se simplicarán a pares articulares. Partiendo de la medición del ángulo del codo realizada con un electrogoniómetro durante una sesión de entrenamiento en press de banca con peso libre. Tomando como referencia una misma cinemática del ejercicio, mediante el modelo matemático se obtendrán y compararán las variables más representativas del ejercicio para el sistema de carga de peso libre y suponiendo un sistema de carga basado en CFM. Para ello se hará uso del software MatLab. De este modo, se completa también parte del cuarto objetivo.

Una vez comparados de forma teórica mediante el modelo matemático los dos sistemas de carga, se realizará un estudio para realizar el rediseño y adaptación del mecanismo de fuerza constante como sistema de carga en una máquina de Smith comercial. Este estudio conllevará la selección del rango de actuación del mecanismo, los diferentes niveles de carga que podrá proporcionar y la modificación de los mismos, etc. Asimismo, se introducirán unas pequeñas modificaciones en la máquina de Smith comercial que permitirán que la misma pueda ser utilizada en peso libre (isoinercial) o con los CFM. También se diseñarán los elementos de conexión necesarios para conectar los CFM a la máquina Smith. Además, se estudiará cómo reducir las masas móviles del mismo para minimizar las fuerzas de inercia. Una vez se obtenga el diseño final del CFM, se encargará la fabricación del mismo a una empresa externa con experiencia en mecanizado de piezas. La máquina Smith modificada será sensorizada con el objetivo de validar experimentalmente y caracterizar el nuevo sistema de carga. Para ello se utilizarán células de carga tipo S (S Type Load Cell, 100kg, modelo CZL301C de Phidgets), un encoder lineal de hilo de 2,5 m y se fabricará una plataforma de fuerza con cuatro sensores de compresión (Button Load Cell, 200kg, modelo CZL204E de Phidgets). La lectura de las células de carga, junto con los registros del encoder que mide el deslazamiento vertical de la barra, permitirá obtener la curva de fuerza-desplazamiento de los CFM. La salida de datos de las tarjetas de adquisición de las células de carga y de la tarjeta del encoder se registran mediante código escrito en Phyton. La caracterización y validación completa del sistema de carga basado en CFM se realizará mediante la obtención de la curva fuerza-desplazamiento para distintos valores de carga a lo largo del rango del mecanismo, quedando así cubierto el tercer objetivo, *implementar un mecanismo de fuerza constante como sistema de carga en una máquina*

de acondicionamiento muscular tipo Smith.

Una vez implementada y validada la máquina de Smith de fuerza constante, se puede terminar de alcanzar el cuarto objetivo, *realizar un análisis comparativo del ejercicio de press de banca para los sistemas de carga con peso libre y con mecanismo de fuerza constante*. Para ello se realizarán una serie de estudios en laboratorio donde un usuario realizará una sesión de entrenamiento utilizando la máquina de Smith en sus dos variantes: peso libre y con CFM. Mediante los sensores instalados en la máquina Smith se obtendrán los datos de posición de la barra mediante (encoder lineal) y de la fuerza que ejerce el deportista (plataforma de fuerza). De este modo se monitoriza al deportista mientras realiza los ejercicios. Mediante el software MatLab se tratarán los datos obtenidos por los sensores y se representarán las respectivas curvas de fuerza para ambos entrenamientos. De este modo, se podrán comparar ambos sistemas de carga.

Para la consecución del último objetivo propuesto se desarrollará un modelo de optimización paramétrica para analizar las formas óptimas de realizar el ejercicio de press de banca. Para ello, se partirá del modelo matemático desarrollado y de un patrón de movimiento medido en el laboratorio mediante un electrogoniómetro colocado en el codo del individuo. La idea principal de la simulación por optimización es parametrizar las trayectorias y los pares articulares (hombro y codo) para encontrar los valores que minimizan una determinada función de coste y satisfacen las ecuaciones de movimiento en determinados puntos de colocación. Por tanto, las trayectorias y los pares articulares serán las incógnitas del problema. Esta metodología tiene como objetivo comprender la realización adecuada del ejercicio de press de banca en dos condiciones de entrenamiento distintas: para ganar resistencia o para realizar el ejercicio de la manera más segura, es decir, evitando las sobrecargas. Se utilizará el software Matlab para resolver este problema de optimización. De este modo, quedarán satisfechos todos los objetivos propuestos en la tesis.

Capítulo 2

Validación experimental de un mecanismo de fuerza constante y análisis de su rendimiento con un modelo multicuerpo calibrado

Mechanism and Machine Theory 173 (2022) 104819

Contents lists available at ScienceDirect

Mechanism and Machine Theory

journal homepage: www.elsevier.com/locate/mechmt

Research paper

Experimental validation of a constant-force mechanism and analysis of its performance with a calibrated multibody model

Silvia Sánchez-Salinas [a], Alfonso García-Agúndez [b], Javier López-Martínez [a,*], Daniel García-Vallejo [b]

[a] CIMEDES Research Center (CeiA3), Department of Engineering, University of Almería, Spain
[b] Department of Mechanical Engineering and Manufacturing, Universidad de Sevilla, Spain

ARTICLE INFO

Keywords:
Constant-force mechanisms
Multibody model
Experimental validation

ABSTRACT

The potential applications of constant-force mechanisms (CFMs) have increased in recent years with the development of new designs. This paper focuses on the experimental evaluation and the mathematical modelling of a CFM. The mechanism is based on the use of cams, rollers and springs, which allows for a large stroke and user-adjustable force value. The evaluation and validation of the mechanism is carried out by performing a series of tests examining the constancy of the input force, and where the influence of friction forces and the manufacturing process on the performance of the mechanism is revealed. A multibody model of the constant-force mechanism is developed and calibrated with the help of the experimental results. This model is based on the assumption of rolling without sliding between the cam and the roller, what makes the multibody model to include velocity constraints. The calibration of the model pursues the development of a mathematical tool to study the performance of the mechanism in conditions that are different from those of the experiments presented. The CFM model is used to perform a sensitivity analysis of some important design parameters of the mechanism.

1. Introduction

Constant-force mechanisms (CFMs) are designed to achieve a constant force value on the input link for a certain prescribed range of displacement. These mechanisms are applied in several fields of engineering, where the design solution given in each case will depend on the intended use.

Constant-force mechanisms can be classified into two main groups according to the type of components that provide mobility to the mechanism [1]. A first group includes those mechanisms based on flexible links, the so-called compliant mechanisms [2–4], where the mobility of these mechanisms is provided by flexible elements and can be designed in one single piece. The flexible parts are usually designed with relatively complex geometries to achieve the characteristic of constant-force in a certain range of movement of the mechanism. The geometry of the flexible element can be obtained from optimization techniques [5–9] and from the pseudo-rigid body method [5,10–13]. Compliant CFMs can be designed for a one directional constant force [14,15] or for a constant torque [7,16]. Some CFMs proposals are based on the use of a positive stiffness element together with a negative stiffness element, so that when acting together the resulting force–displacement curve presents some region with null or almost null slope, i.e. nearly null stiffness [13,17–20]. One way to achieve negative stiffness is by using beam elements subjected to buckling, where

* Correspondence to: CIMEDES Research Center (CeiA3), Department of Engineering, University of Almería, 04120, Almería, Spain.
E-mail addresses: silvia.sanchez@ual.es (S. Sánchez-Salinas), agarciaagundez@us.es (A. García-Agúndez), javier.lopez@ual.es (J. López-Martínez), dgvallejo@us.es (D. García-Vallejo).

https://doi.org/10.1016/j.mechmachtheory.2022.104819
Received 2 December 2021; Received in revised form 2 February 2022; Accepted 3 March 2022
Available online 23 March 2022

the stiffness of the beam can be known from the Euler equation [21–23]. Compliant CFMs are of particular interest in applications that do not require large displacements, have the advantage of being simple and compact construction, and have no friction losses.

The second group of CFMs includes those that use springs together with a non-linear transmission. Compared to compliant CFMs, they have the advantage of being designed for larger displacements [15,24], although in most cases the influence of the friction must be taken into account in the design [14,24,25]. Some proposals are based on the use of rigid links together with springs arranged in a particular configuration [26–28], as is the case of the well known desk lamp holder, which compensates the weight of the lamp for a wide range of positions [29]. In other cases springs are used together with cams with a particular geometry. In some designs a non-circular cam rotates winding a cable around its surface, which lengthens a linear spring. By combining the linear spring characteristic with the variable radius cam, a constant torque can be achieved on the cam's axis of rotation [30,31]. Other designs use springs and rollers, where the springs are lengthened by rolling the rollers over a cam surface [14,15,24,32,33]. The particular geometry of the cam allows maintaining a constant force value on the input link of the mechanism. Some solutions allow the force value to be modified by presetting the initial spring tension [14] or by arranging several springs in parallel [24].

A generalization of the CFMs are mechanisms with user-defined stiffness. Instead of designing the mechanism for zero stiffness (constant force), the same design methods can be applied to obtain a non-linear spring with an specific stiffness curve [34,35]. Bidgoly et al. [36] derive the geometry of several cams to achieve constant torque, cubic, hyperbolic tangent and sinusoidal springs.

Constant-force mechanisms are undergoing considerable development in the field of robotics, where they are used as gravity-balancing mechanism [28], as safety systems against overloads [17], or in the manipulation of objects to limit the gripping force [8,19,37,38], thus avoiding the use of complex force control systems. CFMs have found new applications in fields such as surgery, with the design of grasping forceps to control the clamping force [10,39] or in cardiac ablation catheter [40]; in the development of 2-DOF grippers [41]; in assistive exoskeletons [42]; in end-effectors for polishing/deburring operations [43]; in microgripers for biological cell micromanipulation [44]; in body building machines, where they seek to eliminate the inertia forces present in weight-stack machines [45,46] or for their use in low-gravity environments [47]; in snap-fit connectors [48]; in automotive clutches [49] or in electrical contacts [50].

The multibody modelling of cam mechanisms is a problem that is definitively influenced by the contact modelling between the cam and the follower. Using multibody system dynamics theory, Cardona et al. [51] presented a methodology for the optimal design of the cams of motor engine valve trains including nonlinear geometrical, kinematical and dynamical constraints. Ouyang et al. [52] also utilized a dynamic multibody model of a cam-follower mechanism in the optimal design problem of the cam profile. The contact problem between circular and non-circular bodies, as that of the cam and the follower in general cam mechanisms, has been treated in detail by Xu [53], who proposed a general methodology for planar multibody systems which is applicable in case single and multi-point contact. Since cam profiles are often numerically represented, it is common to use interpolation to reconstruct the cam profile between data points. In this sense, the influence of interpolation errors in the kinematics and dynamics of cam mechanisms is studied by Borboni et al. [54]. Analyses of computational multibody models' results of cam mechanisms in comparison with experimental performance data can be found in the works of [55,56].

In the present work, a CFM based on a cam and springs is experimentally evaluated and mathematically modelled and studied. The CFM prototype evaluated here is based on one of the three conceptual designs of CFMs proposed in a previous work [24], and is intended for the future fabrication of a full-scale CFM for bodybuilding machines [45].

This paper is organized as follows: Section 2 includes, first, a brief description of the conceptual design of the CFM developed, the force equation condition for constant force and the numerical derivation for the cam profile; second, the description of the prototype developed; and third, the evaluation of the manufacturing errors in the fabricated cam. Section 3 contains a series of tests carried out to evaluate the performance of the mechanism and includes some simulations for comparison. Next, Section 4 deals with the formulation of the multibody model of the CFM and Section 5 discusses the influence of different parameters on the constant force characteristic. Lastly, Section 6 draws the main conclusions.

2. The constant-force mechanism

The CFM developed basically comprises a symmetric cam profile, two rollers, and a spring attached to both roller axes (Fig. 1). The pulling force is exerted on a cable (or a rod) aligned with the axis of symmetry of the mechanism, where this cable bifurcates into two braces that are connected to both roller axes respectively. As the cable moves vertically, the rollers move upward by rolling over the cam surface and the spring elongates by exerting a force opposing the movement. With this arrangement, a certain cam profile can be found that allows a constant force value to be maintained throughout the entire stroke of the mechanism.

Once the conceptual design of the CFM has been introduced, this section begins with a summary of the input force equation, the constant force condition, and the numerical integration required to obtain the roller centre trajectory (a more detailed description of this procedure can be found in our former work [24]). Subsequently, the CFM prototype is described. Finally, the manufacturing errors of the cam profile are measured and discussed.

2.1. Force equation and cam profile

Fig. 1 shows the forces acting on the right roller when the roller moves upward. Note that, due to the symmetry of the mechanism, both rollers move at the same time and the force diagrams are also the same for both rollers. From the equilibrium equations in

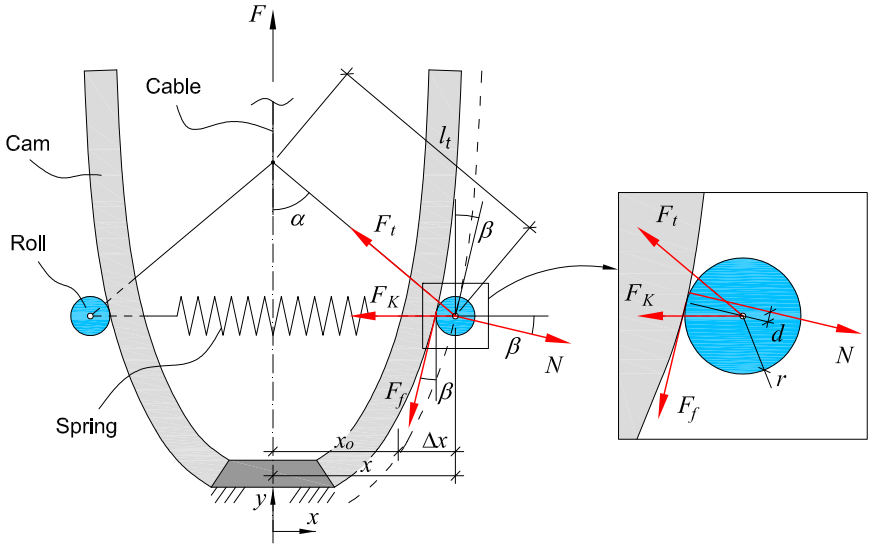

Fig. 1. Conceptual design of the CFM and forces diagram for the roller.

the horizontal and vertical directions, the moment equilibrium equation $F_f r = Nd$, and some basic relations, the input force can be written as [24]

$$F = 4K\,\Delta x \underbrace{\left(\frac{1-\mu_r \tan\beta}{\tan\beta+\mu_r} - \tan\alpha\right)^{-1}}_{A}, \tag{1}$$

where the input force F results as a function of the spring stiffness coefficient K and its elongation Δx, the rolling friction μ_r, the slope of the curve β and the angle α of the brace. Eq. (1) shows that the force F will be constant if the trajectory of the roller centre verifies that the term A keeps constant. It must be noted that Eq. (1) has been obtained for the upward movement of the rollers, while for the downward displacement the sign preceding μ_r must be changed. This means that, due to friction, the cam can only be designed for an exactly constant force curve in one of the two directions of displacement.

Next, from Eq. (1), the following nonlinear first order differential equation can be derived [24]

$$\frac{\mathrm{d}x}{\mathrm{d}y} = \frac{1-\mu_r f(x)}{\mu_r + f(x)}, \tag{2}$$

where

$$f(x) = \frac{1}{A}(x - x_0) + \frac{x}{l_t}\left(1 - \left(\frac{x}{l_t}\right)^2\right)^{-\frac{1}{2}}. \tag{3}$$

To obtain Eq. (2) from Eq. (1), the relations $\tan\beta = \dfrac{\mathrm{d}x}{\mathrm{d}y}$ and $\tan\alpha = \dfrac{x}{l_t}\left(1 - \left(\dfrac{x}{l_t}\right)^2\right)^{-\frac{1}{2}}$ have been used. Then, a first order implicit integration formula can be used to solve the differential Eq. (2) [24], resulting in the trajectory of the roller centre.

Finally, the cam profile can be obtained with the CAD software AutoCAD from AUTODESK. First, the points of the roller centre path obtained from the numerical integration are joined by means of a spline. Secondly, the cam curve is obtained using the equidistance tool provided by the software, where the radius of the roller is used for the equidistance.

2.2. Prototype

In order to experimentally validate the design proposed and to analyse its performance, a prototype of the CFM has been elaborated. Fig. 2 shows the CAD model and a picture of the prototype. The cam profile of the mechanism has been designed for a maximum stroke of 250 mm and to achieve a constant force value F of 50 N for a spring stiffness K of 1.38 N/mm. Table 1 summarizes the main characteristics of the CFM. Due to the initial uncertainty of the value of the rolling friction coefficient, the

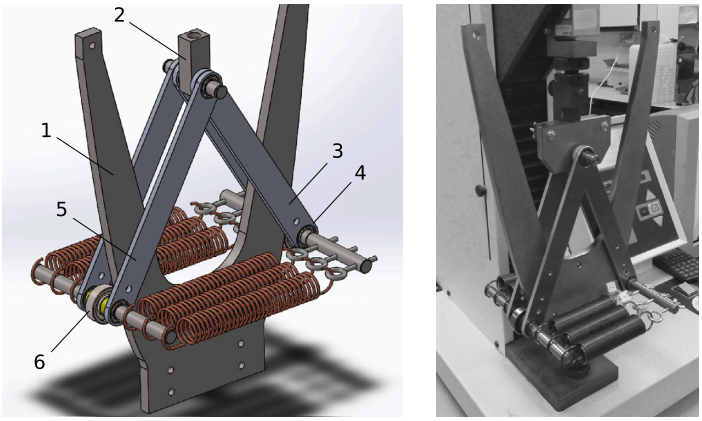

Fig. 2. (a) CAD design of the CFM and (b) an image of the prototype mounted in a H5KS Hounsfield testing machine. Labels in (a): 1 cam, 2 pulling link, 3 and 5 braces (length = 200 mm), 4 and 6 rollers (radius = 16 mm).

Table 1
CFM design parameters.

Constant force, F (see Eq. (1))	$F = 4KA$, with $A = 9.058$
Number of springs in parallel	2/4/6
Possible stiffness, K (N/mm)	1.38/2.76/4.14
Possible force values, F (N)	50/100/150
Stroke (mm)	240
Brace length, l_t (mm)	200
Spring rest length, $2x_o$ (mm)	136
Roller radius, r (mm)	16

cam profile has been derived for $\mu_r = 0$. To achieve a low rolling friction coefficient, the cam is made of stainless steel ASTM A 240 (AISI 304) and two different materials have been tested for the rollers (steel and nylon).

The shaft of the rollers has been prolonged to be able to use up to six springs arranged in parallel. In this way, it is easy to modify the constant force value of the mechanism. According to Eq. (1), the force F is proportional to the spring stiffness. Then, the force value can be changed by adding several springs in parallel or replacing the springs by other with different stiffness constant. In Table 1, three different values of force F are listed (50 N, 100 N, and 150 N), which are achievable by arranging 2, 4, or 6 springs in parallel, with a stiffness of 0.69 N/mm stiffness in each spring. Moreover, others values of force can be obtained using springs with different stiffness. Note that all the springs must have the same rest length, since the distance between the right side and the left side of the cam is conditioned by the spring rest length (defined as $2x_o$ in Fig. 1). To compensate for possible differences in spring length or manufacturing errors, individual spring tensors (M4 × 0.7 mm screws) have been used for each spring to adjust the spring rest length.

2.3. Evaluation of the manufactured cam profile

A precise fabrication of the cam profile is essential to get the constant-force characteristic of the mechanism. The prototype cam has been obtained with a CNC laser cutting machine from the CAD drawing. This manufacturing method has been preferred instead of milling, due to the much lower price of the former. The cam has been obtained from a 10 mm thick steel plate. To evaluate the manufactured cam profile, it has been measured with an optical measuring machine with vision system TESA-VISIO 300 (1 μm resolution) and then compared with the designed profile. Due to the dimensions of the cam and the limited working area of the measuring machine, only the lower half of the cam profile has been measured (first 150 mm of the cam profile). Cam profile measurements were taken at 0.5 mm intervals. The best fit between the set of measured points and the set of model points has been obtained with an iterative closest point (ICP) algorithm, where the registration of the sets of points has been done by iterative reweighted least squares [57]. After the transformation (translation plus rotation) of the measured points sets, a very good fit between both curve points has been obtained, with a root-mean-square error (RMSE) of 0.023 mm and standard deviation (SD) of 0.017 mm. Fig. 3 shows the error in x coordinate between the measured points and the model, for the right and left sides of the cam. Negative values indicate that the measured points of the fabricated cam profile are inside the design profile (lower cam width). These results, which show small manufacturing errors, together with the experimental results described in Section 3, confirm the feasibility of the CNC laser cutting.

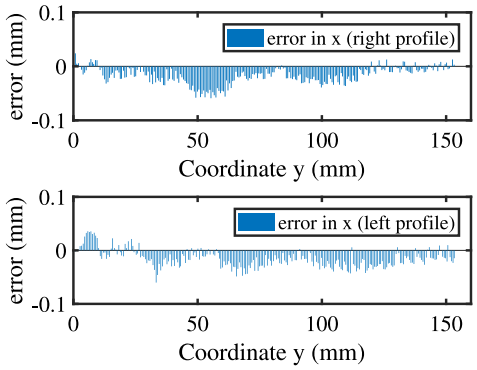

Fig. 3. Error in x coordinate between the measured and the theoretical cam profile.

Table 2
Measured stiffness constant of the springs.

Spring	#1	#2	#3	#4	#5	#6
Stiffness (N/mm)	0.683	0.682	0.681	0.686	0.686	0.679

3. Experimental results

A series of tests have been carried out to analyse the performance of the mechanism. The constant-force mechanism has been tested for three different spring stiffness values and two rollers materials. Previously, some initials tests have been done to obtain the real stiffness constant of the springs and to adjust the spring rest length in the mechanism. All force tests have been done in a H5KS Hounsfield testing machine (see Fig. 2b). This model H5KS includes a 5 kN load cell with a 0.5% load measurement accuracy and 0.001 mm position accuracy. The machine has a maximum stroke of 750 mm and a test speed range from 0.001 mm/min to 1500 mm/min. Tests have been conducted starting with the rollers located at the bottom of the cam and moving upwards. Once the maximum stroke of the mechanism has been reached, with the rollers at the top of the cam, the rollers begin to move downward until they return to the initial position. Most of the tests have been done with a travel speed of 500 mm/min and a sampling rate of 35 Hz.

As described above, the prototype can incorporate up to six springs arranged in parallel (2, 4, or 6 springs are possible). The stiffness of each spring has been obtained through tensile tests. Table 2 lists the stiffness constant values for each spring. The spring rest length will have influence in the force curve of the mechanism, specially in the first section of the cam [24]. For each pair of springs, it has been adjusted the spring rest length from tensile–compression tests results, where the spring rest length can be modified through a screw. Fig. 4 shows the force curves obtained for five different adjustments of the spring rest length of the pair of springs #1 and #2. The step between two consecutive adjustments corresponds to two complete turns of the screw. In Fig. 4, it is represented the upwards and downwards displacements of the mechanism in the same curve, where the resultant hysteresis loop for each test is appreciated. The curve with the best approximation to the constant-force characteristic has been defined as ‘adjust = 0 mm’ in Fig. 4. Variations in the spring rest length result in deviations in the force curve, being more pronounced in the first section of the cam. These results are in accordance with the theoretical results obtained in Ref. [24].

The force value can be modified by adding springs arranged in parallel. Fig. 5 shows the force hysteresis loop measured for 2, 4, and 6 springs. Force curves show some fluctuations due to the errors of the manufactured cam profile and also some noise mainly due to the surface roughness of the cam. In the three force curves, the same fluctuation pattern can be observed. The force curves show larger hysteresis loop for higher spring stiffness, where the area within the hysteresis loop mainly depends on the rolling friction coefficient and the force value. It is interesting to note that the area within the hysteresis loop is not linear with the force (Table 3). For each section of the hysteresis loop (upward and downward displacement), Table 3 summarizes the mean force value, the standard deviation and the maximum and minimum values. Additionally, it is included the theoretical value of the forces, calculated from Eq. (1) with the measured spring stiffness constant and for null friction coefficient. These force values have been represented with dashed lines in Fig. 5.

All force curves obtained in the different tests showed high repeatability. As example, Fig. 6 shows five repetitions of the force test for four springs in parallel.

The tests described so far have been done with rollers of steel. With the aim of studying the effect of other materials in the rolling friction, rollers of nylon have been tested. The curves for the three force levels obtained for steel rollers have been compared with the curves obtained for nylon rollers, showing small differences between the curves. As expected, since the rolling friction for nylon material is slightly higher, the hysteresis loop is somewhat larger when nylon rollers are used. This difference is more easily

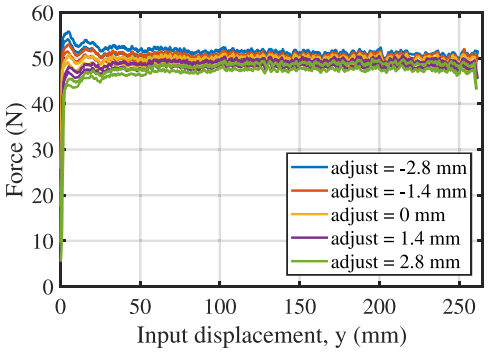

Fig. 4. Force curves for variations in the spring rest length.

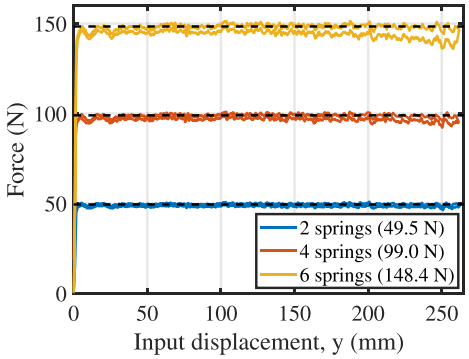

Fig. 5. Force curves for 2, 4, and 6 springs in parallel.

Table 3
Parameters of the force curves in Fig. 5.

Springs arranged in parallel	2 (#1 and #2)	4 (#1 to #4)	6 (#1 to #6)
Spring equivalent stiffness (N/mm)	1.365	2.732	4.097
Theoretical force (N)	49.46	98.99	148.4
Displacement	up/down	up/down	up/down
Mean force (N)	49.67/48.27	98.94/96.62	148.27/144.17
Standard deviation (N)	0.427/0.425	0.949/1.02	1.38/2.12
Max. force (N)	51.00/49.33	101.0/99.00	151.33/148.00
Min. force (N)	48.00/46.33	95.33/92.17	143.17/136.00
Hysteresis loop area (N m)	0.406	0.555	1.069

observed in the curves of higher value of force. Fig. 7 shows the curve force for the two type of rollers and for 6 springs, with hysteresis loop areas of 1.069 Nm and 1.220 Nm for steel and nylon rollers, respectively.

Test displacement speed may influence the force curve results. Previous results were conducted at 500 mm/min. Next, Fig. 8 shows the force curves for five different velocities, from 100 mm/min to 1500 mm/min (maximum allowed by the testing machine). Since the displacement velocity is low in all tests, no appreciable influence of inertia forces is expected. All curves show the same main fluctuation due to the small deviation in the manufacturing process, but the noise due to surface roughness increases with decreasing speed. As representative values, the standard deviations for the upward displacement section of the curves are 0.693 N, 0.551 N, 0.427 N, 0.359 N and 0.318 N for the velocities between 100 mm/min and 1500 mm/min shown in Fig. 8.

Finally, this section presents a comparison between experimental results and simulations using the measured cam profile described in Section 2.3. The simulations were performed with SOLIDWORKS motion commercial software, which uses the ADAMS/Solver simulation engine to solve the equations of motion and calculate the forces on each component of the assembly. The real model has been simplified for simulations. Braces, springs and shafts have been included as virtual links without mass. In addition, no mass has been considered for the rollers. Therefore, no inertial effects are considered, which have no significant

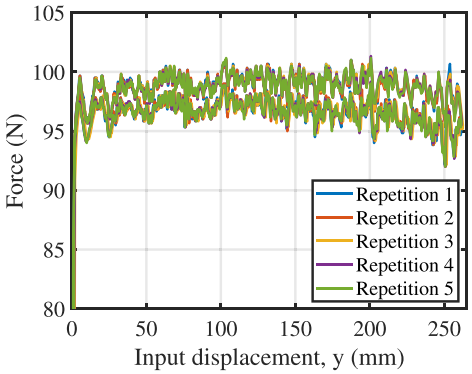

Fig. 6. Force curves for five repetitions of the force test (4 springs).

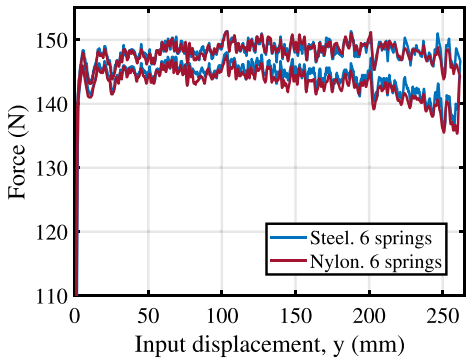

Fig. 7. Force curves for steel rollers and for nylon rollers (6 springs).

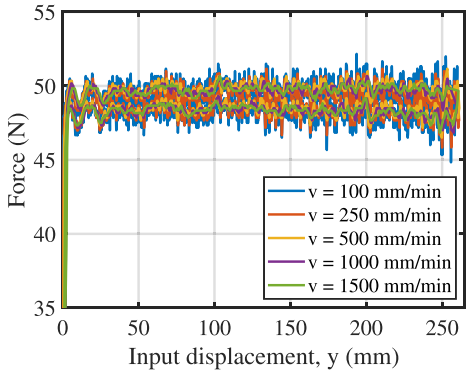

Fig. 8. Force curves for different displacement velocities (2 springs).

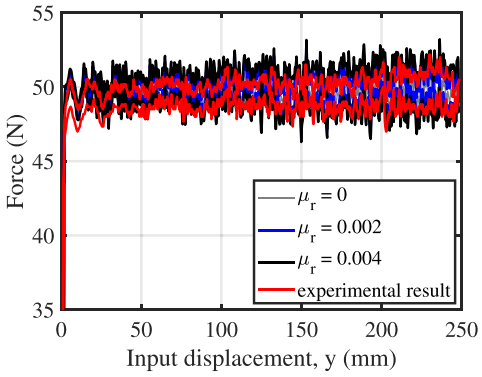

(a)

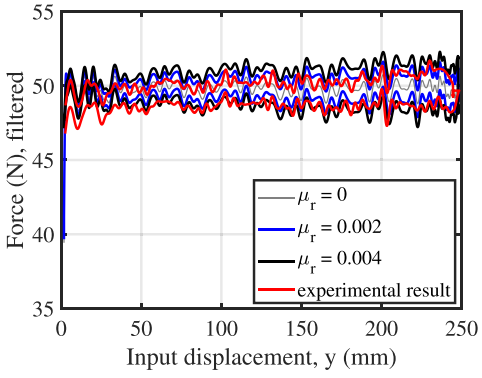

(b)

Fig. 9. Force curves from experimental result and from simulations with the measured cam profile and different values of the rolling friction coefficient. (a) raw data and (b) filtered curves.

influence due to the low accelerations. As in the tests, the simulations were performed with a low displacement velocity of 500 mm/min. Lastly, the contacts between the rollers and the measured cam profile have been imposed as non-penetrating and with allowable separation, and the rolling friction coefficient μ_r has been included.

Fig. 9(a) shows the measured force as well as the simulated results for rolling friction coefficient values of $\mu_r = 0.002$ and $\mu_r = 0.004$, and for no friction. For an easier comparison of the results, the data reported in Fig. 9(a) have been back and forth filtered with a sixth order Butterworth filter with cut-off frequency of 2 Hz, leading to the smoother curves drawn in Fig. 9 (b). From the similarity in the fluctuations shown in the experimentally measured and simulated curves, it is confirmed that the force fluctuations are due to manufacturing errors. The error induced by the machining process defined as the difference between the force measured in the test conducted on the manufactured mechanism and the force obtained by simulation using the profile sent to the manufacturer is studied later on in Section 4, where a dedicated multibody model of the CFM mechanism is developed. Besides the similarity of the curves, a drop in the experimental curve with respect to the simulated curves can be appreciated in the initial section of the displacement. This may be indicative that the spring rest length introduced in the simulation (the theoretical one) does not fit the real one (see Fig. 4). In Fig. 10, the simulation has been repeated for $\mu_r = 0.002$, but a spring rest length of 136.5 mm (0.5 mm longer than the theoretical) has been used instead. In this way, the simulated curves of Fig. 10 follow a more similar pattern in the initial section.

In addition, the results of the simulations allow obtaining an indicative value of the rolling friction coefficient. In Fig. 9(a), the areas of the hysteresis loops in the section between 40 mm and 210 mm of the input displacement result in 0.233 Nm and 0.410 Nm for $\mu_r = 0.002$ and $\mu_r = 0.004$, respectively, and 0.259 Nm for the experimental measurement. In Fig. 10(a), for $\mu_r = 0.002$, the area is 0.232 Nm (almost the same as for Fig. 9(a)). These values indicate that, for this case, the real rolling friction coefficient will be slightly higher than 0.002. Once the value of the rolling friction coefficient has been identified, the cam profile could be designed

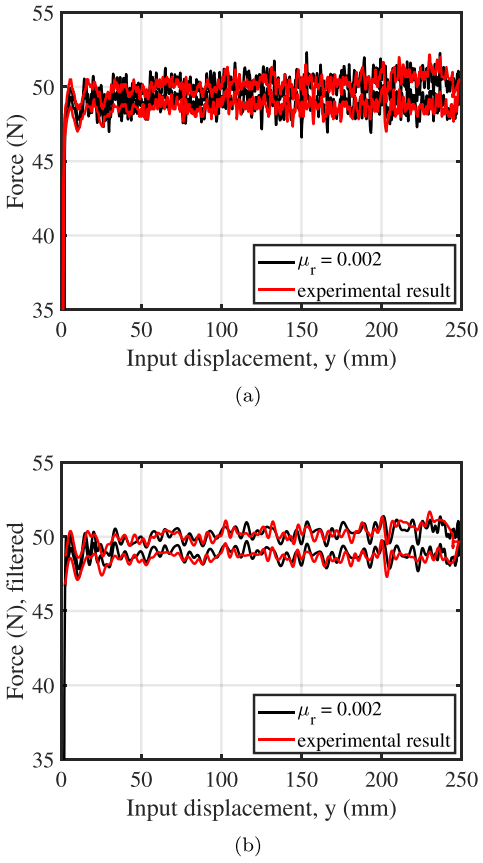

Fig. 10. Force curves from experimental result and from simulation with the measured cam profile, a spring rest length of 136.5 mm and a rolling friction coefficient of 0.002. (a) raw data and (b) filtered curves.

by including that value in Eq. (1). This allows maintaining a more accurate constant force curve in one of the directions of the displacement.

4. Multibody model of the CFM mechanism

The objective of this section is to develop a multibody model of the CFM that reproduces the experimental results presented before. Once the model is validated by comparison with the experimental results, it will be used to investigate the influence of inertial effects and manufacturing tolerances on the CFM performance.

In order to be able to study a wide range of manufacturing errors, the mathematical model of the CFM does not make use of symmetry. Instead, the two cam profiles of the CMF are modelled separately. The model comprises a total of five moving bodies which are described as follows (see Fig. 11). Body 2 is a slider that translates vertically when pulled up by the user. It is the input body of the mechanism. Both bodies 3 and 5 are connecting rods articulated to the slider and the two rollers, bodies 4 and 6, which are assumed to roll without slipping over the left and right cam surfaces. The assumption of no slipping is reasonable as long as the rollers have low inertia torques and low friction torques. They just follow the cam profile as the slider is pulled upwards.

Since the cam profile has a curved shape, the contact between the roller and the cam is implemented by using two non-generalized coordinates to locate the contact point of each roller. The vector of coordinates is as follows:

$$\boldsymbol{x} = \begin{pmatrix} s_2 & \theta_3 & \theta_4 & \xi_4 & y_4 & \theta_5 & \theta_6 & \xi_6 & y_6 \end{pmatrix}^{\mathrm{T}}, \tag{4}$$

where ξ_4 and y_4 are the non-generalized coordinates used to define the contact of roller 4 and the right cam profile, and ξ_6 and y_6 are the non-generalized coordinates used to define the contact of roller 6 and the left cam profile. This set of coordinates is

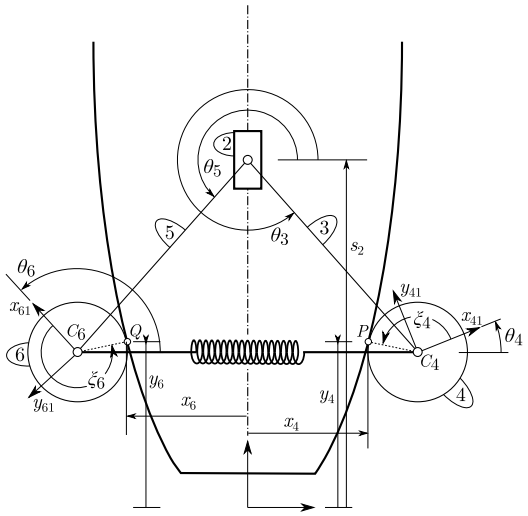

Fig. 11. Sketch of the mathematical model of the constant force mechanism.

constrained by eight constraints (six holonomic plus two velocity constraints). The holonomic constraints are as follows:

$$\boldsymbol{c}_h(\boldsymbol{x}) = \begin{pmatrix} \boldsymbol{r_2} + \boldsymbol{r_3} + \boldsymbol{C_4P} - \boldsymbol{r_1^P} \\ \boldsymbol{t_1^P} \cdot \boldsymbol{C_4P} \\ \boldsymbol{r_2} + \boldsymbol{r_5} + \boldsymbol{C_6Q} - \boldsymbol{r_1^Q} \\ \boldsymbol{t_1^Q} \cdot \boldsymbol{C_6Q} \end{pmatrix} = \boldsymbol{0}_{6\times 1}, \tag{5}$$

with

$$\boldsymbol{r_1^P} = \begin{pmatrix} x_4(y_4) & y_4 & 0 \end{pmatrix}^{\mathrm{T}}, \tag{6}$$

$$\boldsymbol{r_2} = \begin{pmatrix} 0 & s_2 & 0 \end{pmatrix}^{\mathrm{T}}, \tag{7}$$

$$\boldsymbol{r_3} = \begin{pmatrix} L_3\cos\theta_3 & L_3\sin\theta_3 & 0 \end{pmatrix}^{\mathrm{T}}, \tag{8}$$

$$\boldsymbol{C_4P} = \begin{pmatrix} R_4\cos\left(\theta_4+\xi_4\right) & R_4\sin\left(\theta_4+\xi_4\right) & 0 \end{pmatrix}^{\mathrm{T}}, \tag{9}$$

$$\boldsymbol{r_1^Q} = \begin{pmatrix} x_6(y_6) & y_6 & 0 \end{pmatrix}^{\mathrm{T}}, \tag{10}$$

$$\boldsymbol{r_5} = \begin{pmatrix} L_5\cos\theta_5 & L_5\sin\theta_5 & 0 \end{pmatrix}^{\mathrm{T}}, \tag{11}$$

$$\boldsymbol{C_6Q} = \begin{pmatrix} R_6\cos\left(\theta_6+\xi_6\right) & R_6\sin\left(\theta_6+\xi_6\right) & 0 \end{pmatrix}^{\mathrm{T}}, \tag{12}$$

where L_3 and L_5 are the lengths of the bodies 3 and 5, respectively, and R_4 and R_6 are the radii of the rollers 4 and 6. Moreover, $\boldsymbol{t_1^P}$ and $\boldsymbol{t_1^Q}$ are two vectors tangent to the right and left cam profiles at contact points P and Q, respectively. Note that $x_4(y_4)$ and $x_6(y_6)$ are expressed explicitly as functions of y_4 and y_6, respectively. Vectors $\boldsymbol{t_1^P}$ and $\boldsymbol{t_1^Q}$ are calculated from the known functions of the cam profiles, $x_4 = x_4(y_4)$ and $x_6 = x_6(y_6)$, as follows:

$$\boldsymbol{t_1^P} = \frac{\mathrm{d}\boldsymbol{r_1^P}}{\mathrm{d}y_4} = \begin{pmatrix} \dfrac{\mathrm{d}x_4\left(y_4\right)}{\mathrm{d}y_4} & 1 & 0 \end{pmatrix}^{T}, \tag{13}$$

$$\boldsymbol{t_1^Q} = \frac{\mathrm{d}\boldsymbol{r_1^Q}}{\mathrm{d}y_6} = \begin{pmatrix} \dfrac{\mathrm{d}x_6\left(y_6\right)}{\mathrm{d}y_6} & 1 & 0 \end{pmatrix}^{T}. \tag{14}$$

In addition, two velocity constraints expressing the rolling without slipping contacts are added as follows

$$\boldsymbol{c}_{nh}(\boldsymbol{x},\dot{\boldsymbol{x}}) = \begin{pmatrix} \boldsymbol{t_1^P} \cdot \left(\dot{\boldsymbol{r}}_4^{C4} + \boldsymbol{\omega_4} \times \boldsymbol{C_4P}\right) \\ \boldsymbol{t_1^Q} \cdot \left(\dot{\boldsymbol{r}}_6^{C6} + \boldsymbol{\omega_6} \times \boldsymbol{C_6Q}\right) \end{pmatrix} = \boldsymbol{0}_{2\times 1}, \tag{15}$$

where $\dot{\boldsymbol{r}}_4^{C4}$ and $\dot{\boldsymbol{r}}_6^{C6}$ are the absolute velocities of the rollers' centres. Note that the previous equations are linear in the velocities and they can be expressed as $\boldsymbol{c}_{nh}(\boldsymbol{x},\dot{\boldsymbol{x}}) = \boldsymbol{B}(\boldsymbol{x})\,\dot{\boldsymbol{x}}$, being $\boldsymbol{B}(\boldsymbol{x})$ a coordinate dependent 2×9 matrix.

In order to perform the simulations, the motion of the slider, Body 2, is prescribed through the introduction of the following rheonomic constraint:

$$c_{rh}(\boldsymbol{x},t) = s_2 - f(t), \tag{16}$$

being $f(t)$ defined by the following cycloidal displacement profile:

$$f(t) = s_2^0 + A\left(\frac{t}{T} - \frac{1}{2\pi}\sin\left(\frac{2\pi t}{T}\right)\right), \tag{17}$$

where s_2^0 is the vertical initial position of the slider, the parameter T is used to control the speed of the exercise and A is the vertical stroke of the slider. The cycloidal profile has been selected in order to start and end the elevation of the slider at zero velocity and zero acceleration. Observe that by adding the last rheonomic constraint, the kinematics and the dynamics of the mechanism can be solved as follows:

1. Find an admissible initial position coordinate vector, $\boldsymbol{x_0}$, by solving the six holonomic constraints as follows:

$$\boldsymbol{c}_h\left(\boldsymbol{x_0}\right) = \boldsymbol{0}_{6\times1} \quad \text{for} \quad \begin{matrix} s_2(0) = s_2^0 \\ \xi_4(0) = \pi \\ \xi_6(0) = 0 \end{matrix} \tag{18}$$

   where three out of nine coordinates can be prescribed.
2. Numerically integrate the following system of first order differential equations:

$$\dot{\boldsymbol{c}}_h(\boldsymbol{x}) + \beta \boldsymbol{c}_h(\boldsymbol{x}) = \boldsymbol{0}_{6\times1}, \tag{19}$$

$$\boldsymbol{B}(\boldsymbol{x})\,\dot{\boldsymbol{x}} = \boldsymbol{0}_{2\times1}, \tag{20}$$

$$\dot{c}_{rh}(\boldsymbol{x},t) + \beta c_{rh}(\boldsymbol{x},t) = 0_{1\times1}, \tag{21}$$

$$\boldsymbol{x}(0) = \boldsymbol{x_0}, \tag{22}$$

   where β is a positive parameter introduced to stabilize the holonomic and the rheonomic constraints during numerical integration according to Baumgarte's method [58]. Note that, in order to find a first order differential system, both the holonomic and the rheonomic constraints have been differentiated with respect to time. Therefore, if no means were taken to prevent the numerical drift due to the integration, the results could be completely useless. Introducing the holonomic constraints as in Eq. (19) and the rheonomic constraint as in Eq. (21), one may use a conventional numerical integrator avoiding constraint violations. As a result of this step, one finds the trajectories and velocities from initial time to time T.
3. Differentiate the holonomic and rhenomic constraints twice with respect to time and the velocity constraints once with respect to time to find a system of 9 equations in which the acceleration vector, $\ddot{\boldsymbol{x}}$, is the unknown as follows:

$$\frac{\partial \boldsymbol{c}_h(\boldsymbol{x})}{\partial \boldsymbol{x}}\ddot{\boldsymbol{x}} + \frac{\partial}{\partial \boldsymbol{x}}\left(\frac{\partial \boldsymbol{c}_h(\boldsymbol{x})}{\partial \boldsymbol{x}}\dot{\boldsymbol{x}}\right)\dot{\boldsymbol{x}} = \boldsymbol{0}_{6\times1}, \tag{23}$$

$$\boldsymbol{B}(\boldsymbol{x})\,\ddot{\boldsymbol{x}} + \frac{\partial}{\partial \boldsymbol{x}}\left(\boldsymbol{B}(\boldsymbol{x})\,\dot{\boldsymbol{x}}\right)\dot{\boldsymbol{x}} = \boldsymbol{0}_{2\times1}, \tag{24}$$

$$\frac{\partial \boldsymbol{c}_{rh}(\boldsymbol{x},t)}{\partial \boldsymbol{x}}\ddot{\boldsymbol{x}} + \frac{\partial}{\partial \boldsymbol{x}}\left(\frac{\partial \boldsymbol{c}_{rh}(\boldsymbol{x},t)}{\partial \boldsymbol{x}}\dot{\boldsymbol{x}}\right)\dot{\boldsymbol{x}} + 2\frac{\partial^2 \boldsymbol{c}_{rh}(\boldsymbol{x},t)}{\partial \boldsymbol{x}\partial t}\dot{\boldsymbol{x}} + \frac{\partial^2 \boldsymbol{c}_{rh}(\boldsymbol{x},t)}{\partial t^2} = \boldsymbol{0}_{1\times1}, \tag{25}$$

4. Knowing the positions, velocities and accelerations of the mechanism, use the equations of motion to find a set of 9 Lagrange multipliers as follows:

$$\boldsymbol{m}(\boldsymbol{x})\,\ddot{\boldsymbol{x}} + \boldsymbol{D}^T(\boldsymbol{x},t)\,\lambda = \boldsymbol{q}(\boldsymbol{x},\dot{\boldsymbol{x}}) \tag{26}$$

   where $\boldsymbol{m}(\boldsymbol{x})$ is the 9×9 system mass matrix, $\boldsymbol{q}(\boldsymbol{x},\dot{\boldsymbol{x}})$ is the 9×1 generalized applied force vector, which includes gravity forces, λ is the 9×1 Lagrange multipliers vector and $\boldsymbol{D}(\boldsymbol{x},t)$ is the 9×9 constraints' Jacobian, which is built as follows:

$$\boldsymbol{D}(\boldsymbol{x},t) = \begin{pmatrix} \dfrac{\partial \boldsymbol{c}_h(\boldsymbol{x})}{\partial \boldsymbol{x}} \\ \boldsymbol{B}(\boldsymbol{x}) \\ \dfrac{\partial \boldsymbol{c}_{rh}(\boldsymbol{x},t)}{\partial \boldsymbol{x}} \end{pmatrix}. \tag{27}$$

   Since the mechanism is kinematically driven, the Jacobian of the constraints is a full rank square matrix and the Lagrange multipliers are evaluated by inverse dynamics analysis at any time t as follows:

$$\lambda = \left(\boldsymbol{D}^T(\boldsymbol{x},t)\right)^{-1}\left(\boldsymbol{q}(\boldsymbol{x},\dot{\boldsymbol{x}}) - \boldsymbol{m}(\boldsymbol{x})\,\ddot{\boldsymbol{x}}\right). \tag{28}$$

   Finally, the external force required to move the slider, Body 2, according to Eq. (16) is found from the value of the ninth Lagrange multiplier with opposite sign.

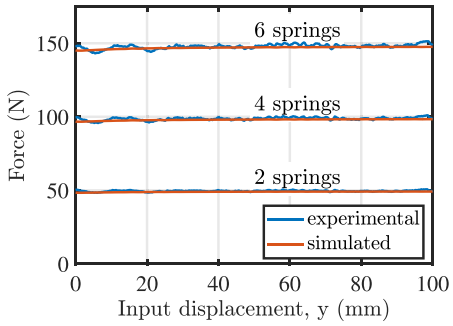

Fig. 12. Comparison of the simulated and experimental results.

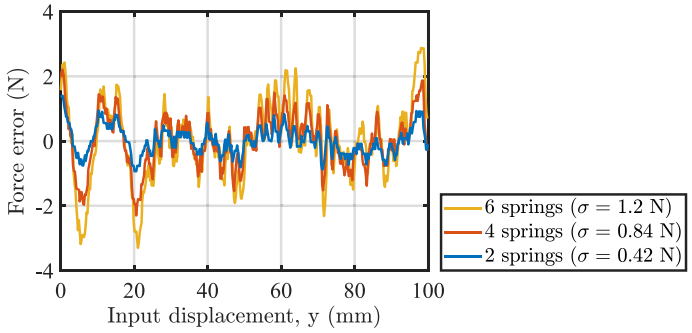

Fig. 13. Analysis of the error in the input force due to the manufacturing process.

Following the previous procedure, the performance of the CFM mechanism, whose design parameters were summarized in Table 1, has been simulated. The measured masses and moments of inertia of the different bodies are: $m_2 = 0.068$ kg, $m_3 = m_5 = 0.077$ kg, $m_4 = m_6 = 0.38$ kg, $I_{G3} = I_{G5} = 2.57 \cdot 10^{-4}$ kg m^2 and $I_{G4} = I_{G6} = 4.61 \cdot 10^{-6}$ kg m^2. In the simulation, the designed cam profile was utilized, which is obviously absent of manufacturing errors. Since the designed profile is obtained by following the numerical procedure described in Section 2.1, the derivatives of the cam profile need to be evaluated numerically, too. To that end, a second order finite difference formula has been used. The obtained derivatives have been low pass filtered to avoid oscillations due to numerical differentiation. The simulation has been conducted starting with a value of s_2^0 of 206.5 mm for a stroke of 100 mm. Eqs. (19)–(21) have been integrated using a conventional fourth order Runge–Kutta method.

The results of the simulations are compared with the experimental ones in Fig. 12. It can be observed that the numerical multibody model captures quite well the behaviour of the CFM mechanism for the three settings selected. The comparison shows a very good agreement in a large part of the simulated stroke. However, there are appreciable differences at the beginning of the stroke that are attributed to manufacturing errors. Such differences are studied and quantified next.

In order to assess the error induced in the input force by the machining process, the difference between the experimental input force and the simulated input force has been analysed and plot in Fig. 13. Note that the simulation is based on the designed cam profile, which was sent to the manufacturer. Therefore, such error force is attributed to deviations of the real cam profile from the designed one due to manufacturing. As shown in Fig. 13, the error increases with the stiffness of the springs set. The standard deviation of the error along the simulated stroke for each set of springs is included in the figure legend. In all cases the standard deviation is approximately 0.8% of the target load.

5. Sensitivity analysis

Once the multibody model has shown a good fit with the experimental results, it is used in this section to study the influence of some decisive design parameters of the CFM, as well as some possible manufacturing or assembly errors, following the previously described solution procedure. The first analysis carried out is aimed at studying the influence of the inertial forces on the force required for the slider to follow the cycloidal profile of Eq. (17), with $A = 100$ mm, starting at $s_2^0 = 220$ mm. The total time taken to elevate the slider, T, is varied from 0.125 s to 1 s, thus generating different acceleration peaks. The results are shown in Fig. 14, where it can be seen that the inertial effects become significant for small enough values of T. The results show that for the set of

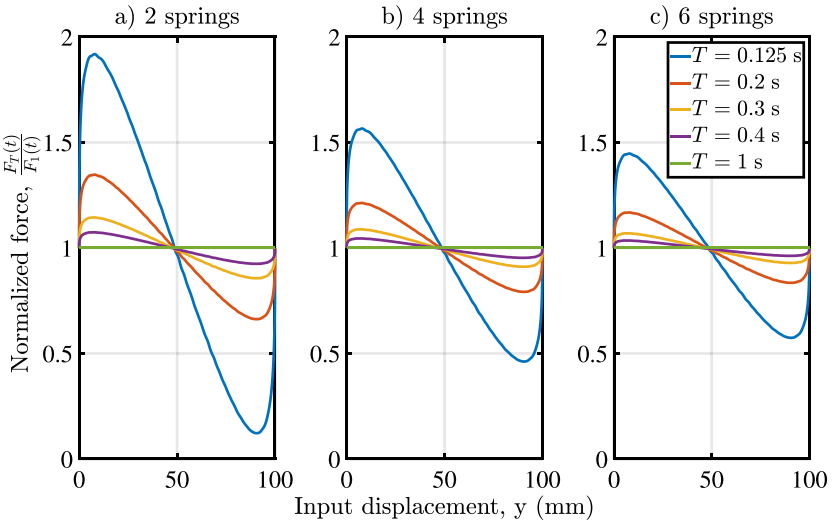

Fig. 14. Analysis of the inertial effect on the CFM response. The normalized force, $F_T(t)/F_1(t)$, is calculated by dividing the input force for an execution time T, $F_T(t)$, by the input force for an execution time of 1 s, $F_1(t)$, for which the inertial effect are negligible.

parameters studied, a reduction of the execution time, T, leads to significant variations of the input force required to perform the stroke following the cycloidal profile. Thus, reducing T from 1 s to 0.125 s results in peaks of the input force of 91.8%, 56.6% and 44.7% for the 2 springs, 4 springs and 6 springs sets, respectively. Remarkably, the influence of the inertial effects becomes less important as the design input force increases. As a mean of comparison, it may be considered that lifting an equivalent death weight following the same cycloidal profile results in peaks that are $\max[\ddot{s}_2(t)]/g$ times larger than the moved weight. This means an increase of 310% for $T = 0.125$ s. Therefore, while the CFM is sensitive to the inertial forces, it shows a more stable input force when compared to a pure weight lifting.

Using the cycloidal lifting profile, an execution time of 0.125 s during a stroke of 0.1 m results in a mean velocity of 0.8 m/s and a maximum velocity of 1.6 m/s, which are values close to those of a typical 60% of 1 RPM execution of bench press exercise according to the literature [59,60].

The CFM is designed for the slider to move along the symmetry axis of the cam. Nevertheless, deviations may occur during the mechanism actuation, as could occur in the case of cable actuation in bodybuilding machines. Therefore, it is interesting to study the influence of a deviation of the slider trajectory from its designed one. The calibrated CFM model has been used to simulate the values of the input force required to move the slider along a cycloidal profile with $A = 100$ mm, $s_2^0 = 212$ mm and $T = 10$ s for different values of the angle of deviation of the slider trajectory. To that end, the cam profiles have been rotated an angle α around the coordinate point (0,0). The results are shown in Fig. 15 for α values from 0° to 5°. Notice that the results are equal no matter the angle α is rotated clockwise or counter clockwise. It can be seen that the load increases significantly during a 100 mm stroke. This allows identifying the importance of caring about the inclination of the input force. The results show that the input load may increase as much as a 20% of the design input force for a deviation of 5°.

Finally, a possible manufacturing error is investigated. In this case, it will be assumed that the profile has been cut so that the cam profiles are rotated symmetrically an angle α around the coordinate point (0,0). This results in the horizontal width of the cam varying linearly from bottom to top with respect to the design profile. The calibrated CFM model has been used to simulate the values of the input force required to move the slider along a cycloidal profile with $A = 100$ mm, $s_2^0 = 220$ mm and $T = 10$ s for different values of the angle α. The results are shown in Fig. 16 for α values from −0.4° to 0.4°. It can be observed that the load varies during a 100 mm stroke. The results show that the input load may increase about an 8% of the design input force for a manufacturing error of 0.4°. According to this simulation, performing a high quality cut of the cam becomes highly important.

6. Summary and conclusions

The design of the constant-force mechanism manufactured has demonstrated good performance with respect to the primary feature of constant force. The design of the mechanism, based on springs and cams, allows achieving large strokes and a changeable force level. The main factors that affect the ideal constant force curve are the friction between the rolling elements and the manufacturing process. Frictional forces inevitably lead to hysteresis loops. In spite of this hysteresis, by identifying the value of the rolling friction coefficient, the cam profile could be designed for a more precise constant force in one of the displacement directions.

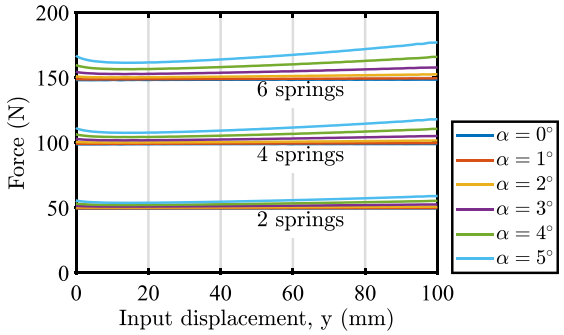

Fig. 15. Analysis of the influence of the slider misalignment on the CFM response.

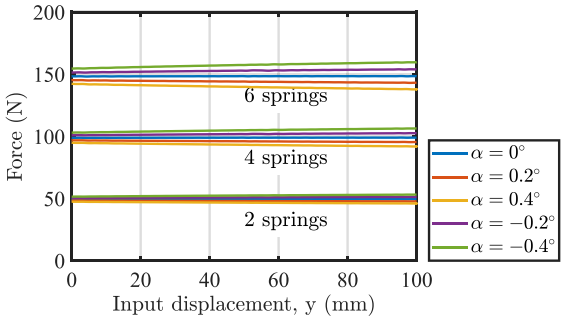

Fig. 16. Analysis of an angular manufacturing defect on the CFM response.

Surface irregularities in the cam surface due to the laser cutting manufacturing process cause noise in the force curve. However, if required, these irregularities could be avoided with more precise manufacturing by CNC milling. Some fluctuations in the force curve, that are present in the experimental results but are absent in the multibody simulation following the design cam profile, could be identified to being caused by an imprecise manufacture of the cam profile.

An ad-hoc multibody model of the CFM has been developed and validated against the experimental results presented in this paper. Thus, by using the multibody model of the CFM, relevant conclusions could be drawn on the influence of the inertial effects, a typical execution error and a possible manufacturing error. In this way, it could be concluded that, by reducing the execution time, T, significant variations of the input force required to perform the stroke following the cycloidal profile may arise. Nevertheless, the analysed CFM shows a much less sensitive behaviour than the pure weight lifting. Therefore, it is an excellent candidate to design training or rehabilitating exercise machines where the resistant force should be as constant as possible.

The simulations also revealed a significant influence of possible manufacturing errors as a linear deviation of the cam profiles. Therefore, controlling the quality of the cam profile becomes highly important. In addition, the simulation showed that significant variations of the input force may arise as a consequence of a deviation in the slider trajectory. Therefore, the importance of caring about the inclination of the input force during the mechanism stroke is clearly identified.

Finally, the multibody model will be useful in the design of future CFMs. Thus, the design and fabrication of a full-scale CFM to be incorporated into a body-building machine is planned for the future.

Declaration of competing interest

The authors declare that they have no known competing financial interests or personal relationships that could have appeared to influence the work reported in this paper.

Acknowledgements

This work has been partially funded by the “Programa Operativo FEDER, Spain 2014–2020” and the Andalusian “Consejería de Transformación Económica, Industria, Conocimiento y Universidades, Spain” under the project UAL2020-CTS-A2100, and supported by Grant FPU18/05598 of the Spanish Ministry of Science, Innovation and Universities.

References

[1] P. Wang, Q. Xu, Design and modeling of constant-force mechanisms: A survey, Mech. Mach. Theory 119 (2018) 1–21, http://dx.doi.org/10.1016/j.mechmachtheory.2017.08.017.
[2] L. Howell, Compliant Mechanisms, John Wiley Sons, New York, 2001.
[3] J. Gallego, J. Herder, Classification for literature on compliant mechanisms: A design methodology based approach, in: Proceedings of the ASME International Design Engineering Technical Conferences and Computers and Information in Engineering Conference 2009, DETC2009, Vol. 7 PART A, 2010, pp. 289–297.
[4] Y. Tian, C. Zhou, F. Wang, K. Lu, D. Zhang, A novel compliant mechanism based system to calibrate spring constant of AFM cantilevers, Sensors Actuators A 309 (2020) 112027.
[5] K. Tolman, E. Merriam, L. Howell, Compliant constant-force linear-motion mechanism, Mech. Mach. Theory 106 (2016) 68–79.
[6] J. Meaders, C. Mattson, Optimization of near-constant force springs subject to mating uncertainty, Struct. Multidiscip. Optim. 41 (1) (2010) 1–15.
[7] H. Prakashah, H. Zhou, Synthesis of constant torque compliant mechanisms, J. Mech. Robot. 8 (6) (2016).
[8] C.-H. Liu, F.-M. Chung, Y.-P. Ho, Topology optimization for design of a 3D-printed constant-force compliant finger, IEEE/ASME Trans. Mechatronics (2021).
[9] B. Ding, X. Li, Y. Li, FEA-based optimization and experimental verification of a typical flexure-based constant force module, Sensors Actuators A 332 (2021) 113083.
[10] A. Lamers, J. Gallego Sánchez, J. Herder, Design of a statically balanced fully compliant grasper, Mech. Mach. Theory 92 (2015) 230–239.
[11] C. Boyle, L. Howell, S. Magleby, M. Evans, Dynamic modeling of compliant constant-force compression mechanisms, Mech. Mach. Theory 38 (12) (2003) 1469–1487.
[12] P. Bilancia, G. Berselli, Design and testing of a monolithic compliant constant force mechanism, Smart Mater. Struct. 29 (4) (2020) 044001.
[13] Y. Tian, C. Zhou, F. Wang, K. Lu, Y. Yuan, M. Yang, D. Zhang, Design of a flexure-based mechanism possessing low stiffness and constant force, Rev. Sci. Instrum. 90 (10) (2019) 105005.
[14] Y. Liu, D.-P. Yu, J. Yao, Design of an adjustable cam based constant force mechanism, Mech. Mach. Theory 103 (2016) 85–97.
[15] M. Li, W. Cheng, Design and experimental validation of a large-displacement constant-force mechanism, J. Mech. Robot. 10 (5) (2018) 051007.
[16] I. Gandhi, H. Zhou, Synthesizing constant torque compliant mechanisms using precompressed beams, J. Mech. Des. 141 (1) (2019) 014501.
[17] H.-T. Pham, D.-A. Wang, A constant-force bistable mechanism for force regulation and overload protection, Mech. Mach. Theory 46 (7) (2011) 899–909.
[18] P. Wang, Q. Xu, Design of a flexure-based constant-force XY precision positioning stage, Mech. Mach. Theory 108 (2017) 1–13.
[19] T. Ye, J. Ling, X. Kang, Z. Feng, X. Xiao, A novel two-stage constant force compliant microgripper, J. Mech. Des. 143 (5) (2021) 053302.
[20] Y.-L. Kuo, C.-C. Lan, A two-dimensional adjustable constant-force mechanism, J. Mech. Des. 142 (6) (2020).
[21] Y. Liu, Y. Zhang, Q. Xu, Design and control of a novel compliant constant-force gripper based on buckled fixed-guided beams, IEEE/ASME Trans. Mechatronics 22 (1) (2017) 476–486.
[22] X. Liu, X. Huang, H. Hua, On the characteristics of a quasi-zero stiffness isolator using Euler buckled beam as negative stiffness corrector, J. Sound Vib. 332 (14) (2013) 3359–3376.
[23] F. Ma, G. Chen, H. Wang, Large-stroke constant-force mechanisms utilizing second buckling mode of flexible beams: Evaluation metrics and design approach, J. Mech. Des. 142 (10) (2020) 103303.
[24] J. López-Martínez, D. García-Vallejo, F. Arrabal-Campos, J. García-Manrique, Design of three new cam-based constant-force mechanisms, Trans. ASME, J. Mech. Des. 140 (8) (2018) http://dx.doi.org/10.1115/1.4040174.
[25] M. Li, W. Cheng, R. Xie, Design and experimental validation of a cam-based constant-force compression mechanism with friction considered, Proc. Inst. Mech. Eng. C 233 (11) (2019) 3873–3887.
[26] R. Nathan, A constant force generation mechanism, Trans. ASME, J. Mech. Des. 107 (4) (1985) 508–512, http://dx.doi.org/10.1115/1.3260755.
[27] Z.-W. Yang, C.-C. Lan, An adjustable gravity-balancing mechanism using planar extension and compression springs, Mech. Mach. Theory 92 (2015) 314–329.
[28] G. Endo, H. Yamada, A. Yajima, M. Ogata, S. Hirose, A passive weight compensation mechanism with a non-circular pulley and a spring, in: Proceedings - IEEE International Conference on Robotics and Automation, 2010, pp. 3843–3848.
[29] M. French, M. Widden, The spring-and-lever balancing mechanism, George Carwardine and the Anglepoise lamp, Proc. Inst. Mech. Eng. C 214 (3) (2000) 501–508.
[30] E. Starostin, Calculating a cam profile for a constant-force mechanism, Sov. Mach. Sci. (4) (1987) 69–76.
[31] E. Duval, Dual pulley constant force mechanism, 2010, US Patent 7,677,540.
[32] G. Keung, C. Chen, Novel design of an adjustable constant force mechanism based on cam and spring, in: IFToMM World Congress on Mechanism and Machine Science, Springer, 2019, pp. 1481–1490.
[33] Q. Xie, S. Liu, H. Jiang, Design of a passive constant-force mechanism based on a five-bar mechanism, Mech. Mach. Theory 143 (2020) 103662.
[34] A. Schepelmann, K. Geberth, H. Geyer, Compact nonlinear springs with user defined torque-deflection profiles for series elastic actuators, in: Proceedings - IEEE International Conference on Robotics and Automation, 2014, pp. 3411–3416.
[35] N. Schmit, M. Okada, Synthesis of a non-circular cable spool to realize a nonlinear rotational spring, in: IEEE International Conference on Intelligent Robots and Systems, 2011, pp. 762–767.
[36] H. Bidgoly, M. Ahmadabadi, M. Zakerzadeh, Design and modeling of a compact rotational nonlinear spring, in: IEEE International Conference on Intelligent Robots and Systems, 2016-November, 2016, pp. 4356–4361.
[37] Y.-H. Chen, C.-C. Lan, An adjustable constant-force mechanism for adaptive end-effector operations, Trans. ASME, J. Mech. Des. 134 (3) (2012).
[38] J.-Y. Wang, C.-C. Lan, A constant-force compliant gripper for handling objects of various sizes, Trans. ASME, J. Mech. Des. 136 (7) (2014) http://dx.doi.org/10.1115/1.4027285.
[39] C.-C. Lan, J.-Y. Wang, Design of adjustable constant-force forceps for robot-assisted surgical manipulation, in: Proceedings - IEEE International Conference on Robotics and Automation, 2011, pp. 386–391.
[40] W.W. Van De Sande, A. Ali, G. Radaelli, Design and evaluation of a passive constant force mechanism for a cardiac ablation catheter, J. Med. Dev. 15 (2) (2021) 021003.
[41] X. Zhang, Q. Xu, Design and analysis of a 2-DOF compliant gripper with constant-force flexure mechanism, J. Micro-Bio Robot. 15 (1) (2019) 31–42.
[42] Y. Liu, Z. Li, S. Bai, Design of a reconfigurable novel constant-force mechanism for assistive exoskeletons, in: IFToMM Symposium on Mechanism Design for Robotics, Springer, 2021, pp. 122–131.
[43] B. Ding, J. Zhao, Y. Li, Design of a spatial constant-force end-effector for polishing/deburring operations, Int. J. Adv. Manuf. Technol. 116 (11) (2021) 3507–3515.
[44] P. Wang, Q. Xu, Design and testing of a flexure-based constant-force stage for biological cell micromanipulation, IEEE Trans. Autom. Sci. Eng. (2017) http://dx.doi.org/10.1109/TASE.2017.2733553.
[45] S. Sanchez-Salinas, C. Nunez-Torres, J. Lopez-Martinez, D. Garcia-Vallejo, J.M. Muyor, Design and analysis of a constant-force bench press, Mech. Mach. Theory 142 (2019) 103612.
[46] L. Howell, S. Magleby, Substantially constant-force exercise machine, 2006, US Patent 7,060,012.
[47] D. Smith, Resistive exercise device, 2005, National Aeronautics and Space Administration (NASA), Washington, DC, US Patent 6,958,032.

[48] Y.-H. Chen, C.-C. Lan, Design of a constant-force snap-fit mechanism for minimal mating uncertainty, Mech. Mach. Theory 55 (2012) 34–50.
[49] Z. Li-Jun, L. Tao, S. Bao-Yu, Optimum design of automobile diaphragm spring clutch, in: 2008 IEEE Vehicle Power and Propulsion Conference, VPPC 2008, 2008, pp. 1–4.
[50] B. Weight, C. Mattson, S. Magleby, L. Howell, Configuration selection, modeling, and preliminary testing in support of constant force electrical connectors, Trans. ASME, J. Electron. Packag. 129 (3) (2007) 236–246.
[51] A. Cardona, E. Lens, N. Nigro, Optimal design of cams, Multibody Syst. Dyn. 7 (3) (2002) 285–305, http://dx.doi.org/10.1023/A:1015278213069.
[52] T. Ouyang, P. Wang, H. Huang, N. Zhang, N. Chen, Mathematical modeling and optimization of cam mechanism in delivery system of an offset press, Mech. Mach. Theory 110 (2017) 100–114, http://dx.doi.org/10.1016/j.mechmachtheory.2017.01.004.
[53] L. Xu, A method for modelling contact between circular and non-circular shapes with variable radii of curvature and its application in planar mechanical systems, Multibody Syst. Dyn. 39 (3) (2017) 153–174, http://dx.doi.org/10.1007/s11044-016-9549-0.
[54] A. Borboni, F. Aggogeri, I. Elamvazuthi, G. Incerti, P. Magnani, Effects of profile interpolation in cam mechanisms, Mech. Mach. Theory 144 (2020) http://dx.doi.org/10.1016/j.mechmachtheory.2019.103652.
[55] P. Danakas, M. Bilodeau, N. Quaegebeur, Cam-follower mechanism for airborne ultrasound generation, Appl. Acoust. 182 (2021) http://dx.doi.org/10.1016/j.apacoust.2021.108225.
[56] R. Rayner, M. Sahinkaya, B. Hicks, Improving the design of high speed mechanisms through multi-level kinematic synthesis, dynamic optimization and velocity profiling, Mech. Mach. Theory 118 (2017) 100–114, http://dx.doi.org/10.1016/j.mechmachtheory.2017.07.022.
[57] P. Bergström, O. Edlund, Robust registration of point sets using iteratively reweighted least squares, Comput. Optim. Appl. 58 (3) (2014) 543–561, http://dx.doi.org/10.1007/s10589-014-9643-2.
[58] J. Baumgarte, Stabilization of constraints and integrals of motion in dynamical systems, Comput. Methods Appl. Mech. Engrg. 1 (1) (1972) 1–16, http://dx.doi.org/10.1016/0045-7825(72)90018-7.
[59] D.M. Frost, J.B. Cronin, R.U. Newton, A comparison of the kinematics, kinetics and muscle activity between pneumatic and free weight resistance, Eur. J. Appl. Physiol. 104 (6) (2008) 937–956.
[60] S. Orange, J. Metcalfe, A. Liefeith, P. Marshall, L. Madden, C. Fewster, R. Vince, Validity and reliability of a wearable inertial sensor to measure velocity and power in the back squat and bench press, J. Strength Cond. Res. 33 (9) (2019) 2398–2408, http://dx.doi.org/10.1519/JSC.0000000000002574.

Capítulo 3

Diseño y análisis de un press de banca de fuerza constante

Mechanism and Machine Theory 142 (2019) 103612

Contents lists available at ScienceDirect

Mechanism and Machine Theory

journal homepage: www.elsevier.com/locate/mechmachtheory

Research paper

Design and analysis of a constant-force bench press

Silvia Sánchez-Salinas[a], Celia Núñez-Torres[a], Javier López-Martínez[a,d,*], Daniel García-Vallejo[b], José M. Muyor[c]

[a] Department of Engineering, University of Almería, Spain
[b] Department of Mechanical Engineering and Manufacturing, Universidad de Sevilla, Spain
[c] Laboratory of Kinesiology, Biomechanics and Ergonomics (KIBIOMER Lab.), Research Central Services, Health Research Centre, University of Almería, Spain
[d] CITE-IIA, Department of Engineering, University of Almería, Almería 04120, Spain

ARTICLE INFO

Article history:
Received 19 July 2019
Revised 4 September 2019
Accepted 5 September 2019

Keywords:
Bench press
Constant-force mechanism
Strength training

ABSTRACT

In strength or resistance training, the patterns of movement of the load and the muscle activation can be adapted to the training objective according to the muscle conditioning machine selected. Traditionally, free-weight bench press is extensively used for athlete training. One of the main features of such kind of machine is the significant influence of the inertial forces in the muscle forces that the athlete has to develop. In this paper, a bench press which is able to maintain an almost constant force resistance is proposed. Then, the proposed constant-force bench press is compared to the traditional free-weight resistance bench press. Experimental data measured in a test session with free-weight resistance are used as an input for a mathematical model of the bench press that allows estimating three meaningful variables of the exercise performance: the shoulder vertical force, the net joint moment at the shoulder and the muscular power. These results are compared with those obtained by assuming a constant-force resistance, finding significant differences between both resistance systems. Constant-force resistance results in a less fluctuating force curve, lower peaks of the joint moment and muscular power, and small variance between different exercise repetitions.

1. Introduction

Strength training also known as resistance training is commonly used to increase muscular strength [1], enhancing muscular power, hypertrophy, and endurance [2] or gaining a particular edge in his or her sport [3].

Following to Frost et al. [4] dynamic strength training can be classified in three different categories that are based on the nature by which the resistance is applied to the muscle: (1) constant, isoinertial or free-weight resistance that is characterized by exercises in which the entire resistant force is dependent on the mass of the object being lifted; (2) accommodating resistance that allows for the development of maximal tension during all range of movement (ROM) in each repetition. In this method, chains are either added on a free-weight bar and combined with traditional plates or added to the bar as the entire load; and (3) variable resistance which increases or decreases the resistant force depending on the ROM.

Currently, constant resistance is the most widely used method to enhance strength and power capacity for sport [4]. However, when training with constant resistance, maximal effort (force) is required at the beginning of the concentric lifting

* Corresponding author at: CITE-IIA, Department of Engineering, University of Almería, Almería 04120, Spain.
E-mail address: javier.lopez@ual.es (J. López-Martínez).

https://doi.org/10.1016/j.mechmachtheory.2019.103612
0094-114X/

phase, decreasing neuromuscular stress throughout the concentric phase [5]. In this sense, several studies have analysed and compared kinematics, kinetics and muscle activation between constant and variable resistances [5–11]. Other studies have evaluated the effectiveness of accommodation and constant resistance training [12–17]. Although the results of these studies sometimes are contradictory, the majority of these studies concluded that the loading motion patterns and the muscle activations could be modified according to the kind of resistance (constant, accommodating or variable) and it is necessary to choose the exercises depending on the training objective.

However, to the best of our knowledge, no study has analysed a constant resistance from the point of view of a device which allows a constant force throughout the concentric and eccentric phases. So, in concordance with Frost et al. [4] an increased understanding of the biomechanical properties that govern each resistance type, and/or how they can be manipulated, will provide the researcher, clinician and practitioner with a much greater appreciation of the benefits and limitations associated with each resistance-training mode.

During isoinertial lifting, the mass is accelerated from zero velocity at the start to a maximum velocity with zero acceleration at an intermediate time. After the lift, a deceleration phase occurs to return to zero velocity at the end of the concentric phase. The deceleration phase may be significant for light or medium masses and increases its importance with the execution velocity of the exercise. In such a situation, the athlete must apply force opposing the motion when the mass must be decelerated to rest. In this way, the concentric portion of a lifting exercise can be subdivided into a propulsive and a braking phase [18]. Sanchez-Medina et al. [19] analysed the contribution of the propulsive and braking phases in the concentric bench press exercise, highlighting the importance of considering both phases in isoinertial strength and power evaluations. Additionally, a large deceleration phase results in a lower activity of the agonist and synergist musculature [20].

Focusing on the bench press exercise, Frost et al. [21] compared the bench press exercise in three testing sessions: free weight, ballistic movement, and using a pneumatic resistance machine. The last one is based on an air compressor and a pneumatic cylinder which in combination with a mechanical linkage, produces a variable resistance force curve [22]. The measured velocity, force and power curves in each session showed significant differences between the three different resistance sources. Since the pneumatic resistance has low inertia forces, results demonstrated considerably less variation in the force curves compared with the free weight and ballistic sessions. As result, pneumatic resistance may offer specific advantages over free weight and ballistic, showing higher force, power and muscle activity during the last 10–20% of the concentric phase [21]. Peltonen et al. [23] compared the neuromuscular response between pneumatic and weight stack devices. Since each device has different properties, they recommend to specifically chose one or another according to the given training goal. Furthermore, Avrillon et al. [24] studied the combination of isoinertial and pneumatic resistances during ballistic movements in bench press.

This work aims at designing a novel bench press that uses a previously designed constant force mechanism. The interest in such a new bench press is justified by the simulated results analyzed in this document on a set of realistic realizations of the bench press exercise in both isoinertial and constant force conditions. Constant-force mechanisms (CFMs) are designed to maintain a nearly constant force along a prescribed range of the mechanism displacement. Different proposals for CFMs can be found in recent literature, showing that attention to this kind of mechanism is gaining interest and the number of applications is increasing. Two main approaches have been used to achieve a constant force characteristic [25]. One approach is based on the use of compliant mechanisms [26], which includes flexible members with particular shapes or configurations to obtain a nearly constant force curve in a certain displacement range [27–30]. Such compliant constant-force mechanisms are mainly used in applications that require small displacements and are implemented in small size components, and therefore its application in strength or resistance training could be limited. In the second approach, one or several springs are used together with a nonlinear transmission to achieve a constant force response. Some designs include a spring with one end hinged to a fixed point and the other attached to a traction cable which is wounded around a noncircular pulley [31]. In other cases, one or both of the spring ends are attached to rollers that can rotate over the surface of a cam [32–35]. In addition, kinematic singularities existing in rigid-body linkages are applied to design mechanisms with zero-stiffness behaviour [36]. Following the last approach, CFMs can be designed for large displacements and for adjustable forces.

Constant-force mechanisms have been used in gravitational force static balancing mechanisms to reduce the total mass and the actuator efforts [28,37], in Robotics to minimize the need for force control schemes in object manipulation [38] or in the interaction with unknown environments [39], in the design of graspers for minimal invasive surgery [40], in biological cell micromanipulation [41], in overload protection devices [42], in snap-fit connectors [43], in grippers and micro grippers [44,45], and in exercise machines among other applications.

In the context of exercise or bodybuilding machines, some patents including constant-force mechanisms as resistance unit can be found. In particular, U.S. Patents No. 2005/0181915 [46] and No. 6685602 [47] are based on the use of multiple parallel negator springs. The National Aeronautics and Space Administration (NASA) registered a resistant exercise device based on springs and cams aiming at being used in low gravity environments [48]. U.S. Patent No. 4231568 [49] uses a spring-cam arrangement which equalizes the force required throughout the exercise stroke. Furthermore, U.S. Patent No. 9358420 [50] is based on the use of a gas spring and a nonlinear transmission. Other patented solutions intended to get constant force exercise devices are based on vacuum cylinders [51] or on pneumatic systems [22,52]. Despite the mentioned patents, to the authors knowledge there is no other commercial machine or prototype based on constant-force mechanisms in the literature.

Apart from their reduced use in low gravity environments, constant-force exercise machines are an interesting alternative to the usual free weight resistance machines. In fact, as mentioned above, the inertia forces of the moving masses in free weight machines make the input force exerted by the user to be variable and highly dependent on the accelerations of the masses. Therefore, the faster the exercise is realized, the larger the fluctuations of the accelerations and input force are. The objective of a constant-force machine is to maintain the constancy of the resistant force throughout the exercise range of movement.

This work proposes a new constant-force exercise machine based on a previous CFM concept presented by the authors [34]. In particular, the aims of the present work are as follow:

(i) To design a bench press with constant-force resistance and, additionally, manufacture and experimentally validate a prototype of the constant-force mechanism used as resistance source of the bench press. This constant-force mechanism is the first prototype of the CFM-2 concept reported by the authors in Ref. [34].
(ii) To develop a mathematical model of the bench press exercise that allows to estimate the forces at the shoulder and wrist of the user, the net moment of the shoulder muscles and the muscular power.
(iii) To compare the response of the constant-force bench press versus a common free-weight one in terms of the resulting forces, the net moment of the shoulder and muscular power, and for two different velocities of execution of the exercise.

This paper is organized as follows: Section 2 presents the design principles as well as the main components of the bench press and the validation of the constant-force mechanism proposed. Section 3 deals with the mathematical model developed for analysing the performance of the proposed bench press in different scenarios. Section 4 discusses the numerical and experimental results obtained by using the mathematical model of the bench press. Finally, some conclusions are drawn in Section 5.

2. Design of the constant-force bench press

One of the most used exercises for upper-body resistance training is the bench press [53], in both athletes and recreational trainers [54]. This section describes the design of a novel bench press that includes a constant-force mechanism as resistance system. Based on the same working principle of the CFM-2 presented by López-Marínez et al. [34], the design of this CFM is adapted for its application to a guided bench press (Smith machine). This CFM solution has been selected among other existing designs due to the performance requirements of the bench press. Together with its low inertia, its greater amplitude of displacement and the ease of load change have been the main reasons for its choice. Finally, for the experimental validation of the CFM, a first prototype is manufactured and tested.

2.1. Working principle of the constant-force mechanism

The constant-force mechanism comprises a symmetric cam, two rollers and a spring that joins both rollers axes (Fig. 1). The rollers are able to roll along the cam surface by the action of an external force *F*. This pulling force is ejected in the

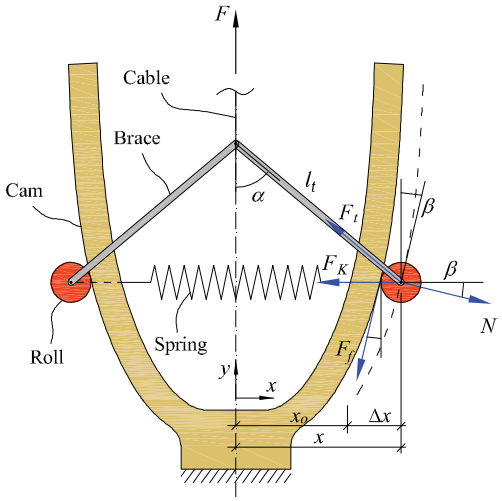

Fig. 1. Conceptual design of the CFM and forces diagram for one roller.

plane of symmetry of the mechanism and transmitted to the rollers through the braces. The value of the force F depends on the cam profile and the spring stiffness coefficient. In this way, it is able to derive a certain cam profile to achieve a constant value of the pulling force along the displacement of the mechanism. The cam profile that meets a constant force value of the mechanism can be derived from the force equilibrium equations of one of the two rollers, since the mechanism is symmetric. Fig. 1 shows the forces acting on the right roller, where N is the normal force at the contact surface with the cam, F_t is the brace tension force, F_K is the spring restitution force and F_f is the friction force between the roller and the cam. The equilibrium equations in the horizontal and vertical directions are written as follows:

$$F_K + F_t \sin\alpha + F_f \sin\beta = N\cos\beta, \tag{1}$$

$$N\sin\beta + F_f \cos\beta = F_t \cos\alpha. \tag{2}$$

where β is the slope of the cam profile and α is the angle between the brace and the direction of force F. Due to the small values of the masses of the braces and the roller, inertial forces are neglected [34] and, therefore, are not included in Eqs. (1) and (2). Assuming a constant value of the coefficient of rolling friction μ_r and a linear spring with stiffness coefficient K, the rolling friction and spring forces can be written as:

$$F_f = \mu_r N. \tag{3}$$

$$F_K = 2\ K\Delta x, \tag{4}$$

where $2\Delta x$ is the elongation of the spring. Finally, using Eqs. (1)–(4) and knowing that the force F is related with the brace force F_t as

$$F = 2F_t \cos\alpha, \tag{5}$$

the pulling force F can be written as

$$F = 4\ \underbrace{K\,\Delta x\left(\frac{1-\mu_r\tan\beta}{\tan\beta+\mu_r} - \tan\alpha\right)^{-1}}_{A}. \tag{6}$$

This equation shows that force F will remain constant for any cam profile that verifies that the term A is constant. Conceptually, as the spring extends when the rollers move up and the normal force N increases, the slope of the cam profile must decrease in order to keep constant the vertical component of the brace force F_t. According to Eq. (6), given a spring stiffness coefficient K and a target value of he force F, one can derive the required cam profile. In a similar way, given a cam profile that verifies that the term A is constant, the value of the pulling force F can be modified by changing the spring stiffness.

The friction force drawn in Fig. 1 occurs in an upward movement of the rollers. In the case of moving the rollers downwards, the friction force changes its direction and Eq. (6) is no longer valid. Instead, the signs preceding the appearances of coefficient of rolling friction change as follows:

$$F = 4\ K\Delta x\left(\frac{1+\mu_r\tan\beta}{\tan\beta-\mu_r} - \tan\alpha\right)^{-1}. \tag{7}$$

Therefore, for a given coefficient of rolling friction, it is not possible to guarantee at the same time a perfectly constant force in both directions of displacement. In an intermediate setting, the cam profile can be designed for a null coefficient of rolling friction. This neutral cam profile is derived from any of Eqs. (6) or (7) for $\mu_r = 0$.

A more detailed description about this CFM, the mathematical procedure to obtain the profile of the cam, and the influence of design parameters in the performance of the mechanism can be found in Ref. [34].

2.2. Constant-force bench press

As an application of the CFM in bodybuilding machines, the bench press has been selected, which is one of the most common exercises. In particular, the CFM has been adapted to be used as resistance system in a Smith-type machine, in which the guided barbell facilitates the use of the CFM. In general, the CFM can be adapted to any other bodybuilding machine that comprises guided weights as loading system.

From the CFM design, the main challenges in adapting it to bodybuilding machines are the large displacement required and the wide number of load values usually required. In the CFM, the displacement is limited for the maximum allowable elongation of the spring. In addition, the cam slope (the value of β in Fig. 1) should be as high as possible to reduce the effect of the rolling friction [34]. This leads to the use of soft springs together with wide cams, i.e. large values of angle β.

In the design of the resistance system (the CFM) for the proposed constant-force bench press the following two main requirements have been specified: (i) a minimum barbell displacement of 0.7 m and (ii) resistance capacity up to 140 kp at intervals of 5 kp. Additionally, the components design and selection have been made to minimize the moving masses of the mechanism, and therefore to reduce the influence of the inertial forces, as well as to reduce the friction forces in the

(a)

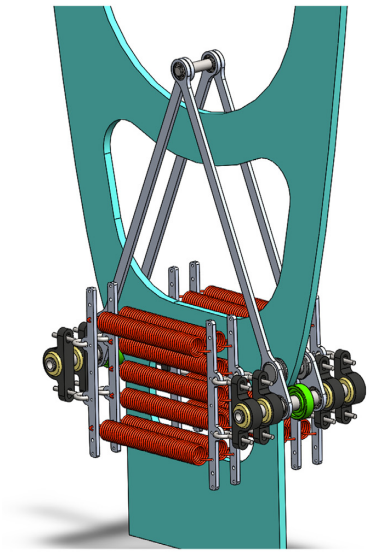

(b)

Fig. 2. (a) The constant-force bench press and (b) detail of the resistance system based in a CFM.

contact between the rollers and the cam. Although commercial Smith machines may work with higher resistance capacity and greater bar displacement, it should be noted that the proposed constant-resistance bench press is primarily oriented to this research work and therefore the above design requirements are considered suitable for its evaluation in future studies with subjects.

Fig. 2 shows the 3D CAD model of the constant-resistance bench press, which includes one CFM attached to each of the two ends of the barbell. Each CFM has a stroke of 0.7 m, which allows the same displacement of the barbell. It can be mounted up to 28 springs in pairs to maintain the stability of the roller axle (one on each side of the roller), where each

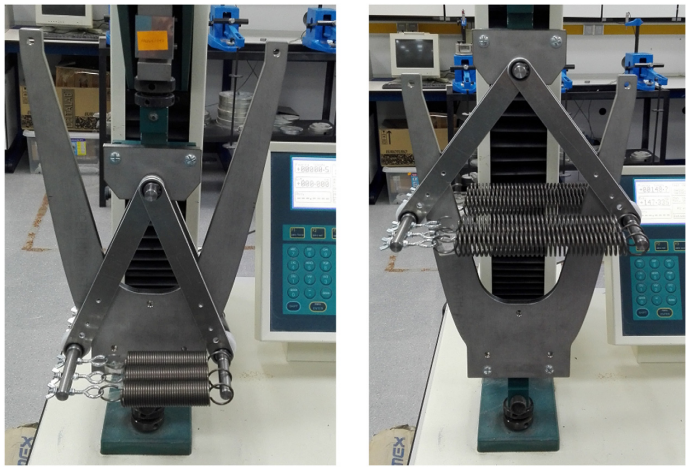

(a) (b)

Fig. 3. Two positions of the prototype with 6 springs during the force tests: (a) initial position and (b) intermediate position.

Table 1
Values of the measured force curves (Fig. 4).

Theoretical force (N)	49.1	98.1	147
Displacement	up/down	up/down	up/down
Mean force (N)	49.67/48.27	98.94/96.62	148.27/144.17
Force variance	0.18/0.18	0.90/1.05	1.91/4.48
Max. force (N)	51.00/49.33	101.0/99.00	151.33/148.00
Min. force (N)	48.00/46.33	95.33/92.17	143.17/136.00

pair of springs increases the resistance force by 5 kp, with a maximum resistance of 70 kp when all the spring are mounted. Since there is one CFM at each barbell end, the bench press has a maximum resistance of 140 kp.

2.3. Validation of the constant-force mechanism

Prior to the fabrication of a complete constant-force bench press, a prototype of the CFM has been elaborated and experimentally validated. The CFM prototype, mounted in a testing machine, is showed in Fig. 3. The prototype has been designed for a maximum displacement of 250 mm and for a constant force value of 5 kp (49.1 N) when two springs of 0.69 N/mm stiffness constant are arranged in parallel (one at each side of the cam). The force value can be doubled or tripled by arranging four or six springs, respectively. Also, the force value could be modified using springs with different stiffness constants.

Force tests have been carried out in a model H5KS Hounsfield testing machine (Fig. 3). This testing machine is equipped with a load cell of 5 kN, has a load measurement accuracy of 0.5% of the applied load, a position measurement accuracy of 0.001 mm, a test speed range from 0.001 mm/min to 1500 mm/min and a maximum stroke of 750 mm. The tests were performed at a speed of 500 mm/min with a total displacement of 260 mm. Each test starts with the rollers at the bottom of the cam (smaller elongation of the springs) and moving upwards. Once the maximum displacement of the mechanism is achieved, when the rollers are at the top of the cam, it returns to the starting position. Fig. 4 shows the force curves measured for 2, 4 and 6 springs arranged in parallel. The results depict a good performance of the mechanism. The force curves maintain a near constant value along the stroke of the mechanism, especially for the upward displacement, and fit quite well to the theoretical values of 5 kp (49.1 N), 10 kp (98.1 N) and 15 kp (147 N). Table 1 provides the mean value, variance and maximum and minimum values of the three force curves shown in Fig. 4. Differences between the upward and downward curves are due to the friction forces, increasing the difference for larger input displacement, that results in higher friction forces (higher spring extension and normal forces). In the same way, results show larger hysteresis loops (defined as the region inside the upward and downward curves) for higher force values. As discussed in Ref. [34], rolling friction plays an important roll in the deviations from the target constant force.

To reduce the influence of the friction forces and the hysteresis loops, wide cam profiles (large values of the cam slope β) should be used in combination with springs of low stiffness coefficients. For this work a neutral cam profile designed for null rolling friction has been used. The noise and small fluctuations of the force curves are attributable to the surface roughness of the cam and to possible small manufacturing errors in the laser cutting process of the cam. Due to the low inertia of the

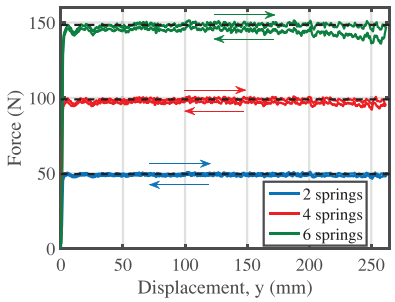

Fig. 4. Measured force curves for 2, 4 and 6 springs arranged in parallel.

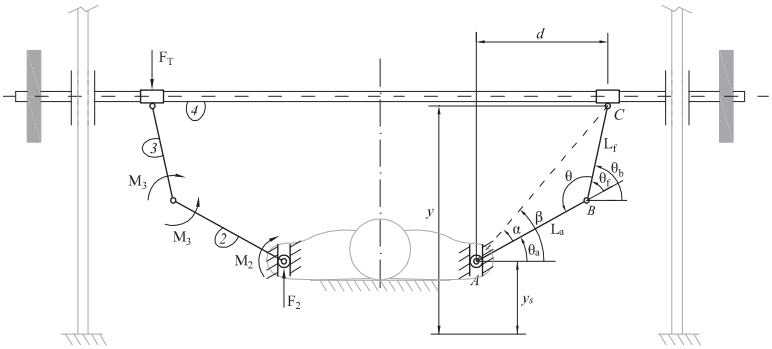

Fig. 5. Bench press model.

moving parts of the mechanism no dynamic effects on the results obtained are appreciable at the tested speeds. The same force level test has been repeated at different speeds, ranging from 250 mm/min to 1500 mm/min (machine limit), obtaining force curves without appreciable differences that could be attributed to dynamic effects.

Based on these results it can be concluded that the proposed design of CFM is suitable for its use as a resistance device in bodybuilding machines. The requirement of changing the load level of these machines can be fulfilled by adding springs in parallel or by replacing them with others with different stiffness constant.

3. Mathematical model of the bench press exercise

In this section, the mathematical model of the bench press exercise is described. The model is based on the one presented by Rahmani et al. [55,56] while it has been modified in the following points: (i) the rotational inertia of the upper limbs segments is included, and (ii) the net joint moment and forces can be computed. In addition, a more meaningful expression to calculate the power is proposed.

The bench press exercise can be realized with a traditional bench press or in a Smith machine. The mathematical model described is based on a Smith machine [57] where the barbell is guided and restricted to remain horizontal at any time. The upper limbs segments are considered as rigid bodies and joined through ideal joints, see Fig. 5. The bench press exercise is modeled as follows. The arm of length L_a is joined with revolute joints to the forearm and trunk, additionally the vertical displacement at the shoulder is allowed. The forearm of length L_f is articulated to the hand through a revolute joint. The hand can be modeled as a point of lumped mass with the same displacement as the barbell. Since a Smith machine is used, two prismatic joints at each side of the barbell are included to allow the vertical displacement. Thus, the hand is only able to move vertically and the horizontal distance between the shoulder and the arm, d, remain constant. Also, since the barbell is forced to keep centered and horizontally, the bench press exercise is assumed to be performed in a symmetrical manner [56]. Based on this assumption, any half of the model depicted in Fig. 5 can be used to analyse the dynamics of both halves of the symmetrical model during the weight lift.

In Fig. 5, y is the vertical position of the hand, y_s is the vertical position of the shoulder and θ is the angle between the forearm and the arm. The model described has two d.o.f, this means that knowing a set of two independent coordinates one can determine the mechanism position. Usually, in a bench press exercise the hand position (coordinate y) is measured using optical encoders [58] or linear transducer [59] and the elbow angle coordinate θ is measured using a goniometer [55].

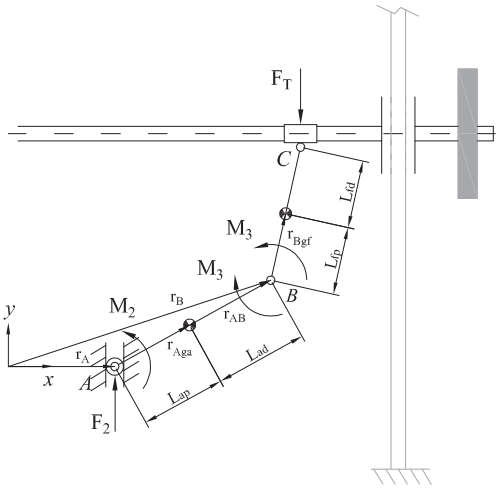

Fig. 6. CGs and representative distances of the arm and forearm.

3.1. Inverse kinematic model

An inverse kinematic analysis is required to derive the position, velocity and acceleration of the limb segments from the measured time curves of the hand height, y, and elbow angle θ. In Fig. 5, the arm and forearm define a triangle with vertices A, B and C. From the cosine theorem the distance $\overline{AC}$ can be written as:

$$\overline{AC}^2 = d^2 + (y - y_s)^2 = L_a^2 + L_f^2 - 2L_aL_f\cos\theta, \tag{8}$$

where L_a and L_f are the limb segment lengths, d is the horizontal distance between wrist and shoulder and y_s is the position of the shoulder axis. Using the previous equation, the shoulder axis position, y_s, can be computed from the constants of the model and the values of y and θ. In addition, if the shoulder axis displacement can be assumed to be negligible, Eq. (8) can be used to compute y from the constants of the model and the value of θ.

The absolute angle θ_a of the arm, defined with respect the horizontal axis, can be expressed as:

$$\theta_a = \beta - \alpha \tag{9}$$

where $\beta = \tan^{-1}\left(\frac{y-y_s}{d}\right)$ and $\alpha = \tan^{-1}\left(\frac{L_f\sin\theta_f}{L_a+L_f\cos\theta_f}\right)$.

The absolute angle of the forearm θ_b is obtained as:

$$\theta_b = \theta_f + \theta_a = \pi - \theta + \theta_a \tag{10}$$

Eqs. (8) –(10) must be solved for each instant of time in order to know the position of the limb segments over time. The numerical differentiation of the position coordinates (y, y_s, θ_a, θ_b) can be computed to obtain the velocities ($\dot{y}$, $\dot{y}_s$, $\dot{\theta}_a$, $\dot{\theta}_b$) and the accelerations ($\ddot{y}$, $\ddot{y}_s$, $\ddot{\theta}_a$, $\ddot{\theta}_b$).

Next, for the inverse dynamical analysis, the acceleration of the center of gravity (CG) of each limb segment is necessary. The velocities of the CGs of the arm, $\dot{\boldsymbol{r}}_{\boldsymbol{ga}}$, and forearm, $\dot{\boldsymbol{r}}_{\boldsymbol{gf}}$, can be written as (see Fig. 6):

$$\dot{\boldsymbol{r}}_{\boldsymbol{ga}} = \dot{\boldsymbol{y}}_{\boldsymbol{s}} + \dot{\boldsymbol{\theta}}_{\boldsymbol{a}} \times \boldsymbol{r}_{\boldsymbol{Aga}} \tag{11}$$

$$\dot{\boldsymbol{r}}_{\boldsymbol{gf}} = \dot{\boldsymbol{r}}_{\boldsymbol{B}} + \dot{\boldsymbol{\theta}}_{\boldsymbol{b}} \times \boldsymbol{r}_{\boldsymbol{Bgf}} \tag{12}$$

$$\dot{\boldsymbol{y}}_{\boldsymbol{s}} = \dot{y}_s\,\hat{\boldsymbol{j}}$$

$$\dot{\boldsymbol{\theta}}_{\boldsymbol{a}} = \dot{\theta}_a\,\hat{\boldsymbol{k}}$$

$$\dot{\boldsymbol{\theta}}_{\boldsymbol{b}} = \dot{\theta}_b\,\hat{\boldsymbol{k}}$$

$$\boldsymbol{r}_{\boldsymbol{Aga}} = L_{ap}\cos\theta_a\,\hat{\boldsymbol{i}} + L_{ap}\sin\theta_a\,\hat{\boldsymbol{j}}$$

$$\boldsymbol{r}_{\boldsymbol{Bgf}} = L_{fp}\cos\theta_b\,\hat{\boldsymbol{i}} + L_{fp}\sin\theta_b\,\hat{\boldsymbol{j}}$$

$$\dot{\boldsymbol{r}}_{\boldsymbol{B}} = \dot{\boldsymbol{y}}_{\boldsymbol{s}} + \dot{\boldsymbol{\theta}}_{\boldsymbol{a}} \times \boldsymbol{r}_{\boldsymbol{AB}}$$

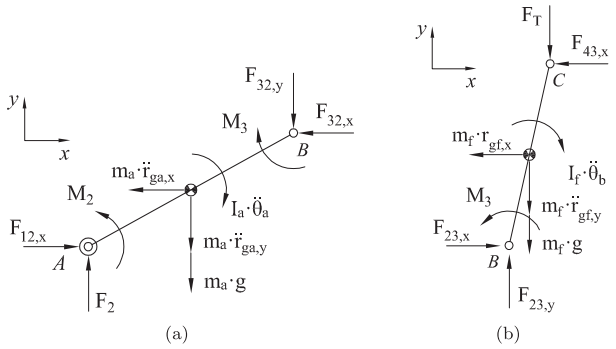

Fig. 7. Forces diagrams of the (a) arm and (b) forearm.

and,

$$\boldsymbol{r_{AB}} = L_a \cos\theta_a \,\hat{\boldsymbol{i}} + L_a \sin\theta_a \,\hat{\boldsymbol{j}}$$

Finally, the accelerations of the CGs of the arm, $\ddot{\boldsymbol{r}}_{\boldsymbol{ga}}$, and forearm, $\ddot{\boldsymbol{r}}_{\boldsymbol{gf}}$, can be obtained from:

$$\ddot{\boldsymbol{r}}_{\boldsymbol{ga}} = \ddot{\boldsymbol{y}}_{\boldsymbol{s}} + \ddot{\boldsymbol{\theta}}_{\boldsymbol{a}} \times \boldsymbol{r}_{\boldsymbol{Aga}} + \dot{\boldsymbol{\theta}}_{\boldsymbol{a}} \times (\dot{\boldsymbol{\theta}}_{\boldsymbol{a}} \times \boldsymbol{r}_{\boldsymbol{Aga}}) \tag{13}$$

$$\ddot{\boldsymbol{r}}_{\boldsymbol{gf}} = \ddot{\boldsymbol{r}}_{\boldsymbol{B}} + \ddot{\boldsymbol{\theta}}_{\boldsymbol{b}} \times \boldsymbol{r}_{\boldsymbol{Bgf}} + \dot{\boldsymbol{\theta}}_{\boldsymbol{b}} \times (\dot{\boldsymbol{\theta}}_{\boldsymbol{b}} \times \boldsymbol{r}_{\boldsymbol{Bgf}}) \tag{14}$$

3.2. Forces and moment calculation

The bench press exercise involves several muscles groups to generate the movement of the upper limbs, mainly the pectoralis major, the anterior deltoid brachial and the triceps brachii [60]. In a simplified mathematical model of the muscle action, the sum of the contribution of all individual muscles in a joint is reduced to a net joint moment. In Fig. 6, M_2 and M_3 are the net joint moments at the shoulder and elbow, respectively; F_2 is the vertical force at shoulder, which corresponds to the force usually measured with force plates located under the user's back [21,55]; and F_T is the vertical force acting on the user's wrist. In the model the net joint moment at the wrist has been neglected. It must be noted that the mechanism is overactuated by the moments at the shoulder and elbow. This mean that there is an infinite number of combinations of M_2 and M_3 that allows lifting the load along the same trajectory.

Fig. 7 shows the free body diagrams of the arm and the forearm, where the mass and rotational inertia of the bodies and the internal and external forces at joints have been included.

According to Fig. 7(a), the equilibrium equations for horizontal forces, vertical forces and moments with respect to the CG of the arm read as:

$$F_{12,x} - F_{32,x} = m_a \ddot{r}_{ga,x} \tag{15}$$

$$F_2 - F_{32,y} = m_a \ddot{r}_{ga,y} + m_a g \tag{16}$$

$$\begin{aligned} &F_{12,x} L_{ap} \sin\theta_a + F_{32,x} L_{ad} \sin\theta_a - F_2 L_{ap} \cos\theta_a \\ &\quad - F_{32,y} L_{ad} \cos\theta_a + M_2 - M_3 = I_a \ddot{\theta}_a, \end{aligned} \tag{17}$$

where L_{ap} and L_{ad} are the proximal and distal distances from the center of gravity of the arm, respectively, I_a is the moment of inertia of the arm with respect to its CG and g is the gravity acceleration. Similarly, from Fig. 7(b), the equilibrium equations for the forearm are written as:

$$F_{23,x} - F_{43,x} = m_f \ddot{r}_{gf,x} \tag{18}$$

$$F_{23,y} - F_T = m_f \ddot{r}_{gf,y} + m_f g \tag{19}$$

$$F_{23,x} L_{fp} \sin\theta_b + F_{43,x} L_{fd} \sin\theta_b - F_{23,y} L_{fp} \cos\theta_b - F_T L_{fd} \cos\theta_b + M_3 = I_f \ddot{\theta}_b, \tag{20}$$

where L_{fp} and L_{fd} are the proximal and distal distances from the center of gravity of the forearm, respectively, and I_f is the moment of inertia of the forearm with respect to its CG. The term of force F_T includes the force due to the resistance system F_R, the force due to the hand mass m_h and the friction F_f that appears at the vertical guides of the Smith machine [55] as follows:

$$F_T = F_R + m_h (g + \ddot{y}) + F_f \tag{21}$$

Eqs. (15) –(20) form an undetermined system of 6 equations with 7 unknowns, being $F_{23,x} = -F_{32,x}$ and $F_{23,y} = -F_{32,y}$. The 7 unknowns are the two net joint moments M_2 and M_3, the vertical force at the shoulder F_2, the internal forces at the elbow $F_{23,x}$ and $F_{23,y}$, the horizontal force at the shoulder $F_{12,x}$ and the horizontal force at the wrist $F_{43,x}$. As mentioned above, having an undetermined system of equations derives from the fact that the mechanism is over-actuated by the moments M_2 and M_3. Thus, posing this dynamical problem as an optimum control problem may help to find the optimal combination of M_2 and M_3. There might be different criteria that could be used to formulate an objective function for the optimization. However, the optimization problem is out of the scope of this work and it is not addressed here. To overcome this inconvenience, it is assumed that the net joint moment at the elbow M_2 is much smaller than the net joint moment at the shoulder M_3 and will not be included in the model. In this way, Eqs. (15)–(20) reduces to a determined system that can be solved over time.

In this work, it has been assumed that the net joint moment at the elbow M_2 is much smaller than the net joint moment at the shoulder M_3. This assumption is reasonable since the literature about studies on electromyography activity and strength training carried out in the bench press exercise have reported that the primary muscle in the bench press exercise is the pectoralis major and anterior deltoid, which mobilize the shoulder joint for performing the movement of lifting the barbell. In this sense, the horizontal bench press involves horizontal adduction and abduction of the shoulder [61]. Secondly, for ending the movement of lifting the barbell, the triceps brachii is activated for elbow extension. All studies consulted about this topic have reported that to lift the same mass, there is a significantly higher EMG activity in the pectoralis major and the anterior deltoid than triceps brachii is performing during the bench press exercise [60–63].

3.3. Power calculation

The calculation of the muscular power helps at improving muscular characteristics in individual training. In the bench press exercise the power value is usually calculated as $P = F \cdot v$, where F is the force exerted by the subject and v is the velocity of the barbell. The velocity of the barbell can be derived from the measures of an appropriated kinematic device located in the Smith machine (encoder, linear position transducer). Regarding the term of force, it is calculated as $F = m(a+g)$, where a is the acceleration of the barbell, g is the acceleration due to gravity and m is the moving mass. Some authors include in the term of mass m only the lifting mass [19,64] or the sum of the lifting mass and the upper-limb mass [55]. Rambaud et al. [58] compared the force values obtained including the upper-limb mass and using only the lifted mass, showing significant differences in both cases. Additionally, they found a good match between the force calculated taking into account the upper-limb mass and the force measured with a force plate. As result, they underlined the importance of taking into account the upper-limb mass to ensure precise evaluation of muscular characteristics. Other authors also use force plates to measure the force value [21,55].

While the force value calculated adding the upper-limb inertia or the force directly measured from force plates are used in the power equation $P = F \cdot v$, it must be noted that those forces are not applied to the barbell and therefore the power calculated as the product of that force and the velocity of the barbell is less meaningful in a physical sense. In this work, based on the mathematical model of the bench press exercise, it is proposed to calculate the mechanical power as the product of the net joint moment by the angular velocity of the corresponding upper-limb segment, plus the product of the vertical force in the shoulder by its vertical velocity. The equation of power can be written as, see Fig. 6:

$$P = |M_2 \dot{\theta}_a| + |M_3 \dot{\theta}_f| + |F_2 \dot{y}_s| \tag{22}$$

where the absolute value $|\cdot|$ is taken to account for the muscle power. During the raise of the load, the mechanical power is positive. However, it must be noted that during the descent of the load, the net mechanical power of the mechanism is negative, that is, the muscles need to be contracted to work as a brake, developing power. Finally, due to the assumption of $M_3 \approx 0$, the power is evaluated as $P = |M_2 \dot{\theta}_a| + |F_2 \dot{y}_s|$.

4. Comparative study between constant-force resistance and isoinertial resistance

The mathematical model of the bench press exercise described in the previous section is used for a comparative between the isoinertial resistance and the constant-force bench press proposed in this work. The isonertial or free-weight resistance is the most commonly used method to improve strength and power capacity in sport. It is based on the lifting of masses where the resistance force depends on the masses weight and its acceleration, $F = m(g+a)$. In contrast, the constant-force bench press has small moving masses and provides an almost constant resistance force, where the force value is independent of the accelerations.

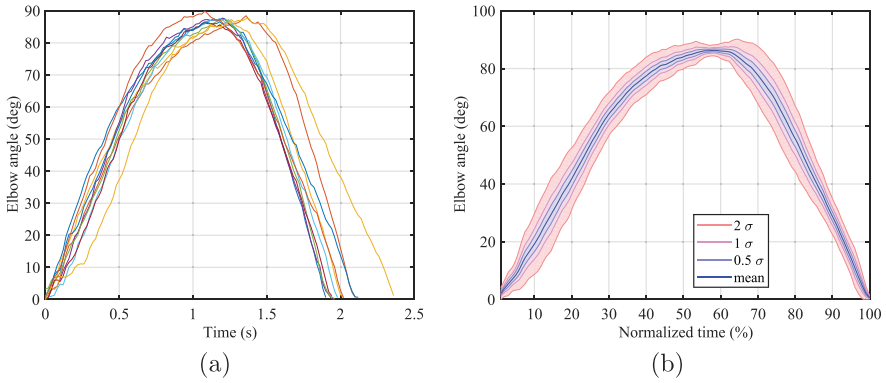

Fig. 8. Experimental results obtained in ten repetitions of the bench press exercise: (a) all repetitions and (b) mean and deviations calculated using the ten repetitions.

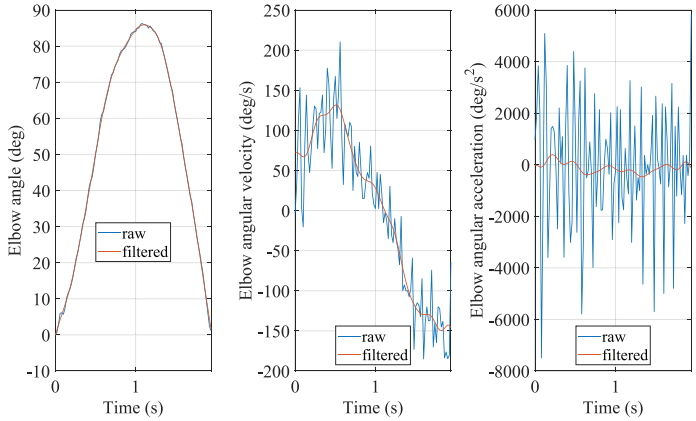

Fig. 9. Electrogoniometer raw signal and the calculated angular velocity and acceleration (in blue) besides its filtered curves (in red). (For interpretation of the references to colour in this figure legend, the reader is referred to the web version of this article.)

4.1. Test session

The comparative analysis is based on data measured in a test session. A trained man with 5 years experience in bench press lifting volunteered to participate in this study. Subject's age, height and body mass were 22 years, 1.79 m and 75 kg, respectively. The bench press exercise was done with a Smith machine and isoinertial resistance following a procedure similar to that described by Muyor et al. [60]. At the start of each repetition the subject lifts the barbell with the elbow extended and begins the eccentric phase, which ends when the bars reach around 2 cm over the subject's chest. The concentric phase is then carried out to the starting position. The results described below correspond to a session of 12 repetitions of the exercise using a mass of 66 kg, which was the 60% of the one repetition maximum (1RM). Grip distance was 150% of the distance between acromiums. Regarding the instrumentation, the elbow angle was measured with an electrogoniometer (Biometrics Ltd., Newport, UK) placed on the lateral side of the ulna and the humerus.

From the set of twelve repetitions, the first and the last were excluded to avoid the possible bias induced by the knowledge of the volunteer of being the first and the last of the series. Therefore, a smaller set of ten repetitions is used in what follows. Fig. 8(a) shows the selected repetitions starting from the same time point. As can be seen in the figure, the durations of the repetitions are slightly different. In order to find a mean representative motion, the selected ten repetitions have been statistically analysed after normalizing each time vector with its duration. Therefore, in Fig. 8(b) a mean motion can be represented against a normalized time vector expressed in percentage. This figure shows also the bands delimited by 0.5, 1 and 2 standard deviations. It is interesting to see how the dispersion of the measurements significantly decreases at the frontier of the concentric and eccentric phases of the exercise, with an average value of 86 degrees of elbow flexion. In addition, a larger dispersion in the results is found at the beginning of the concentric phase.

Table 2
Model parameters values.

Parameter	Value
Arm length, L_a	0.330 m
Arm distal CG length, L_{ad}	0.186 m
Arm proximal CG length, L_{ap}	0.144 m
Arm mass, m_a	2.10 kg
Arm CG inertia moment, I_a	0.0237 kg m^2
Forearm length, L_f	0.260 m
Forearm distal CG length, L_{fd}	0.148 m
Forearm proximal CG length, L_{fp}	0.112 m
Forearm mass, m_f	1.20 kg
Forearm CG inertia moment, I_f	0.0074 kg m^2
Shoulder-wrist distance, d	0.208 m
Wrist mass, m_h	0.450 kg

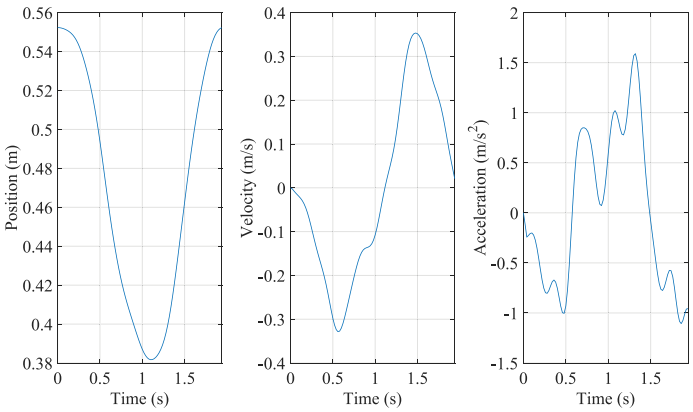

Fig. 10. Vertical position, velocity and acceleration of the barbell for one repetition.

The measures of the electrogoniometer, sampled at 50 Hz, include a certain level of noise from different sources that makes difficult the inverse dynamics simulations. As an example, the measures of the electrogoniometer during the eighth repetition are shown in Fig. 9. While the noise is not too apparent in the angle measurement, calculating the angular velocity and angular acceleration from this signal results in very noise velocity and acceleration curves. In order to avoid this inconvenience the signal from the goniometer has been back and forth filtered with a sixth order Butterworth filter with cut-off frequency of 4 Hz. This way the goniometer signal is smoothed without causing lag and leading to smooth and representative time derivatives.

Upper limb segments length were measured during the test session. The values of the measured parameters that will be used later on for inverse dynamics simulations are listed in Table 2.

4.2. Inverse kinematic

The bench press model described in the preceding section has two degrees of freedom and, as it was stated before, two independent coordinates are required to determine the limb segments position. In the test session the exercise was realized keeping the shoulder without appreciable vertical displacement, thus it has been assumed $y_s = 0$ at any time. Accordingly, the d.o.f. of the model has been reduced to 1 d.o.f. In this way, knowing the elbow angle θ, the arm and forearm positions can be determined. Again, as an example, Fig. 10 shows the calculated position, velocity and acceleration of the barbell (y, $\dot{y}$, $\ddot{y}$) for the eighth repetition. These curves have been obtained from the filtered signal of the electrogoniometer, which measures the elbow angle. This exercise repetition was done in 1.94 s (1.13 s for eccentric phase and 0.81 s for concentric phase). The frontier of the concentric and eccentric phases is identified as the time in which the position of the barbel is minimal and its velocity is accordingly zero.

4.3. Force, moment and power results for isoinertial resistance

From the previous kinematic results one can obtain the forces and net joint moment required to realize the exercise. To do that, besides the upper limbs segment lengths their inertial properties are required. Table 2 summarizes the values

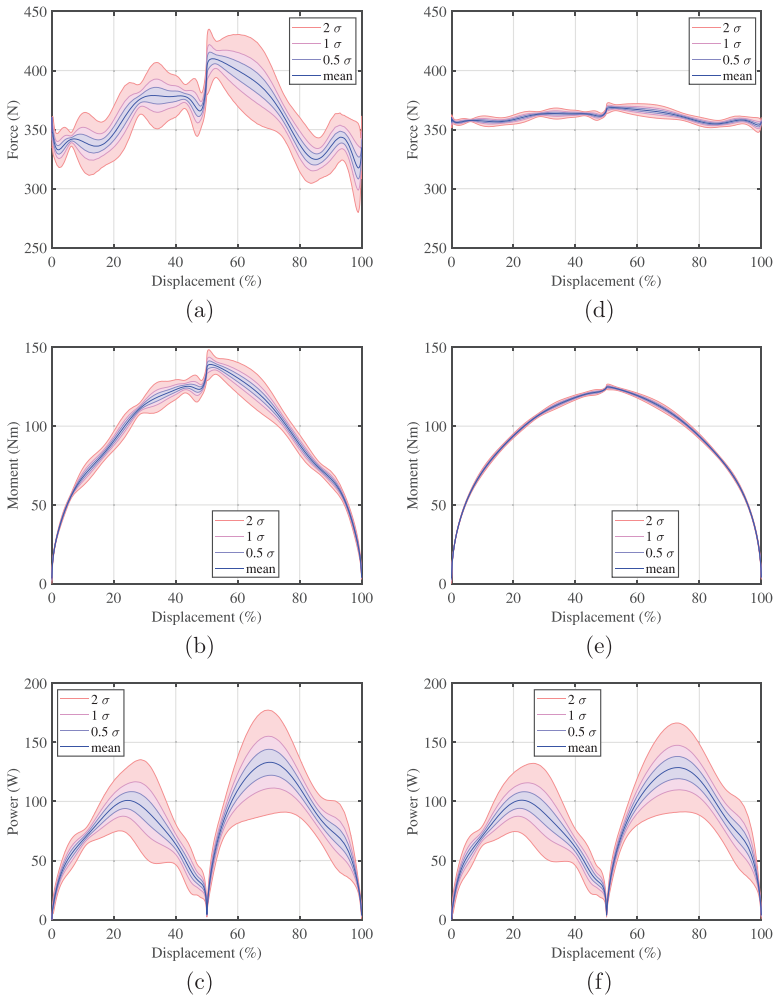

Fig. 11. Mean and deviations calculated using ten repetitions. On the left, for isoinertial resistance: (a) shoulder vertical force, (b) shoulder net moment and (c) power. On the right for simulated constant-force resistance: (d) shoulder vertical force, (e) shoulder net moment and (f) power. Eccentric phase goes from 0 to 50%, while concentric phase goes from 50%–100%.

of the parameters used for the simulations, where the masses, moments of inertia and positions of the centers of gravity of the arm and forearm have been estimated from the data provided by Contini [65] and Winter [66]. To overcome the overactuation of the model due to simultaneous action of the shoulder and elbow moments, in the following it has been considered that the shoulder is able to realize the exercise by itself and there is no moment at the elbow as explained before. It is worth of noting that this simplification does not affect the resultant vertical force at the shoulder and the power values.

The ten selected repetitions of the free-weight bench press exercise have been used in inverse dynamics analysis to obtain the shoulder force and moment histories, respectively. Later, using Eq. (22) the instantaneous power developed in each repetition by the actuating muscles is calculated. Fig. 11 shows, for the ten analysed repetitions, the mean values and standard deviations of the vertical force at the shoulder, the net moment at the shoulder, and the power curves versus the percentage of displacement, where the eccentric phase goes from 0–50% and the concentric phase from 50%–100%. Due to the relatively low repeatability of the exercise, it can be observed a considerable dispersion of the results, especially in the power graph.

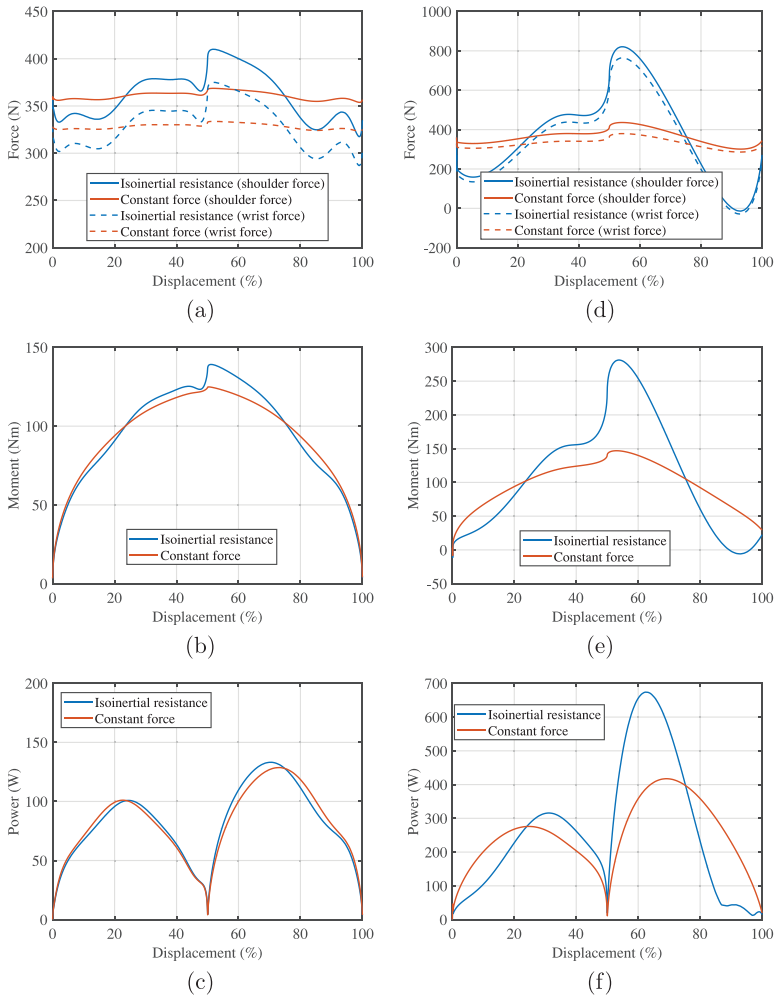

Fig. 12. Comparative curves between isoinertial resistance and constant-force resistance. On the left, for the real velocity exercise: (a) wrist and shoulder vertical forces, (b) shoulder net moment and (c) power. On the right, for a simulated three times higher velocity exercise: (d) wrist and shoulder vertical force, (e) shoulder net moment and (f) power. Eccentric phase goes from 0–50%, while concentric phase goes from 50%–100%.

It must be noted that these results correspond to one half of the symmetrical bench press model. Thus, the resulting vertical force, that would be measured with a force plate located at the user's back, would be double, and the total power would be also doubled.

4.4. Constant-force resistance vs. isoinertial resistance

Since the resistance response of the proposed bench press is different from the traditional isoinertial resistance, it is expected to find significant differences in the muscle action. Due to the lack of experimental data of the proposed constant-force bench press, the time-position curve of the barbell in the isoinertial exercise has been utilized to analyze the performance of the constant-force exercise. Obviously, in a real case the kinematics for both resistance systems will not be the same. However, the simulated results obtained here are of interest for a qualitative comparison of both systems. In the simulations, a total moving mass of 7 kg (lightened barbell + CFM masses) was considered. The remaining, up to 66 kg (to equals the isoinertial resistance), is supplied by the CFM.

Besides the isoinertial resistance curves, the right column of Fig. 11 shows the results obtained for the simulated constant-force bench press, where there is a clear smaller dispersion in the force and moment graphs. This is not the case for the power results, where the dispersion of the results is quite similar. Additionally, the curves of the mean values showed in Fig. 11 for the two resistance systems are represented together, for a better comparison, in the left column of the Fig. 12. Also, in Fig. 12(a) it has been included the curve of the mean force at the wrist. For the mean curves there are significant differences between both resistance systems. The constant-force resistance results in almost constant force values at the wrist and at the shoulder compared with the isoinertial resistance results. Differences between wrist and shoulder force curves are due to the arm and forearm masses. For constant-force resistance, maximum fluctuations of wrist and shoulder forces during the repetition are 10.4 N (3.2%) and 14.9 N (4.6%), respectively; where these small fluctuations are due to: the barbell and CFM masses in the cases of the wrist force; and also to arm and forearm masses in the case of the shoulder force. The maximum peak force to be supported by the shoulder is 369 N and takes place at the beginning of the concentric phase, at the time the masses must be accelerated to start the lift. In the case of the isoinertial resistance, larger fluctuations and larger peaks in the force are clearly observed. The maximum values of the fluctuations of the wrist and shoulder forces during the repetition are 88.0 N (27.2%) and 92.4 N (28.5%), respectively. These values are more than six times larger than those obtained for the constant-force resistance simulation. The maximum peak force at the shoulder is 410 N, a value which is 11% larger than that of the constant-force simulation. Regarding the shoulder net moment, a higher value is appreciable for the isoinertial resistance at the beginning of the concentric phase, Fig. 12(b). Smaller differences have been found for the maximum values of the power curves, Fig. 12(c).

Next, to extend the comparative study to higher velocities of the bench press exercise, the time history of the goniometer lecture has been scaled accordingly. To simulate a faster execution of the bench press exercise it has been supposed that the exercise was realized in a third of the time, i.e. the eccentric phase is realized in 0.37 s and the concentric phase in 0.27 s. Again, this is a virtual situation, but may be used for comparison. The right column of Fig. 12 shows the vertical forces at wrist and shoulder joints, shoulder net moment and power curves for this simulated exercise for both isoinertial resistance and constant-force resistance. In this faster exercise execution, much larger differences are found between both resistance systems. Forces at wrist and shoulder remain quite constant for the constant resistance system, while high fluctuations are remarkable in the case of the isoinertial resistance, where a maximum value of 764 N and a minimum of - 29 N for the force at the wrist are shown in Fig. 12(d). Negative values of the force indicates the braking phase that typically occurs in fast and explosive executions for isoinertial resistance. On the contrary, for the proposed constant-force resistance the braking phase is not likely to happen. Regarding the shoulder net moment and power curves for this faster exercise execution, also larger differences are appreciable. A peak moment of 281 Nm at the beginning of the concentric phase is found for the isoinertial resistance, see Fig. 12(e), value 91% higher than for constant-force resistance (147 Nm). In the same way, larger peak values of power (61% higher) are required for the isoinertial resistance than for the constant-force resistance, see Fig. 12(f).

5. Summary and conclusions

This work proposed a new design of a bench press which is based on the use of a constant-force mechanism and was compared with an isoinertial resistance one. Due to the low inertia of the moving parts of the constant-force mechanism, the proposed bench press is able to maintain a nearly constant resistance force which may be adapted to different values by adding spring in a parallel layout. A prototype of the constant-force mechanism has been manufactured and tested to validate its performance. A mathematical model of the bench press exercise including arm, forearm and hand has been developed. By properly feeding the model with a recorded motion, it can be used to evaluate the force, moment and muscular power curves. A set of repetitions has been recorded in the laboratory and analyzed by inverse dynamics. The results from ten repetitions of the bench press exercise have been analyzed from a statistical point of view showing mean values and standard deviations.

The results show that the constant-force bench press has qualitative differences in the vertical forces at the shoulder and wrist, the net moment at the shoulder and muscle power curves as compared to the traditional isoinertial (free-weight) resistance. Due to the low inertia of the moving masses of the constant-force resistance device, force curves show much more constant patterns than those of the isoinertial resistance, and avoids the braking phase that typically occurs in fast and explosive executions. Large peak values in the force and moment curves at the beginning of the concentric phase are practically eliminated. In addition, the maximum power required is reduced. In general, smoother curve patterns, and less dispersion between exercise repetitions are obtained for the constant-force resistance. This could have advantages in strength and resistance training, decreasing the risk of injury, or in sports physiotherapy in the recovery of musculoskeletal pathologies. These hypotheses should be analyzed in future works. In addition, future work will include experiments in the constant force bench press aimed at validating the proposed mathematical model.

Acknowledgment

This work has been partially funded by the Spanish "Ministerio de Economía y Competitividad" under the project DEP2016-80296-R (AEI/FEDER, UE).

References

[1] S. Fleck, W. Kraemer, Designing Resistance Training Programs, 4th ed., Human Kinetics, 2004.
[2] P. Sorace, T. LaFontaine, Resistance training muscle power: design programs that work!, ACSM's Health Fitness J. 9 (2) (2005) 6–12.
[3] D. Murray, S. Bera, L. Brown, B. Findley, Strength assesment, in: LE. Brown (Ed.), Strength Training. Champaign, IL, Human Kinetics, 2007, pp. 97–112.
[4] D. Frost, J. Cronin, R. Newton, A biomechanical evaluation of resistance: fundamental concepts for training and sports performance, Sports Med. 40 (4) (2010) 303–326, doi:10.2165/11319420-000000000-00000.
[5] A. Saeterbakken, V. Andersen, R. Van Den Tillaar, Comparison of kinematics and muscle activation in free-weight back squat with and without elastic bands, J. Strength Condition. Res. 30 (4) (2016) 945–952, doi:10.1519/JSC.0000000000001178.
[6] R. Häberle, F. Schellenberg, R. List, M. Plüss, W. Taylor, S. Lorenzetti, Comparison of the kinematics and kinetics of shoulder exercises performed with constant and elastic resistance, BMC Sports Sci. Med. Rehabilit. 10 (1) (2018), doi:10.1186/s13102-018-0111-7.
[7] S. Walker, H. Peltonen, J. Avela, K. Häkkinen, Kinetic and electromyographic analysis of single repetition constant and variable resistance leg press actions, J. Electromyogr. Kinesiol. 21 (2) (2011) 262–269, doi:10.1016/j.jelekin.2010.12.004.
[8] S. Walker, H. Peltonen, J. Avela, K. Häkkinen, Neuromuscular fatigue in young and older men using constant or variable resistance, Eur. J. Appl. Physiol. 113 (4) (2013) 1069–1079, doi:10.1007/s00421-012-2526-2.
[9] S. Walker, J. Hulmi, M. Wernbom, K. Nyman, W. Kraemer, J. Ahtiainen, K. Häkkinen, Variable resistance training promotes greater fatigue resistance but not hypertrophy versus constant resistance training, Eur. J. Appl. Physiol. 113 (9) (2013) 2233–2244, doi:10.1007/s00421-013-2653-4.
[10] V. Andersen, M. Fimland, M. Kolnes, A. Saeterbakken, Elastic bands in combination with free weights in strength training: neuromuscular effects, J. Strength Condit. Res. 29 (10) (2015) 2932–2940, doi:10.1519/JSC.0000000000000950.
[11] V. Andersen, M. Fimland, M. Kolnes, S. Jensen, M. Laume, A. Saeterbakken, Electromyographic comparison of squats using constant or variable resistance, J. Strength Condit. Res. 30 (12) (2016) 3456–3463, doi:10.1519/JSC.0000000000001451.
[12] J. Ataee, M. Koozehchian, R. Kreider, L. Zuo, Effectiveness of accommodation and constant resistance training on maximal strength and power in trained athletes, PeerJ 2014 (1) (2014), doi:10.7717/peerj.441.
[13] R. Nijem, J. Coburn, L. Brown, S. Lynn, A. Ciccone, Electromyographic and force plate analysis of the deadlift performed with and without chains, J. Strength Condit. Res. 30 (5) (2016) 1177–1182, doi:10.1519/JSC.0000000000001351.
[14] P. Swinton, A. D. Stewart, J. Keogh, I. Agouris, R. Lloyd, Kinematic and kinetic analysis of maximal velocity deadlifts performed with and without the inclusion of chain resistance, J. Strength Condit. Res. 25 (11) (2011) 3163–3174, doi:10.1519/JSC.0b013e318212e389.
[15] K. Neelly, J. Terry, M. Morris, A mechanical comparison of linear and double-looped hung supplemental heavy chain resistance to the back squat: a case study, J. Strength Condit. Res. 24 (1) (2010) 278–281, doi:10.1519/JSC.0b013e3181b2977a.
[16] D. Baker, R. Newton, Effect of kinetically altering a repetition via the use of chain resistance on velocity during the bench press, J. Strength Condit. Res. 23 (7) (2009) 1941–1946, doi:10.1519/JSC.0b013e3181b3dd09.
[17] J. Bernentg, C. Coker, D. Briggs, The biomechanical and perceptual influence of chain resistance on the performance of the olympic clean, J. Strength Condit. Res. 22 (2) (2008) 390–395.
[18] B. Jidovtseff, J.-L. Croisier, N. Scimar, C. Demoulin, D. Maquet, J.-M. Crielaard, The ability of isoinertial assessment to monitor specific training effects, J. Sports Med. Phys. Fitness 48 (1) (2008) 55–64.
[19] L. Sánchez-Medina, C. Pérez, J. González-Badillo, Importance of the propulsive phase in strength assessment, Int. J. Sports Med. 31 (2) (2010) 123–129, doi:10.1055/s-0029-1242815.
[20] R. Newton, W. Kraemer, K. Häkkinen, B. Humphries, A. Murphy, Kinematics, kinetics, and muscle activation during explosive upper body movements, J. Appl. Biomech. 12 (1) (1996) 31–43, doi:10.1123/jab.12.1.31.
[21] D. Frost, J. Cronin, R. Newton, A comparison of the kinematics, kinetics and muscle activity between pneumatic and free weight resistance, Eur. J. Appl. Physiol. 104 (6) (2008) 937–956, doi:10.1007/s00421-008-0821-8.
[22] D. Keiser, Pneumatic exercising device, 1981, US Patent 4,257,593.
[23] H. Peltonen, K. Häkkinen, J. Avela, Neuromuscular responses to different resistance loading protocols using pneumatic and weight stack devices, J. Electromyogr. Kinesiol. 23 (1) (2013) 118–124, doi:10.1016/j.jelekin.2012.08.017.
[24] S. Avrillon, B. Jidovtseff, F. Hug, G. Guilhem, Influence of isoinertial-pneumatic mixed resistances on force-velocity relationship, Int. J. Sports Physiol. Perform. 12 (3) (2017) 385–392, doi:10.1123/ijspp.2016-0226.
[25] P. Wang, Q. Xu, Design and modeling of constant-force mechanisms: a survey, Mechan. Mach. Theory 119 (2018) 1–21, doi:10.1016/j.mechmachtheory.2017.08.017.
[26] L. Howell, Compliant Mechanisms, John Wiley Sons, New York, 2001.
[27] J. Gallego, J. Herder, Classification for literature on compliant mechanisms: a design methodology based approach, in: Proceedings of the ASME International Design Engineering Technical Conferences and Computers and Information in Engineering Conference 2009, DETC2009, 7 PART A, 2010, pp. 289–297.
[28] K. Tolman, E. Merriam, L. Howell, Compliant constant-force linear-motion mechanism, Mech. Mach. Theory 106 (2016) 68–79, doi:10.1016/j.mechmachtheory.2016.08.009.
[29] P. Wang, S. Yang, Q. Xu, Design and optimization of a new compliant rotary positioning stage with constant output torque, Int. J. Precis. Eng. Manufactur. 19 (12) (2018) 1843–1850, doi:10.1007/s12541-018-0213-x.
[30] G. Hao, A framework of designing compliant mechanisms with nonlinear stiffness characteristics, Microsyst. Technol. 24 (4) (2018) 1795–1802.
[31] G. Endo, H. Yamada, A. Yajima, M. Ogata, S. Hirose, A passive weight compensation mechanism with a non-circular pulley and a spring, in: Proceedings of the IEEE International Conference on Robotics and Automation, 2010, pp. 3843–3848.
[32] H. Bidgoly, M. Ahmadabadi, M. Zakerzadeh, Design and modeling of a compact rotational nonlinear spring, in: Proceedings of the IEEE International Conference on Intelligent Robots and Systems, 2016, pp. 4356–4361, November
[33] Y. Liu, D.-P. Yu, J. Yao, Design of an adjustable cam based constant force mechanism, Mech. Mach. Theory 103 (2016) 85–97, doi:10.1016/j.mechmachtheory.2016.04.014.
[34] J. López-MartÃnez, D. García-Vallejo, F. Arrabal-Campos, J. García-Manrique, Design of three new cam-based constant-force mechanisms, J. Mech. Des. Trans. ASME 140 (8) (2018), doi:10.1115/1.4040174.
[35] M. Li, W. Cheng, Design and experimental validation of a large- displacement constant-force mechanism, J. Mech. Robot. 10 (5) (2018), doi:10.1115/1.4040437.
[36] B. Li, G. Hao, Nonlinear behaviour design using the kinematic singularity of a general type of double-slider four-bar linkage, Mech. Mach. Theory 129 (2018) 106–130.
[37] R. Nathan, A constant force generation mechanism, J. Mech. Des. Trans. ASME 107 (4) (1985) 508–512, doi:10.1115/1.3260755.
[38] C.-C. Lan, J.-Y. Wang, Design of adjustable constant-force forceps for robot-assisted surgical manipulation, in: Proceedings of the IEEE International Conference on Robotics and Automation, 2011, pp. 386–391.
[39] Y.-H. Chen, C.-C. Lan, An adjustable constant-force mechanism for adaptive end-effector operations, J. Mech. Des. Trans. ASME 134 (3) (2012).
[40] A. Lamers, J. Gallego Sánchez, J. Herder, Design of a statically balanced fully compliant grasper, Mech. Mach. Theory 92 (2015) 230–239, doi:10.1016/j.mechmachtheory.2015.05.014.
[41] P. Wang, Q. Xu, Design and testing of a flexure-based constant-force stage for biological cell micromanipulation, IEEE Trans. Autom. Sci. Eng. 15 (3) (2018) 1114–1126, doi:10.1109/TASE.2017.2733553.
[42] H.-T. Pham, D.-A. Wang, A constant-force bistable mechanism for force regulation and overload protection, Mech. Mach. Theory 46 (7) (2011) 899–909, doi:10.1016/j.mechmachtheory.2011.02.008.

[43] Y.-H. Chen, C.-C. Lan, Design of a constant-force snap-fit mechanism for minimal mating uncertainty, Mech. Mach. Theory 55 (2012) 34–50, doi:10.1016/j.mechmachtheory.2012.04.006.
[44] X. Zhang, Q. Xu, Design and testing of a novel 2-dof compound constant-force parallel gripper, Precis. Eng. 56 (2019) 53–61, doi:10.1016/j.precisioneng.2018.09.004.
[45] G. Hao, J. Mullins, K. Cronin, Simplified modelling and development of a bi-directionally adjustable constant-force compliant gripper, Proc. Inst. Mech. Eng. Part C J. Mech. Eng. Sci. 231 (11) (2017) 2110–2123, doi:10.1177/0954406216628557.
[46] D. Hoecht, M. Ross, F. Bohm, Constant resistance exercising apparatus and system, 2005, US Patent 2005/0181915 A1.
[47] P. Colosky, T. Ruttley, Gravity-independent constant force resistive exercise unit, 2004, US Patent 6,685,602.
[48] D. Smith, Resistive exercise device, 2005, US Patent 6,958,032.
[49] R. Riley, D. Carey, Exercise machine with spring-cam arrangement for equalizing the force required through the exercise stroke, 1980, US Patent 4,231,568.
[50] N. Funk, J. Funk, Portable exercise device providing constant force output, 2016, US Patent 9,358,420.
[51] J. Raboin, J. Niebuhr, S. Cruz, C.D. Lamoreaux, Advance resistive exercise device, 2008, US Patent 7,462,141.
[52] R. Wilmarth, Pneumatic exercising device, 1983, US Patent 4,397,462.
[53] J. Padulo, G. Laffaye, A. Chaouachi, K. Chamari, Bench press exercise: the key points, J. Sports Med. Phys. Fitness 55 (6) (2015) 604–608.
[54] A. Saeterbakken, M. Fimland, Electromyographic activity and 6RM strength in bench press on stable and unstable surfaces, J. Strength Condit. Res. 27 (4) (2013) 1101–1107, doi:10.1519/JSC.0b013e3182606d3d.
[55] A. Rahmani, O. Rambaud, M. Bourdin, J.-P. Mariot, A virtual model of the bench press exercise, J. Biomech. 42 (11) (2009) 1610–1615, doi:10.1016/j.jbiomech.2009.04.036.
[56] A. Rahmani, B. Morel, P. Samozino, A Simple Method for Measuring Force, Velocity, Power and Force-Velocity Profile of Upper Limbs, Springer International Publishing, 2018, doi:10.1007/978-3-319-05633-3_7.
[57] D. Baker, Comparison of upper-body strength and power between professional and college-aged rugby league players., J. Strength Condit. Res. 15 (2001) 30–35.
[58] O. Rambaud, A. Rahmani, B. Moyen, M. Bourdin, Importance of uper-limb inertia in calculating concentric bench press foce, J. Strength Condit. Res. 22 (2) (2008) 383–389, doi:10.1123/ijspp.2016-0226.
[59] A. García-Ramos, S. Jaric, P. Padial, B. Feriche, Force-velocity relationship of upper body muscles: traditional versus ballistic bench press, J. Appl. Biomech. 32 (2) (2016) 178–185, doi:10.1123/jab.2015-0162.
[60] J. Muyor, D. Rodríguez-Ridao, I. Martín-Fuentes, J. Antequera-Vique, Evaluation and comparison of electromyographic activity in bench press with feet on the ground and active hip flexion, PLoS ONE 14 (6) (2019), doi:10.1371/journal.pone.0218209.
[61] P. Gentil, J. Fisher, J. Steele, A review of the acute effects and long-term adaptations of single-and multi-joint exercises during resistance training, Sports Med. 47 (5) (2017) 843–855.
[62] P.W. Marshall, B.A. Murphy, Increased deltoid and abdominal muscle activity during swiss ball bench press, J. Strength Condit. Res. 20 (4) (2006) 745–750.
[63] Y.d.A.C. Campos, S.F.d. Silva, Comparison of electromyographic activity during the bench press and barbell pulloverexercises, Motriz. J. Phys. Educat. 20 (2) (2014) 200–205.
[64] C. Bosco, A. Belli, M. Astrua, M. Tihanyi, R. Pozzo, S. Kellis, O. Tsarpela, C. Foti, R. Manno, C. Tranquilli, A dynamometer for evaluation of dynamic muscle work., Eur. J. Appl. Physiol. 70 (1995) 379–386.
[65] R. Contini, Body segment parameters, Part ii., Artif. Limbs 16 (1972) 1–19.
[66] D. Winter, Biomechanics and Motor Control of Human Movement, 4th ed., John Wiley & Sons, Inc., New York, 2009.

Capítulo 4

Diseño de trayectorias y pares mediante optimización paramétrica para el ejercicio de press de banca en una máquina Smith

Mechanism and Machine Theory 155 (2021) 104089

Contents lists available at ScienceDirect

Mechanism and Machine Theory

journal homepage: www.elsevier.com/locate/mechmachtheory

Design of trajectories and torques by parameter optimization for the bench press exercise on a Smith machine

Silvia Sánchez-Salinas[a], Daniel García-Vallejo[b], Javier López-Martínez[a,*], José M. Muyor[c]

[a] CITE-IIA, Department of Engineering, University of Almería, Spain
[b] Department of Mechanical Engineering and Manufacturing, Universidad de Sevilla, Spain
[c] Laboratory of Kinesiology, Biomechanics and Ergonomics (KIBIOMER Lab.), Research Central Services, Health Research Centre, University of Almería, Spain

ARTICLE INFO

Article history:
Received 3 February 2020
Revised 22 July 2020
Accepted 23 August 2020
Available online 1 September 2020

Keywords:
Multibody
Optimized trajectory
Optimal control
Collocation

ABSTRACT

The bench press exercise on a Smith machine, frequently used in training programs, can be analyzed as a redundantly actuated biomechanical system. In this exercise, a simplified model having one degree of freedom, actuated at the shoulder and the elbow, provides a meaningful representation of its dynamics. Due to the actuation redundancy, many different combinations of actuations that lead to the same motion can be found. The present optimization framework for the bench press exercise is intended at understanding the appropriate performance of this exercise when it is used to gain endurance or to perform the exercise in the safest manner, that is, avoiding overloads. The dynamic simulation is solved by parameter optimization and direct collocation. The kinematics of the bench press exercise performed by a trained subject and recorded with an electro-goniometer is used as a reference motion for the optimization. The results show that it is possible to mathematically obtain better realizations of the exercise, what suggests the potential of this methodology in the design of training programs in sports or rehabilitation exercises.

1. Introduction

The bench press exercise is receiving an increasing interest as a field testing, training and/or therapeutic modality to improve neuromuscular performance [1]. Moreover, this exercise has been defined as the simplest and the most suitable test for evaluating upper body strength [2]. Increasing upper body strength is of utmost importance in any activity or sport that puts a premium on body-to-body contact or where an implement is carried and thrown using the upper body [3].

Positive innce of endurance and strength on potentiation could suggest the existence of some association between maximum strength and muscular endurance [4]. The muscular endurance is necessary in physical employment such as firefighters, militaries and professional athletes that require high levels of physical fitness [5,6]. However, a program for a person wishing to increase maximal strength differs greatly from a program for a person wishing to increase muscular endurance. If muscular endurance is the goal, one should use a lighter load, which in turn allows a greater number of repetitions [7]. For

* Corresponding author.
E-mail addresses: sss043@ual.es (S. Sánchez-Salinas), dgvallejo@us.es (D. García-Vallejo), javier.lopez@ual.es (J. López-Martínez), josemuyor@ual.es (J.M. Muyor).

https://doi.org/10.1016/j.mechmachtheory.2020.104089
0094-114X/

this reason, in terms of muscular efficiency it would be interesting to perform a muscular task as the bench press optimizing its performance.

In fitness and strength training contexts, the Smith machine is frequently used for training and improving the performance of the pectoral major and upper limb muscles. It is a piece of free weight exercise equipment in which a horizontal Olympic-size barbell moves up and down on a set of vertical guiding rods [8]. Its main characteristic is that the stability requirements are lower in this machine, which creates a guided one-dimensional movement pattern [9]. In this sense, a drawback could be that the unnatural barbell path of the Smith machine forces the participants to press the barbell in a linear path [10]. However, the Smith machine is more secure for the users [1] because it constrains the barbell movements in the mediolateral and anterior-posterior directions, focusing on the vertical direction [8]. In addition, the guiding system of the Smith machine avoids measurement errors resulting from extraneous horizontal motions [11].

Human motion analysis by computational mechanics techniques has been a significant area of research interest for many years [12]. Multibody system dynamics (MSD) techniques are potentially very powerful in this field, and there are many contributions from the MSD community to the problem of gait simulation [13–16]. Among other approaches, parameter optimization techniques have been frequently used for motion synthesis of biped robots [17]. These techniques have been proven to be powerful in two-dimensional human walking research as shown in Refs. [18,19]. In this approach muscle forces and generalized coordinates are described in terms of a specific set of parameters, whose optimal values are found by minimizing cost functions that include an energy expenditure estimation and a measure of deviation from normal gait patterns. The method is mainly based on inverse dynamics since an inverse dynamic problem is solved by using the motion reconstructed from the design parameters at each iteration of the optimization algorithm. The main advantage of this approach is the complete elimination of the forward time integrations of the equations of motion, which significantly reduces the computational cost of simulation. In Ref. [20] parameter optimization was successfully used to solve a combined optimal control and optimal design problem, since at the same time the trajectories, muscle forces, etc., and the optimal parameters of an active orthosis model could be obtained. In recent years, the research on physic-based prediction of human movement has experienced a great development by the incorporation of computationally efficient techniques, among which the use of algorithmic differentiation has made possible a significant reduction of simulation time by direct collocation and optimization. Remarkable examples can be found in the three-dimensional simulation of human gait in Falisse et al. [21,22] or in the simulation of sit-to-stand movements in Serrancolí et al. [23]. In addition, the combination of the computational tools provided by Matlab© with the musculoskeletal modeling capabilities of OpenSim have been efficiently used by Lee and Umberger [24] to create a framework for generating predictive simulations of musculoskeletal movement based on direct collocation optimal control techniques.

The objective of this work is to find appropriate controls and trajectories for the bench press exercise by using parameter optimization and collocation. The main idea of the method used in this research is that the controls and trajectories must fulfil the equations of motion as well as minimizing a certain performance criterion specified as a cost function. The cost function includes a quadratic term to encourage the model to stay close to a realistic movement, which has been measured in the lab, see Van Den Bogert et al. [24], as well as other cost function components based on effort considerations that will encourage the model to use its muscle torques efficiently. In addition, other kinematic constraints have to be added to the optimization problem. This way, a realization obtained by optimization of the exercise might be used to design training programs for athletes. As shown by Sánchez-Medina et al. [25], assessing the velocity when lifting light and medium loads is particularly useful to evaluate the level of effort during resistance training as well as an indicator of the degree of fatigue. The knowledge of the optimal velocity profile to decrease the effort made, which translates into a decrease in the fatigue of the considered muscle groups, or the understanding of the muscular work done during the exercise stroke, allowing the athlete to modify the torque exerted by specific muscle groups during the exercise, based on the concept of internal attentional focus [26,27], will be useful in the planning of sport training as well as in the prescription of physical exercise. The optimization of the bench press exercise studied in this document is intended at understanding the appropriate performance of the bench press exercise in conditions of training to gain endurance or to perform the exercise in the safest manner, that is avoiding overloads. This method can be used to study the muscular response to different resistance systems [28] and define the most appropriate exercise realization in each case. Specifically, in the case of under-studied resistance devices such as the constant-force resistance [29]; or even for the development of future user-defined variable-force resistance devices based on nonlinear springs [30,31].

The paper is structured as follows. In Section 2, the model of the bench press exercise is presented, summarizing the simplifying assumption taken to achieve a representative model. In Section 3, the experiments carried out in the laboratory are described. These experiments are statistically analysed and are later used as a reference motion for the optimization. Section 4 presents the framework designed to solve the problem of simulating trajectories and controls by optimization. Later on, a numerical result section is included to demonstrate the usability of the procedure. The conclusions drawn from the analysis are summarized in Section 6.

2. Model description

The mathematical model of the bench press exercise described in this Section is based on the one presented by Rahmani et al. [32,33]. In addition to all the features of the model in Refs. [32,33], the rotational inertias of the upper limbs segments have been included in this research.

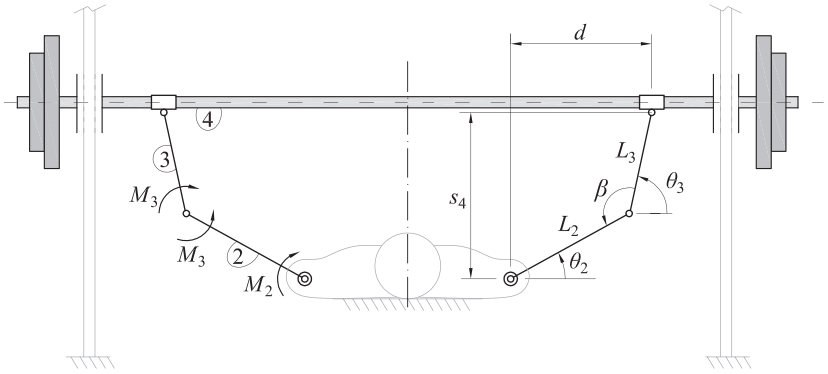

Fig. 1. Craniocaudal view of the bench press model with the anatomical transverse plane in vertical position.

The mathematical model described here is based on a Smith machine [34], in which the barbell is guided and restricted to remain horizontal at any time. This machine is attractive to the lifter involved in rehabilitation, novice lifters, or very young and old lifters. Also, those experienced lifters looking for maximal fatigue at the end of a workout routine might nd the Smith machine useful [3]. The upper limb segments are assumed to be rigid bodies joined through ideal joints, see Fig. 1. The bench press exercise is modelled as follows. The upper arm of length L_2 is joined with revolute joints to the forearm and trunk. In addition, the horizontal and vertical displacements of the shoulder axis are not allowed. The forearm of length L_3 is articulated to the hand through a revolute joint. The hand is modelled as a lumped mass that experiences the same displacement as the barbell. Due to the translation of the barbell, two prismatic joints at each side are included to allow the vertical displacement. Therefore, the hand is only able to move vertically and the horizontal distance between the shoulder and the hand, d, remains constant. Prior to the execution of the bench press exercise, the volunteer was instructed to realize a scapular retraction. This preparatory movement helps at maintaining the shoulder flat on the bench. In this way, during the exercise the shoulder did not show any appreciable vertical displacement. Because the barbell is constrained to move linearly in the vertical plane in the Smith machine, the stability requirements are lower than in the traditional bench press with barbell or dumbbell [35], in which other muscle groups (biceps brachii and deltoid) work to stabilize the barbell in the mediolateral and anterior-posterior directions [9,35]. Additionally, since the horizontal translation and rotation of the barbell is constrained, the effects of the natural upper limb asymmetry in the barbell displacements are eliminated. Equal properties (lengths, masses and moments of inertia) have been used for both upper limbs. Then, the bench press exercise is assumed to be performed in a symmetrical manner [33]. Based on this symmetry, any half of the model depicted in Fig. 1 can be used to analyse the dynamics during the weight lift.

In Fig. 1, s_4 is the vertical position of the hand, the position of the shoulder is fixed and β is the relative angle between the forearm and the arm. The model described has only one independent geometrical parameter. This means that given a value of the independent parameter one can determine the mechanism position. Usually, in a bench press exercise the hand position (coordinate s_4) is measured using optical encoders [36] or linear transducer [37] while the elbow angle, β, is measured using a goniometer [32].

Fig. 2 shows the simplified model that will be used in this research due to the symmetry of the full model. Note that the athlete is assumed to be grasping the barbell tightly. Therefore, the horizontal sliding of the wrist along the barbell is not allowed and, as a consequence, a constraint force appears between body four and the vertical guide in Fig. 2. The mechanism in Fig. 2 is overactuated by torques M_2 and M_3 to lift a load m_4 from a height s_4^0 to a larger height s_4^f. Note that m_4 includes the weight of the hand and half of the weight of the barbell. As the mechanism has one degree of freedom, there should be an infinite number of combinations of M_2 and M_3 that allows lifting the weight m_4 from s_4^0 to s_4^f in the same manner. Thus, posing this dynamical problem as an optimization problem may help to find an appropriate distribution of M_2 and M_3 for a given trajectory.

In this research, the optimization will be performed over a time interval of duration t_f. During that period of time, M_2 and M_3 are allowed to vary with time. All the required time derivatives of dynamical variables of the model are achieved by discretizing the simulation interval using finite difference formulae.

3. Test session

As it will explained in the next sections, the optimization framework proposed in this document utilizes the motion measured in a test session as a reference. In the test session, a trained man with 5 years of experience in bench press lifting volunteered to participate in this study. Subject's age, height and body mass were 22 years, 1.79 m and 75 kg, respectively. The bench press exercise was done with a Smith machine with isoinertial resistance following a procedure similar to that

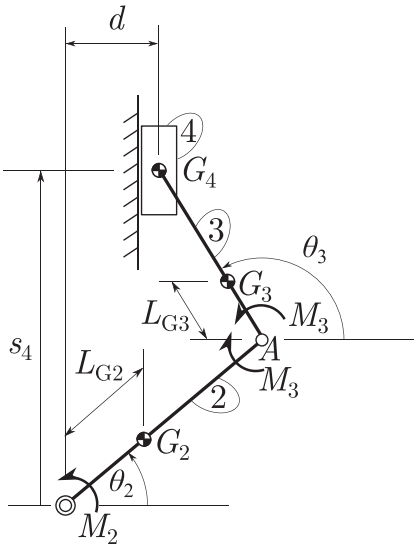

Fig. 2. Reduced bench press model based on the assumption of symmetry along the anatomical sagittal plane.

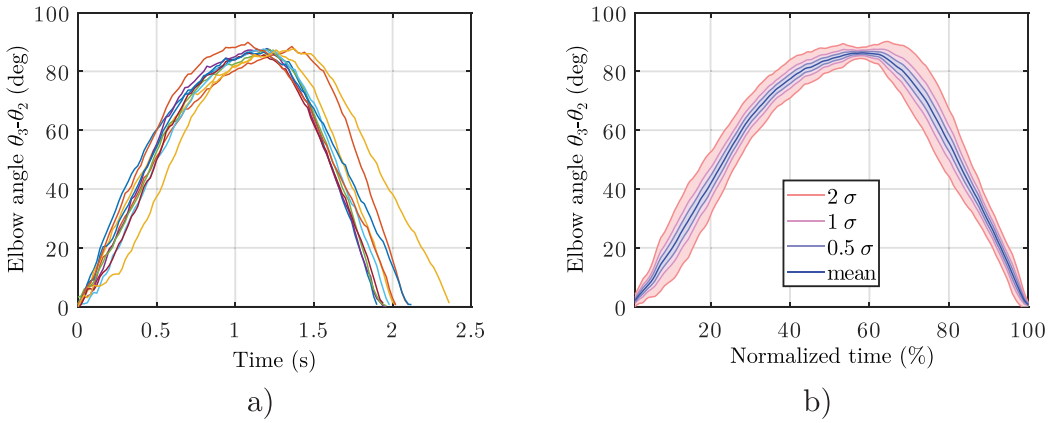

Fig. 3. Experimental results obtained for the angle $\theta_3 - \theta_2$ (supplementary angle of β) in ten repetitions of the bench press exercise: a) all repetitions and b) mean and deviations.

described by Muyor et al. [38]. At the start of each repetition the subject is asked to lift the barbell, to maintain it with the elbow extended and to begin the eccentric phase (drop the weight), which ends when the bars is 2 cm close to the subject's chest. Then, the concentric phase is carried out until the weight reaches the starting position. The results described below correspond to a session of 12 repetitions using a mass of 66 kg, which was the 60% of the one repetition maximum (1RM). This intensity (60% 1RM) has been thoroughly used in several studies for monitoring the bench press performance [38–40]. Grip distance was 150% of the distance between acromiums. Regarding the instrumentation, the elbow angle was measured with a electrogoniometer (Biometrics Ltd., Newport, UK) placed on the lateral side of the ulna and the humerus. Since the guiding system of the Smith machine forces the barbell to move in a vertical plane and the athlete was laying on the bench with the shoulders slightly above the plane defined by the guides, the motion of the arms mainly happened in the vertical plane.

From the twelve repetitions, the first and the last were excluded to avoid the possible bias induced by the knowledge of the volunteer of being the first and the last of the series. Therefore, a set of ten repetitions is used in what follows. Fig. 3a) shows the selected repetitions starting from the same time point. As can be seen in the figure, the durations of the repetitions are slightly different. Fig. 3b) shows a significant dispersion in the measured motions. Such dispersion is

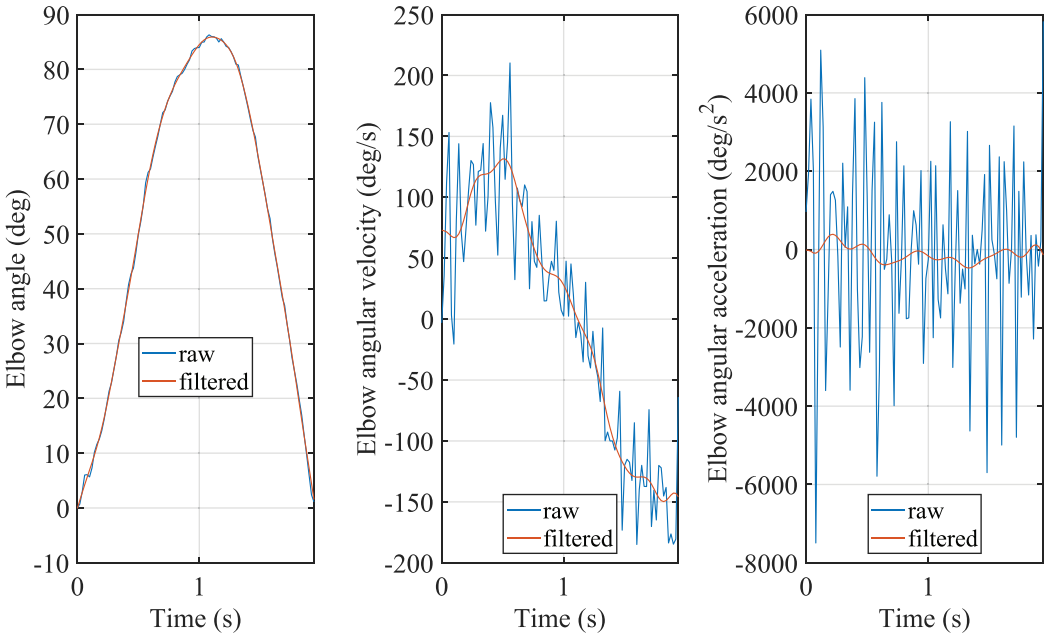

Fig. 4. Electrogoniometer raw signal and the calculated angular velocity and acceleration (in blue) besides its filtered curves (in red). (For interpretation of the references to colour in this figure legend, the reader is referred to the web version of this article.)

Table 1
Values of the model parameters.

Parameter	Value
Arm length (L_2)	0.330 m
Arm proximal CG length (L_{G2})	0.144 m
Arm distal CG length ($L_2 - L_{G2}$)	0.186 m
Arm mass (m_2)	2.10 kg
Arm CG inertia moment (I_{G2})	0.0237 kg m^2
Forearm length (L_3)	0.260 m
Forearm proximal CG length (L_{G3})	0.112 m
Forearm distal CG length ($L_3 - L_{G3}$)	0.148 m
Forearm mass (m_3)	1.20 kg
Forearm CG inertia moment (I_{G3})	0.0074 kg m^2
Shoulder-wrist distance (d)	0.208 m
Hand mass (m_4)	0.450 kg

attributed to different sources, among which are the errors of the measurement system, the presence of skin artifacts and the different trajectories followed by the athlete. The most important of those dispersion sources is that the athlete could not repeat the same trajectory for each exercise execution. However, the measurement system was accurate enough to detect differences between the different executions. In order to find a mean representative motion, the selected ten repetitions have been statistically analysed after normalizing each time vector. Therefore, in Fig. 3b) a mean motion is represented against a normalized time vector expressed in percentage, including the bands of 0.5, 1 and 2 standard deviations. According to Fig. 3b) the dispersion of the measurements significantly decreases at the frontier of the concentric and eccentric phases of the exercise, with an average value of 86 degrees of elbow flexion. In addition, a larger dispersion in the results is found at the beginning of the concentric phase.

The measures of the electrogoniometer, sampled at 50 Hz, include a certain level of noise from different sources that may difficult the inverse dynamics simulations. As an example, the measures of the electrogoniometer during the eighth repetition are shown in Fig. 4. The signal from the goniometer has been back and forth filtered with a sixth order Butterworth filter with cut-off frequency of 4 Hz in order to avoid noisy velocity and acceleration curves. This way the goniometer signal is smoothed without causing lag and leading to smooth and representative time derivatives.

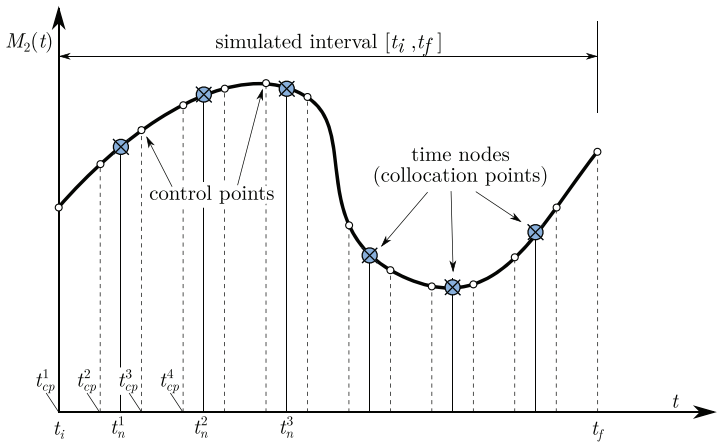

Fig. 5. Example of the distribution of time nodes and control points in the shoulder joint torque, M_2, where the number of control points is larger than that of time nodes.

The mechanical properties of the body segments included in the model are listed in Table 1. The lengths of the upper limb segments were measured during the test session, while the inertial properties: masses, moments of inertia and positions of the centres of gravity of the arm and forearm, have been estimated from the data provided by Contini [41] and Winter [42]. The arm and forearm lengths used in the model have been those measured for the dominant arm of the volunteer.

4. Optimization framework

This section describes the optimization framework designed to simulate a realization of the bench press exercise. The main idea of the simulation by optimization is to parametrize the trajectories and controls to find the values that minimize a certain cost function and satisfy the equations of motion at certain collocation points. Therefore, the trajectories and controls are unknowns in this problem. In order to generate realistic trajectories, one may either reduce the domain of possible solutions by properly adding constraints or add a quadratic term in the cost function to encourage the model to stay close to a reference trajectory. The last option has been taken in this research and a quadratic term that measure deviations with respect to a reference motion as explained in Refs. [19,24] has been included. To do that, a reference motion is obtained as explained in the previous section, by recording the measures of the electrogoniometer in a realization of the bench press exercise by a trained subject.

For the simulation by parameter optimization, the following two different set of points are used:

- Time nodes. This set of points is used to parametrize the trajectories and the controls. The number of time nodes depends on the smoothness of the parametrized function. This number is denoted as N_n in this work and it is in general smaller than the number of control points, N_{cp}. The time nodes are equidistant in time.
- Control points. This set of N_{cp} points is used to enforce the fulfilment of the equations of motion. In principle, the equations of motion are not satisfied in between control points. Therefore, for a realistic simulation the gaps between control points should be as small as possible or, in order words, the number of control points should be as large as possible. Control points are equidistant in time, too.

The number of nodal values should be as large as possible to have a good definition of the parametrized variables, but as small as possible to keep the size of the vector of design variables to a reasonable size. On the other hand, if the gaps between control points are large, the violation of constraints may be unacceptable. The idea of having more control points than time nodes is to find a compromise between a high definition of dynamic variables and an accurate fulfillment of constraints. Based on previous experience [19], the increase in the number of control points has a less negative effect on the computational efficiency of the numerical optimization problem and, therefore, the number of control points can be increased further than that of time nodes without significantly decreasing the computational performance.

To better explain the distribution of time node and control points, a typical situation has been represented in Fig. 5. The vector of time nodes is defined as follows:

$$\boldsymbol{t_n} = \left[t_n^1, \quad t_n^2, \quad \ldots \quad t_n^{N_n}\right] \tag{1}$$

where N_n is the number of time nodes. On the other hand, the control points time vector is written as follows:

$$\boldsymbol{t_{cp}} = \left[t_{cp}^1, \quad t_{cp}^2, \quad \ldots \quad t_{cp}^{N_{cp}}\right] \tag{2}$$

where as explained before $N_n < N_{cp}$. For simplicity, in this research the number of control points has been defined equal to the number of points where the goniometer recorded a value of the elbow angle. For example, the eighth realization of the bench press was performed with 96 measurements of the elbow angle, that is, $N_{cp} = 96$. For the optimization, the SQP [43] algorithm included in the `fmincon` subroutine in Matlab© has been used showing to converge to a solution in a reasonably low number of iterations in all cases.

4.1. Description of the vector of design variables

Once the trajectories and controls are parametrized, the vector of design variables of the optimization problem can be built as follows:

$$\boldsymbol{\chi} = \left[\boldsymbol{\theta}_2^T,\ \boldsymbol{M}_2^T,\ \boldsymbol{M}_3^T\right]^T \tag{3}$$

The vector of design variables is built of $3 \times N_n$ scalar variables. The components of the vector of design variables are built of nodal values as follows:

$$\boldsymbol{\theta}_2 = \left[\theta_2(t_n^1),\quad \theta_2(t_n^2),\quad \ldots\quad \theta_2(t_n^{N_n})\right]^T \tag{4}$$

$$\boldsymbol{M}_2 = \left[M_2(t_n^1),\quad M_2(t_n^2),\quad \ldots\quad M_2(t_n^{N_n})\right]^T \tag{5}$$

$$\boldsymbol{M}_3 = \left[M_3(t_n^1),\quad M_3(t_n^2),\quad \ldots\quad M_3(t_n^{N_n})\right]^T \tag{6}$$

Note that given the vector $\boldsymbol{\theta}_2$, since the mechanism has one degree of freedom, it is possible to calculate the value of any other kinematic variable at any time node.

The reconstruction of the trajectory $\theta_2(t)$ and the controls $M_2(t)$ and $M_3(t)$ at any time t is made by using cubic spline and the nodal values. This way a smooth description of trajectories and controls is achieved.

In this research, the total time, t_f, will be fixed to moderately low real values, what helps at teaching an appropriate performance of the exercise to an athlete who will have more control of movements and will be able to maintain the technique during several repetitions. Nevertheless, the exercise duration could be included in the vector of design variables to investigate the influence of this parameter on the exercise.

4.2. Numerical differentiation

Since the equations of motion are written in terms of positions, velocities and accelerations, the time derivatives of θ_2 will be required for the evaluation of the equations of motion. In order to do that, numerical differentiation is used to estimate the time derivatives of the design variable $\boldsymbol{\theta}_2$. The time increment can be calculated from the number of control points and the time duration. The following centred finite differences formula is used to calculate the time derivative of a variable, for instance θ_2, as

$$\dot{\theta}_2^j = \frac{\theta_2^{j+1} - \theta_2^{j-1}}{2h} + O(h^2) \approx \frac{\theta_2^{j+1} - \theta_2^{j-1}}{2h}, \quad j = 2,\ 3, \ldots N_{cp} - 1 \tag{7}$$

where the notation $\theta_2^j = \theta_2(t_{cp}^j)$ has been used for the sake of simplicity. The numerical derivative at the first and last time instant are calculated by using forward and backward formulae of the same error order, that is, the same order of accuracy, respectively. Thus, the time derivative of θ_2 at the first time instant, t_{cp}^1, is evaluated as

$$\dot{\theta}_2^1 = \frac{-3\theta_2^1 + 4\theta_2^2 - \theta_2^3}{2h} + O(h^2) \approx \frac{-3\theta_2^1 + 4\theta_2^2 - \theta_2^3}{2h} \tag{8}$$

while the time derivative of θ_2 at the last time instant, $t_{cp}^{N_{cp}}$, is evaluated as

$$\dot{\theta}_2^{N_{cp}} = \frac{3\theta_2^{N_{cp}} - 4\theta_2^{N_{cp}-1} + \theta_2^{N_{cp}-2}}{2h} + O(h^2) \approx \frac{3\theta_2^{N_{cp}} - 4\theta_2^{N_{cp}-1} + \theta_2^{N_{cp}-2}}{2h} \tag{9}$$

The same finite difference formulae are used to obtain the second time derivative of θ_2, that is, the first time derivative of $\dot{\theta}_2$. There is no need to numerically differentiate other coordinates as θ_3 or s_4, since given one velocity and one acceleration one can calculate any other velocity and acceleration in a single degree of freedom mechanism.

4.3. Objective function

There might be different criteria that could be used to formulate an objective function for the optimization. Such criteria should resemble the muscle recruitment criteria of the Central Nervous System and may be based on pain, energy consumption and/or aesthetics [19]. In this research, since the physical activity studied is intended at training strength, a muscle recruitment criterion based on the mechanical power seems to be appropriate. Being able to do a strength exercise with the least amount of energy consumption would result in less muscle fatigue and therefore greater endurance. On

the other hand, one can also seek to perform the movements in a way that involves the smallest joint torque values. This might be of interest to decrease neuromuscular stress, to avoid overloads, and then to reduce the risk of injury; and it could also be applicable to create appropriate rehabilitation programs. By defining appropriate cost functions, the methodology proposed could also be used to generate motions that tend to achieve the maximum effort for muscle training. Based on the previous explanations, two different muscle recruitment criteria will be studied, one based on joint torque values and another based on mechanical power values. Each cost function will be constructed as a sum of different components as it is explained in this section.

As a feasible joint torque recruitment criterion, the dynamic effort cost function used for lifting simulation by Xiang et al. [44] is utilized in this research. It is formulated as follows:

$$f_d(\boldsymbol{\chi}) = \int_0^{t_f} (M_2(t))^2 + (M_3(t))^2 \mathrm{d}t \tag{10}$$

where t_f is the duration of the exercise. This value is taken from the reference motion, but could be changed to explore the performance at higher velocities.

In addition, as stated above, it makes sense to study other criteria as the mechanical power developed by the joint torques. This idea has been used by other authors in the literature, see for example Ref. [45]. In this research, the mechanical power is used to form a cost function component as follows:

$$f_p(\boldsymbol{\chi}) = \int_0^{t_f} \left(M_2(t)\dot{\theta}_2(t)\right)^2 + \left(M_3(t)\left(\dot{\theta}_3(t) - \dot{\theta}_2(t)\right)\right)^2 \mathrm{d}t \tag{11}$$

During optimization, it is possible to find converged solutions showing an oscillatory behavior in the joint torques. In addition, it is reasonable to consider that the rate of joint torque development must be limited. In other words, humans can not modify their joint torques as fast as desired since muscle force is dependent on contraction velocity [46]. In order to include these two effects, the following component is also included:

$$f_r(\boldsymbol{\chi}) = \int_0^{t_f} \left(\dot{M}_2(t)\right)^2 + \left(\dot{M}_3(t)\right)^2 \mathrm{d}t \tag{12}$$

where $\dot{M}_2(t)$ and $\dot{M}_3(t)$ are the joint torque rates that can be evaluated numerically during optimization using finite difference formulae as explained in Section 4.2. The consideration of the joint torque rates to achieve solutions by optimization can be found also in the literature, see for example Ref. [47].

In addition to the cost functions in Eqs. (10) to (12), a quadratic cost function intended at driving the model to stay close to a real trajectory will be added. Such component is based on the deviation from a reference motion that has been measured in the lab and has been presented previously in Section 3. The deviation from the reference motion is formulated as follows:

$$J(\boldsymbol{\chi}) = \int_0^{t_f} \left(\frac{\theta_2(t) - \bar{\theta}_2(t)}{\max\left[\bar{\theta}_2(t)\right] - \min\left[\bar{\theta}_2(t)\right]} \right)^2 \mathrm{d}t \tag{13}$$

where $\bar{\theta}_2(t)$ is the reference motion, which is defined as the mean motion depicted in Fig. 3. It is worth of note here that including $J(\boldsymbol{\chi})$ in the cost function does not force the generated motion to be equal to the one measured in the lab. Instead the generated motion will show some similarity with the reference motion.

Finally, the functions $f_d(\boldsymbol{\chi})$, $f_p(\boldsymbol{\chi})$, $f_r(\boldsymbol{\chi})$ and $J(\boldsymbol{\chi})$ are combined with the help of weighting factors to formulate two different cost functions. The first cost function is mainly based on dynamic effort as

$$f_{dyn}(\boldsymbol{\chi}) = \omega_d \frac{f_d(\boldsymbol{\chi})}{f_d^0} + \omega_r \frac{f_r(\boldsymbol{\chi})}{f_r^0} + \omega_J J(\boldsymbol{\chi}) \tag{14}$$

where ω_d, ω_r and ω_J are weighting factors used to give different importance to the dynamic effort, the joint torque rate component or the measure of the similarity to the reference motion. In addition, f_d^0 and f_r^0 are reference values used to bring the quotients to magnitudes that are similar to that of $J(\boldsymbol{\chi})$. The previous cost function is referred in this document as *cost function based on dynamic effort*, since that is its main component.

The second cost function considered in this research is based on mechanical power as

$$f_{pow}(\boldsymbol{\chi}) = \omega_p \frac{f_p(\boldsymbol{\chi})}{f_p^0} + \omega_r \frac{f_r(\boldsymbol{\chi})}{f_r^0} + \omega_J J(\boldsymbol{\chi}) \tag{15}$$

where ω_p is a weighting factor and f_p^0 is a reference value used again to bring the magnitude of the first quotient in the right hand side of Eq. (15) to the order of $J(\boldsymbol{\chi})$. It is worth of noting here that due to the construction of component $J(\boldsymbol{\chi})$, its order of magnitude is unity ($\sim 10^0$). The previous cost function is referred in this document as *cost function based on squared mechanical power*, since that is its main component.

4.4. Bounds

As in every optimization problem, a set of lower and upper bounds may be fixed. The lower and upper bounds are defined in terms of the trajectory of θ_2 and joint torques, M_2 and M_3 as

$$-\pi/2 \le \theta_2^j \le \pi/2, \quad j = 1,\ 2, \ldots N_n \tag{16}$$

$$M_2^{min} \le M_2^j \le M_2^{max}, \quad j = 1,\ 2, \ldots N_n \tag{17}$$

$$M_3^{min} \le M_3^j \le M_3^{max}, \quad j = 1,\ 2, \ldots N_n \tag{18}$$

In this research, Ref. [48] has been used to select the values of the bounds. According to this reference, normal values of $M_2^{\min} = -91$ Nm, $M_2^{\max} = 127$ Nm, $M_3^{\min} = -70$ Nm and $M_3^{\max} = 101$ Nm have been used. Note that the positive sign indicates flexion while negative indicates extension. The lower and upper bounds that apply to the independent coordinate, θ_2, have been selected to avoid non feasible positions.

4.5. Constraints

The optimization problem is subject to a number of constraints, being some linear and other nonlinear. The nature of these constraints is mainly the kinematics and the dynamics of the bench press exercise. The constraints added to the optimal control problem are summarized next.

4.5.1. Linear constraints

The exercise should start and end at the same angular position. Therefore, a linear constraint is added to enforce such condition. It is written as follows:

$$\theta_2\left(t_{cp}^1\right) - \theta_2\left(t_{cp}^{N_{cp}}\right) = 0 \tag{19}$$

4.5.2. Nonlinear constraints

As it will be seen in this section, the number of nonlinear constraints is larger than that of the linear ones. The nonlinear constraints arising from the kinematics are first described. The first constraint is a inequality equation which is used to express that the realization of the exercise should lift the load at least the same height as the reference motion, that is,

$$\max[s_4(t)] - \min[s_4(t)] \le H \tag{20}$$

where H is the distance along which the load is lifted in the reference motion. Notice that this constraint is nonlinear since s_4, see Fig. 2, has to be calculated using the following position constraints:

$$L_2 \cos\theta_2 + L_3 \cos\theta_3 = d \tag{21}$$

$$L_2 \sin\theta_2 + L_3 \sin\theta_3 = s_4 \tag{22}$$

where L_2, L_3 and d are defined in Fig. 2. Since the elbow extension is limited to the alignment of the arm and the forearm, it is required to ensure that for any time t the angle of the forearm, $\theta_3(t)$, is larger than the angle of the arm, $\theta_2(t)$. This constraint will prevent *hyperextension* in the simulated motion. This relation must hold at any control point as

$$\theta_2(t_{cp}^j) - \theta_3(t_{cp}^j) \le 0 \quad j = 1,\ 2 \ldots N_{cp} \tag{23}$$

In addition, the exercise should start at the same height, s_4^0, as the reference motion. This leads to the following constraint:

$$s_4\left(t_{cp}^1\right) = s_4^0 \tag{24}$$

The initial velocity at the beginning of the load drop should be zero, since the subject start the exercise from rest. This condition can be numerically expressed as follows:

$$-3s_4\left(t_{cp}^1\right) + 4s_4\left(t_{cp}^2\right) - s_4\left(t_{cp}^3\right) = 0 \tag{25}$$

where the finite difference formula of Eq. (8) has been applied to $\dot{s}_4\left(t_{cp}^1\right)$. Note that the first control point, t_{cp}^1, is located at the beginning of the exercise when the athlete start dropping the load from rest.

Finally, the constraint equations arising from the equations of motion have to be fulfilled at each time point. The equations of motion will be written in terms of the independent coordinate θ_2, instead of the probably most natural choice s_4, to avoid singular configurations in the search domain. Using the parameters of Table 1, it is easy to show that the possible singular configurations are out of the interval defined by the lower and upper bounds of θ_2. To find a compact set of

constraints, the Virtual Power Principle (VPP) is used to avoid dealing with constraint forces and minimizing the number of dynamical constraints. In the case represented in Fig. 2, the application of the VPP leads to the following equation:

$$M_2\omega_{21}^{*} + m_2\boldsymbol{g}\cdot\boldsymbol{v}_{21}^{G2*} - m_2\boldsymbol{a}_{21}^{G2}\cdot\boldsymbol{v}_{21}^{G2*} - I_{G2}\alpha_{21}\omega_{21}^{*} - M_3\omega_{21}^{*} + M_3\omega_{31}^{*} + m_3\boldsymbol{g}\cdot\boldsymbol{v}_{31}^{G3*} - m_3\boldsymbol{a}_{31}^{G3}\cdot\boldsymbol{v}_{31}^{G3*} - I_{G3}\alpha_{31}\omega_{31}^{*} + m_4\boldsymbol{g}\cdot\boldsymbol{v}_{41}^{G4*} - m_4\boldsymbol{a}_{41}^{G4}\cdot\boldsymbol{v}_{41}^{G4*} = 0 \tag{26}$$

where the subscript ij means 'of body i with respect to body j'. In what follows, subscript 1 is given to the fixed reference frame. Observe that since the motion is planar, any applied or inertial torque as well as any angular velocity vector has only one non-null component corresponding to the direction perpendicular to the plane of motion. The virtual power of torques is therefore written using only the non-null component of the involved torque and angular velocity vectors appearing as scalar quantities in Eq. (26). Virtual velocities can be expressed as $\omega_{i1}^{*} = J_{Ri}(s_4,\theta_2,\theta_3)\dot{\theta}_2^{*}$ $(i=2,3)$ and $\boldsymbol{v}_{i1}^{Gi*} = \boldsymbol{J}_{Ti}(s_4,\theta_2,\theta_3)\dot{\theta}_2^{*}$ $(i=2,3,4)$, being J_{Ri} and $\boldsymbol{J}_{Ti}$ the jacobian matrices of rotation and translation of body i, respectively. As it is known for holonomic systems, the jacobian matrices depend only on generalized coordinates (s_4, θ_2, θ_3). In addition, the accelerations in Eq. (26) can be expressed as $\alpha_{i1} = J_{Ri}(s_4,\theta_2,\theta_3)\ddot{\theta}_2 + \dot{J}_{Ri}(s_4,\theta_2,\theta_3)\dot{\theta}_2$ $(i=2,3)$ and $\boldsymbol{a}_{i1}^{Gi} = \boldsymbol{J}_{Ti}(s_4,\theta_2,\theta_3)\ddot{\theta}_2 + \dot{\boldsymbol{J}}_{Ti}(s_4,\theta_2,\theta_3)\dot{\theta}_2$ $(i=2,3,4)$. Introducing the previous kinematic relations in the equation derived from the Virtual Power Principle, one can find a nonlinear equation, which depends on coordinates s_4, θ_2 and θ_3, on the independent velocity, $\dot{\theta}_2$, on the independent acceleration, $\ddot{\theta}_2$, and on the driving torques M_2 and M_3. Such equation can be written as follows:

$$g^{dyn}(\theta_2,\theta_3,s_4,\dot{\theta}_2,\ddot{\theta}_2,M_2,M_3) = m(\theta_2,\theta_3,s_4)\ddot{\theta}_2 - q(\theta_2,\theta_3,s_4,\dot{\theta}_2,\dot{\theta}_3,\dot{s}_4,M_2,M_3) \tag{27}$$

where $m(\theta_2,\ \theta_3,\ s_4)$ is the generalized mass term, which is detailed in Eq. (A.1) of Appendix A and $q(\theta_2,\theta_3,s_4,\dot{\theta}_2,\dot{\theta}_3,\dot{s}_4,M_2,M_3)$ is a generalized force term including gravity forces, applied joint torques and Coriolis and quadratic velocity terms. Its expression is detailed in the Eq. (A.2) of Appendix A. The equation of motion must be fulfilled in all time points as

$$g^{dyn}(\theta_2^j,\theta_3^j,s_4^j,\dot{\theta}_2^j,\ddot{\theta}_2^j,M_2^j,M_3^j) = 0, \quad j = 1,\ 2,\ldots N_{cp} \tag{28}$$

5. Numerical results

In this section, some numerical simulations are used to demonstrate the performance of the optimal control problem presented in the previous sections. The first simulation is carried out for a reference motion that elapses for 1.94 s. The load lifted is fixed to 66 kg, coinciding with the load lifted by the subject during the test session. This simulation is aimed at demonstrating if the performance of the trained subject can be improved by the optimal control solver, according to the objective functions. Prior to the numerical optimization, the design variables as well as the constraints were scaled so that the resulting normalized variables and constraints are of order one.

It is important to emphasize that the weight factors are established based on the authors' subjective perception of the importance of each component of the cost function. Including the muscle contraction and activation dynamics would help at avoiding physiologically unrealistic trajectories. However, since the muscle dynamics has not been modeled, to avoid unrealistic solution it has been attributed the same importance to the deviation from the reference motion than to the combination of the other components of the cost function. The importance of each component is estimated as 50% for $J(\boldsymbol{\chi})$, 45% for $f_d(\boldsymbol{\chi})/f_d^0$ (or $f_p(\boldsymbol{\chi})/f_p^0$) and 5% for $f_r(\boldsymbol{\chi})/f_r^0$. As explained before, the muscle torque rate component has been included to prevent oscillations in the torque, what is achieved with a small contribution of this term.

5.1. Cost function based on dynamic effort

This section describes the results predicted when the cost function based on dynamic effort, as detailed in Eq. (14), is used. The values of the weighting factor are selected as $\omega_d = 0.45$, $\omega_r = 0.05$ and $\omega_J = 0.5$ while f_d is equal to 10^3 Nm^{2}s. Although in this case the joint torque rate component is not needed to avoid oscillations in the muscle torque, the values of the weights are the same to those of the next simulation to allow for a fair comparison. The number of control points used in this simulation is 96 while the number of time nodes is 60.

Fig. 6 shows the simulated shoulder torque. It has to be explained that the initial estimation used in the optimization is found by inverse dynamics using the reference motion and static optimization, see Ref. [18], by minimizing at each time point the measure $\sqrt{M_2^2 + M_3^2}$. Such initial estimation is dependent on the reference motion, therefore does not correspond to an optimal realization of the exercise. Note that the results of the static optimization are used as a reasonable initial estimate here. A more accurate estimate could be achieved if an external reaction force could be measured. In such case, M_2 and M_3 could be calculated by using Eq. (28) together with an equilibrium equation involving the measured constraint force and the torques. In Fig. 6, the torques are represented against time and stroke, where stroke means the distance traveled by the barbell.

Note that while Fig. 6b) seems to show a peak at 50% of total stroke, it must be emphasized that this is due to the slow variation of the displacement at that part of the cycle. In fact, Fig. 6a) shows that, at the same part of the cycle, the slope of $M_2(t)$ changes smoothly from positive to negative and, therefore, the muscle torque is differentiable, suggesting continuous jerk as it is physiologically expected.

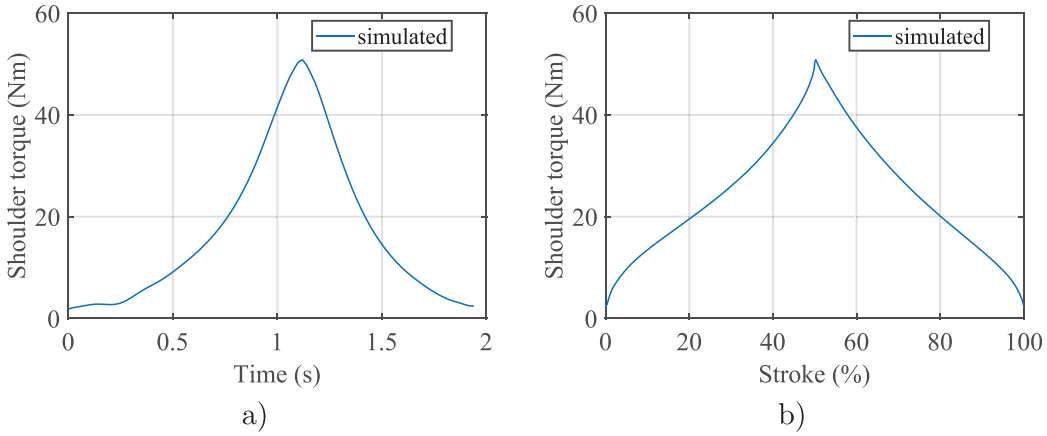

Fig. 6. Shoulder torque simulated using $f_{dyn}(\boldsymbol{\chi})$ as cost function: a) represented against time; b) represented against stroke.

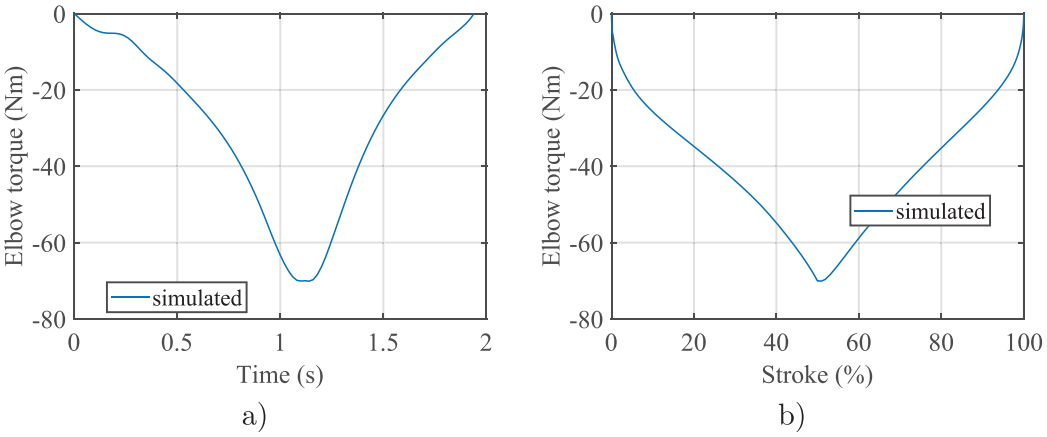

Fig. 7. Elbow torque simulated usingg $f_{dyn}(\boldsymbol{\chi})$ as cost function: a) represented against time; b) represented against stroke.

Fig. 7 shows the simulated elbow torque. It is interesting to emphasize that the realization of the exercise obtained by optimization enforces the elbow torque to achieve the maximum allowable torque as defined by the lower and upper bounds, which can be seen clearly in Fig. 7a) where the elbow torque becomes flat after time 1.0 s. In addition, the elbow torque is larger than the shoulder torque throughout the exercise. This behavior does not seem to approach a realistic realization of the exercise since, according to the literature, the shoulder has a larger torque capacity than the elbow, and the muscle excitation (EMG activity) during the bench press exercise is also higher for the shoulder muscles [38,49–51].

As a representative result, the vertical position of the barbell, represented by coordinate s_4 in Fig. 2, is shown in Figs. 8 a) and b). As shown in the figure, the realization generated by optimization shows larger slopes resulting in a more explosive realization. Also, the variation of barbell displacement is concentrated in the central part of the exercise. It is interesting to observe that while the term $J(\boldsymbol{\chi})$ of the cost function helps at finding trajectories by optimization, the reference and simulated trajectories are not necessarily very similar. It may be explained that Fig. 8b) shows an interesting perspective of the exercise, where both graphs are represented along the stroke of the reference motion. The straight lines correspond to the reference motion and, therefore if the optimal control problem can not significantly improve such reference motion, the simulated motion should be close the straight lines. In other words, this plot shows how different from the reference motion the trajectory generated by optimization needs to be to minimize the performance criterion included in the cost function.

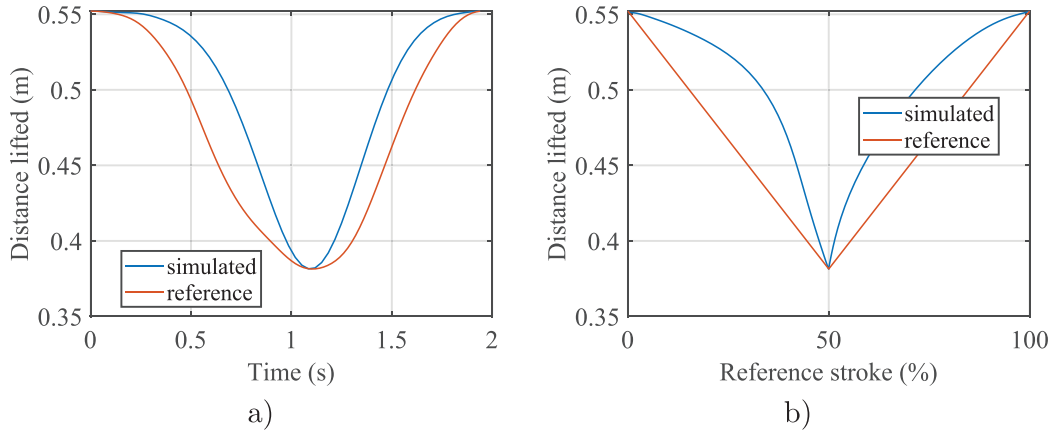

Fig. 8. Comparison of the distance lifted in the reference and the simulated motion using $f_{dyn}(\boldsymbol{\chi})$ as cost function: a) represented against time; b) represented against stroke.

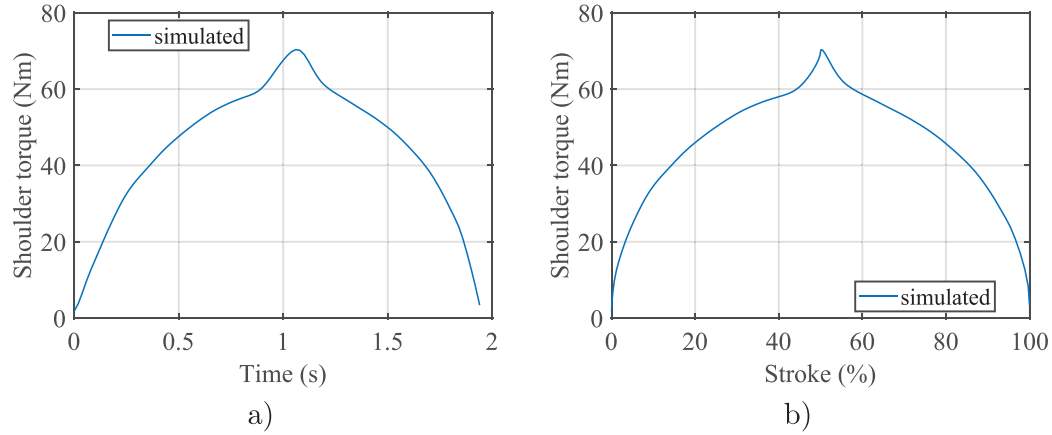

Fig. 9. Shoulder torque simulated using $f_{pow}(\boldsymbol{\chi})$ as cost function: a) represented against time; b) represented against stroke.

5.2. Cost function based on the integral of the squared mechanical power

This section describes the results predicted when the cost function detailed in Eq. (15) is used. The values of the weighting factors are selected as $\omega_p = .45$, $\omega_r = 0.05$ and $\omega_J = 0.5$ while f_p is equal to 10^3 W^{2}s and f_r is equal to 10^4 Nm^2/s. In this case, the joint torque rate component has been used to prevent solutions of the optimization for the joint torques with high frequency oscillations.

Regarding the joint torques obtained, unlike what happens with the dynamic effort criterion, the shoulder shows larger contribution to the movement than the elbow, which is a more realistic result. This can be observed by comparing Figs. 9 to 10. In addition, in order to follow this distribution the patterns obtained for $M_2(t)$ and $M_3(t)$ have lower slopes than those obtained when using the dynamic effort criterion. In such smoother way, the subject is able to control the exercise achieving minimal values of the mechanical power. Note that the shoulder and elbow torques used as initial estimates to obtain the torques in Figs. 9 and 10 are found by using inverse dynamics and a static optimization aiming at minimizing at each time point the cost function $\sqrt{M_2^2 + M_3^2}$. Therefore, they are not direct measures of the torques.

Both shoulder and elbow torque curves show a small peak in the middle of the cycle due to the fast change of direction of the barbell in the frontier of the eccentric and concentric phases.

A relevant result is that, minimizing the squared mechanical power, the predicted motion remains closer to the motion measured in the lab during the test sessions. As can be seen in Fig. 11a, the barbell displacement, $s_4(t)$, in the simulation

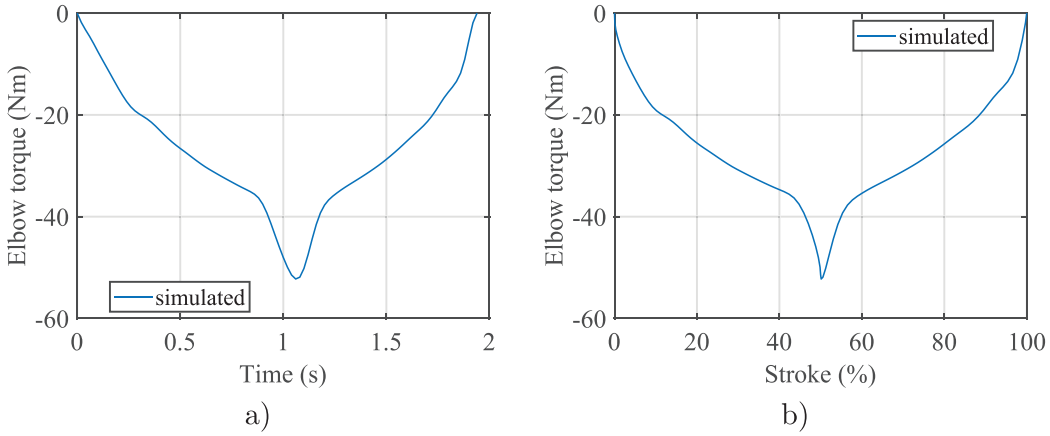

Fig. 10. Elbow torque simulated using $f_{pow}(\boldsymbol{\chi})$ as cost function: a) represented against time; b) represented against stroke.

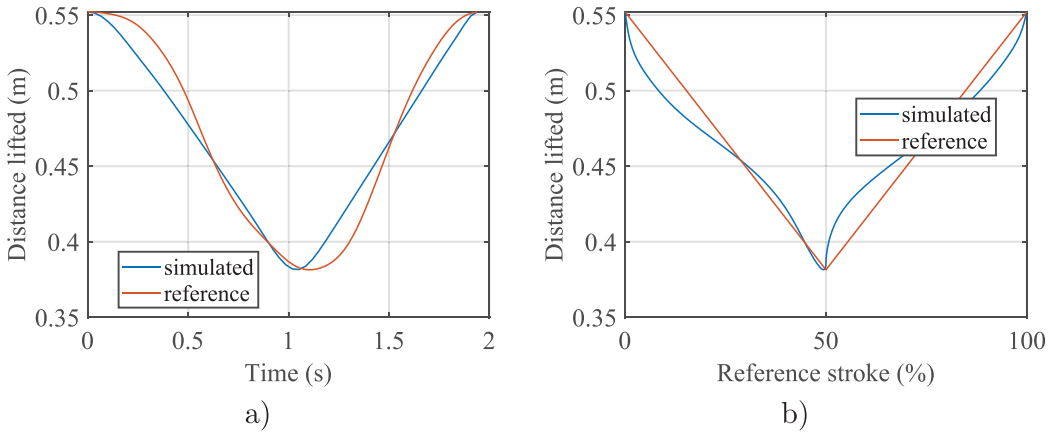

Fig. 11. Comparison of the distance lifted in the reference and the simulated motion using $f_{pow}(\boldsymbol{\chi})$ as cost function: a) represented against time; b) represented against stroke.

closely follows the curve obtained from the angle measured with the goniometer. From this result it could be concluded that the execution of the exercise is adequate in terms of the energy expenditure of the volunteer. On the other hand, some differences between both curves can be observed in Fig. 11a. A first difference is that in the predicted motion the time duration of the eccentric and the concentric phases of the exercise tend to be equalized, which makes sense from an energetic point of view, while in the measured motion the eccentric phase took longer than the concentric one. Another difference to mention is that the subject adapts the change from the eccentric phase to the concentric phase faster when using this criterion, i.e. the barbell stays less time in its lowest position near the chest. This pattern can also be seen in the predicted $s_4(t)$ curve (Fig. 11), which differs significantly from the results of the dynamic effort criterion as can be concluded when comparing Figs. 8 and 11.

The dynamic effort cost function results in lower values of the shoulder torque and higher values of the elbow torque as compared with the results of the squared mechanical power cost function. However, the sum of the squares of the shoulder and elbow torques, $(M_2(t))^2 + (M_3(t))^2$, achieves lower values for the results of the dynamic effort criterion than for those of the squared mechanical power cost function as it is expected.

5.3. Effect of lifted weight

The optimal control problem is solved in this case for different values of the weight of the lifted load using the two mentioned cost functions. In all the simulations the reference motion has been the same. As it is expected, when the lifted

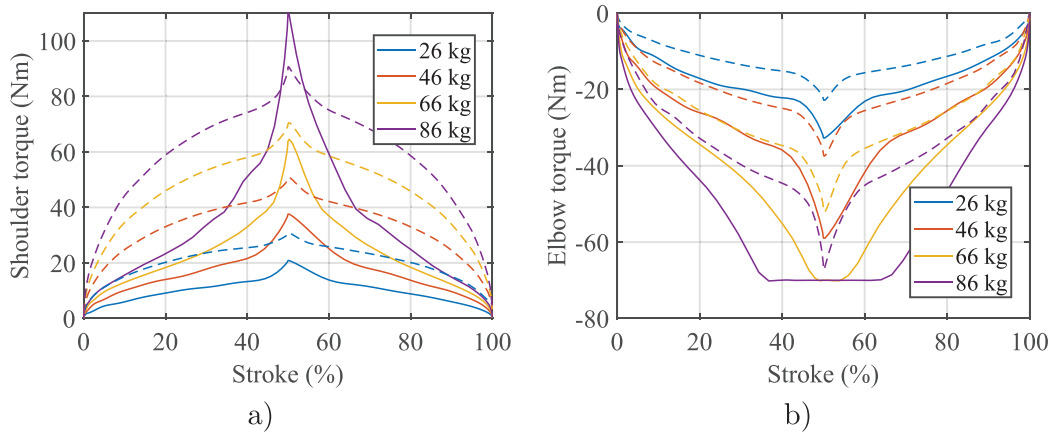

Fig. 12. Joint torques simulated for different values of the weight lifted: a) shoulder torque; b) elbow torque. Solid lines correspond to solutions of the optimization problem generated with cost function based on the dynamic effort while dashed lines correspond to solutions of the optimization problem generated with cost function based on the squared mechanical power.

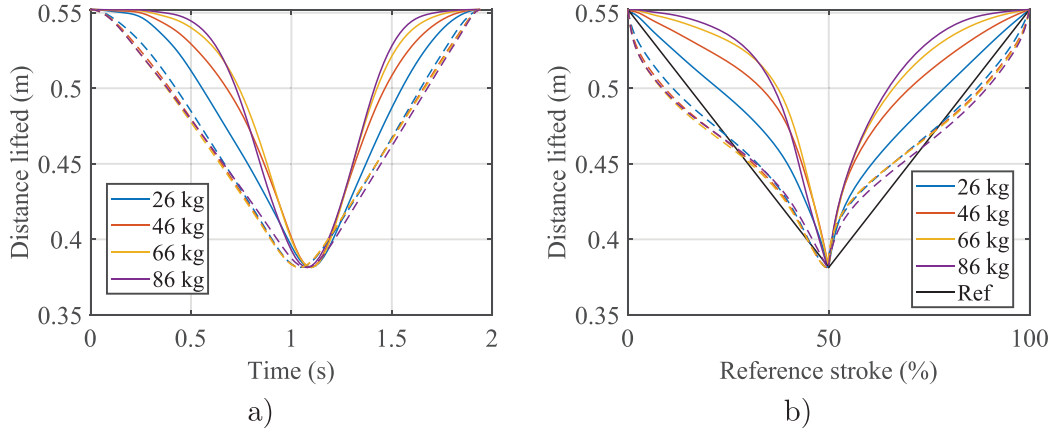

Fig. 13. Distance lifted for different values of the weight lifted. Solid lines correspond to solutions of the optimization problem generated with cost function based on the dynamic effort while dashed lines correspond to solutions of the optimization problem generated with cost function based on the squared mechanical power.

load is smaller than the one used in the previous simulations, the performance generated by optimization can be achieved with smaller values of the joint torques, see Fig. 12a and b. In particular, it is interesting that for the weights 26 kg and 46 kg, the elbow torque does not achieve the limiting value of −70 Nm.

The largest differences are found for the dynamic effort criterion, where the maximum shoulder torque grows from 20.8 Nm for a load of 26 kg to 109.5 Nm for a load of 86 kg, while for the mechanical power criterion the maximum shoulder torque grows from 30.7 Nm for a load of 26 kg to 90.7 Nm for a load of 86 kg.

Fig. 13a and b show the different solutions in terms of the position of the barbell. As shown in Fig. 13a the larger the load the larger are the slopes of the $s_4(t)$ curve. On the other hand, Fig. 13b shows how different to the reference motion is each one of the $s_4(t)$ curves when represented against the reference stroke.

5.4. Effect of exercise duration

The exercise duration is an interesting parameter since it is related to velocities and accelerations and therefore affects the equations of motion using the two previously mentioned cost functions. The simulations shown in this case are obtained for values of the weight load of 46 kg. The reference motion is the same in all cases. As it is shown in Fig. 14a and b

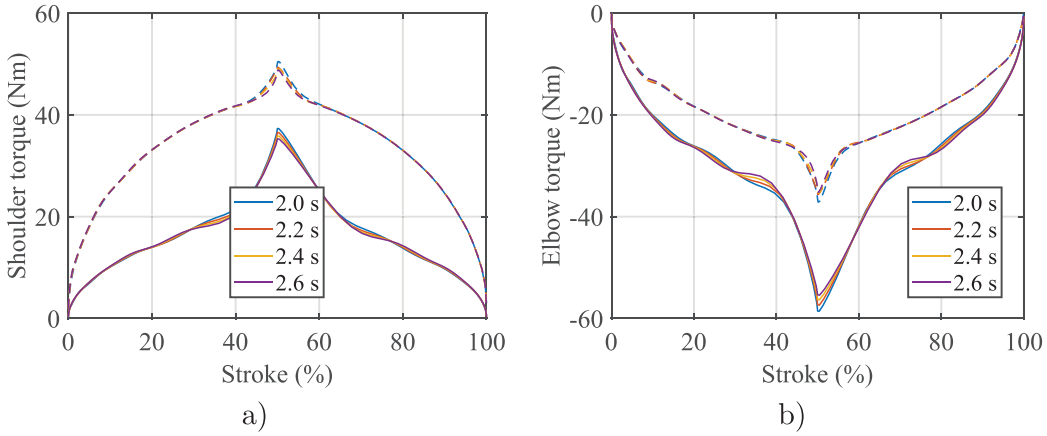

Fig. 14. Joint torques simulated for different values of the exercise duration: a) shoulder torque; b) elbow torque. Solid lines correspond to solutions of the optimization problem generated with cost function based on the dynamic effort while dashed lines correspond to solutions of the optimization problem generated with cost function based on the squared mechanical power.

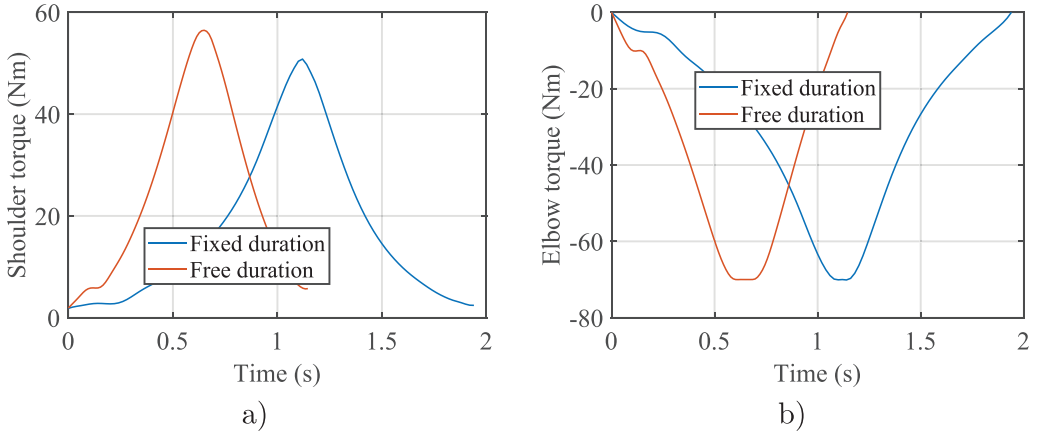

Fig. 15. Comparison of shoulder and elbow torques obtained using $f_{dyn}(\boldsymbol{\chi})$ as cost function for a fixed duration and for the duration obtained by optimization.

changing the exercise duration from 2.0 s to 2.6 s does not result in significant modification of the torque distribution generated by optimization. Interestingly, the different solutions show a common trend what suggests that the optimization framework shown a reasonable convergent behavior.

To investigate the influence of the exercise duration, t_f, on the solution of the optimization, this parameter is included in the vector of design variables, which is now written as follows:

$$\boldsymbol{\chi} = \left[\boldsymbol{\theta}_2^T,\ \boldsymbol{M}_2^T,\ \boldsymbol{M}_3^T,\ t_f\right]^T \tag{29}$$

The lower and upper bounds selected for the new design variable, t_f, are 0 and twice the exercise duration for the reference motion. When using $f_{dyn}(\boldsymbol{\chi})$ as cost function a solution of the optimization is found for a shorter time as represented in Fig. 15. For very fast realizations of the exercise, the inertial effects result in larger joint torques and therefore in larger values of the dynamic effort function. On the other hand, when the exercise realization is performed very slow, the inertial effects are probably negligible, but the athlete has still to move the load quasi-statically and therefore the muscle torques can not decrease below certain values. In such case, the area below the curve $\sqrt{(M_2(t))^2 + (M_3(t))^2}$ would increase with the exercise duration. It is found that the exercise duration obtained by optimization seems to be around 1.2 s. When the cost function $f_{pow}(\boldsymbol{\chi})$ is used, it is observed that the value of the total time, t_f, obtained by optimization is always at the upper bound, no matter the large the upper bound is. This is because the mechanical power involves a product of the torque

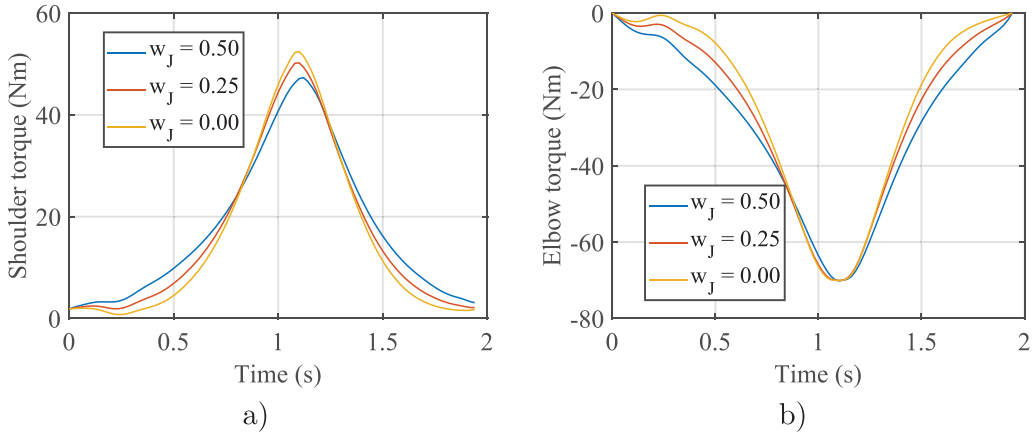

Fig. 16. Comparative of results obtained using $f_{dyn}(\boldsymbol{\chi})$ for three different combinations of weight factors: i) $\omega_d = 0.45$, $\omega_r = 0.05$ and $\omega_J = 0.5$; ii) $\omega_d = 0.675$, $\omega_r = 0.075$ and $\omega_J = 0.25$; and iii) $\omega_d = 0.9$, $\omega_r = 0.1$ and $\omega_J = 0.0$. Figure a) shows the shoulder torque, while Figure b) shows the elbow torque.

and the joint angular velocity. Then, if the velocity is small the squared power function will be small. Finally, the slowest the exercise is realized the lower the cost function value is. Therefore, including the total time as a design variable does not provide meaningful solutions for the $f_{pow}(\boldsymbol{\chi})$ criterion.

5.5. Influence of $J(\chi)$ on the generated motion

In the previous simulations, the combination of weights has been unique ($\omega_d = 0.45$, $\omega_r = 0.05$ and $\omega_J = 0.5$). Such combination of weights attributes the same importance to the deviation from a reference motion as to the sum of the dynamic effort and the muscle torque rate components. It is clear that the reference motion has an influence on the generated torque pattern. To investigate the influence of $J(\boldsymbol{\chi})$ in the solution, three simulations have been carried out with different combinations of the weight factors: i) $\omega_d = 0.45$, $\omega_r = 0.05$ and $\omega_J = 0.5$; ii) $\omega_d = 0.675$, $\omega_r = 0.075$ and $\omega_J = 0.25$; and iii) $\omega_d = 0.9$, $\omega_r = 0.1$ and $\omega_J = 0.0$. A comparative of the results obtained using $f_{dyn}(\boldsymbol{\chi})$ and three combinations of weights can be found in Fig. 16. It can be seen that the combination of weights that gives the largest importance to $J(\boldsymbol{\chi})$ provides the smoothest shoulder torque history. The relative differences in the maximum shoulder torque are within a 10%.

The same three combinations of weights have been used with the cost function based on the squared mechanical power, $f_{pow}(\boldsymbol{\chi})$. In such case, the shoulder and elbow torque did not vary with the value of ω_J. That is, the problem converged to the same solution. In addition, it was observed that both when using $f_{dyn}(\boldsymbol{\chi})$ and $f_{pow}(\boldsymbol{\chi})$, the use of $J(\boldsymbol{\chi})$ in the solution, by setting ω_J different from zero, resulted in a faster convergence to the solution (fewer iterations of the optimization solver).

6. Summary and conclusion

This paper presents a methodology for designing trajectories and controls by optimization for the bench press exercise. In particular, this methodology is intended at understanding the appropriate performance of the bench press exercise in conditions of training to gain endurance or to perform the exercise in the safest manner, that is avoiding overloads. The optimal control problem is formulated as a nonlinear constrained optimization problem. The design variables are the trajectory and the joint torques at the time nodes. A number of kinematic and dynamic constraints must be fulfilled by the solution at a set of collocation points, the so-called control points. Two different cost functions are formulated in this study. One is based on the dynamic effort and the other on the mechanical power developed.

The optimization framework previously described is used to study the bench press performance from the point of view of a subject who trains to gain endurance or to avoid joint torque overloads. To that end, the two criteria have been tested and compared by generating trajectories and joint torques by optimization following a reference realization of the bench press in the lab. It must be emphasized that the combination of values used for the weight factors plays an important role on the solution. Therefore, the trajectories and muscle torque histories obtained by optimization must be interpreted as optimal for the particular combination of weights used. It is found that minimizing the dynamic effort leads to trajectories that are executed with larger values of the elbow torque, what might not be a realistic distribution of the joint torques according to the literature. It must be noted that the bench press model used did not included muscle properties, and that the results obtained may vary by incorporating realistic muscle models. As a future work, the implementation of a reduced muscle model in the bench press exercise, with the use of muscle-torque-generators as described in Ref. [48] is expected to enhance the prediction achieved by the proposed optimization framework.

Unlike the dynamic effort criterion, the squared mechanical power criterion provides results that adjust to more realistic trajectories and joint torque distribution. Specifically, the predicted motion resembles reasonably well the motion of the volunteer in the tests. This suggests that the subject performs the exercise efficiently in terms of its energy cost. In this case, the proposed methodology is useful for predicting the performance of strength exercises performed under conditions of endurance improvement.

In this work, the effect of the lifted weight and the time duration of the exercise have been studied. The load variation results in significantly different joint torque histories, where as explained before the dynamic effort criteria provide larger values for the elbow torque, leading to its saturation at the maximum achievable elbow torque defined.

The natural differences in mechanical properties of the left and right arms will result in slight variations in the predicted values for the shoulder angle and the muscle torques. As a future step, a sensitivity analysis will be performed on a full model of the bench press exercise to see the influence of the natural asymmetry of the human body.

Analysing the influence of the different possible joint torque recruitment criteria, as the dynamic effort or the mechanical power criterion, by carrying out simulations allows the possibility to study coordination aspects of human activities and shows a potential application of this approach to the design of rehabilitation therapies and to the design of training programs. The results of the optimization offer relevant information in the planning of sport training as well as in the prescription of physical exercise since they provide an appropriate velocity profile to decrease the effort made, which translates into a decrease in the fatigue of the considered muscle groups, and they offer information on muscular work during the exercise stroke. Thus, it will be possible to ask the athlete to adapt the execution speed in a certain phase of the exercise to the trajectory generated by optimization. In addition, by EMG monitoring it will be possible to train the athlete in focusing on particular muscle groups during certain phases of the exercise. Efficient methods as presented in this research for the simulation of human activities are most important to understand the way the human body executes some interesting physical tasks.

Declaration of Competing Interest

The authors declare that they do not have any conflict of interest

Acknowledgment

This work has been partially funded by the Spanish Ministerio de Economía y Competitividad under the project DEP2016-80296-R (AEI/FEDER, UE).

Appendix A. Terms of the equations of motion

The generalized mass is written as follows:

$$\begin{aligned} m(\theta_2,\theta_3,s_4) = \frac{1}{{L_3}^2 \sin(\theta_3)^2}\big(& I_{G3}{L_2}^2\sin(\theta_2)^2 + I_{G2}{L_3}^2\sin(\theta_3)^2 + {L_2}^2{L_3}^2 m_3 \sin(\theta_3)^2 \\ & + {L_2}^2{L_3}^2 m_4 \sin(\theta_2)^2 + {L_2}^2{L_3}^2 m_4 \sin(\theta_3)^2 + {L_2}^2{L_{G3}}^2 m_3 \sin(\theta_2)^2 + {L_3}^2{L_{G2}}^2 m_2 \sin(\theta_3)^2 \\ & - 2{L_2}^2{L_3}^2 m_4 \sin(\theta_2)^2 \sin(\theta_3)^2 - 2{L_2}^2 L_3 L_{G3} m_3 \sin(\theta_2)^2 \sin(\theta_3)^2 \\ & - 2{L_2}^2{L_3}^2 m_4 \cos(\theta_2)\cos(\theta_3)\sin(\theta_2)\sin(\theta_3) - 2{L_2}^2 L_3 L_{G3} m_3 \cos(\theta_2)\cos(\theta_3)\sin(\theta_2)\sin(\theta_3)\big) \end{aligned} \tag{A.1}$$

while the generalized force vector is written as follows:

$$\begin{aligned} & q(\theta_2,\theta_3,s_4,\dot\theta_2,\dot\theta_3,\dot s_4,M_2,M_3) \\ & = -\frac{1}{{L_3}^2\sin(\theta_3)^3}\big({L_3}^2 M_3 \sin(\theta_3)^3 \\ & - {L_3}^2 M_2 \sin(\theta_3)^3 + L_2 L_3 M_3 \sin(\theta_2)\sin(\theta_3)^2 + L_2{L_3}^2 g m_3 \cos(\theta_2)\sin(\theta_3)^3 \\ & + L_2{L_3}^2 g m_4 \cos(\theta_2)\sin(\theta_3)^3 + {L_3}^2 L_{G2} g m_2 \cos(\theta_2)\sin(\theta_3)^3 - I_{G3}{L_2}^2\dot\theta_2\dot\theta_3\cos(\theta_3)\sin(\theta_2)^2 \\ & - L_2{L_3}^3 m_4 \dot\theta_3^2 \cos(\theta_2)\sin(\theta_3)^4 + I_{G3}{L_2}^2\dot\theta_2^2\cos(\theta_2)\sin(\theta_2)\sin(\theta_3) \\ & - L_2{L_3}^2 L_{G3} m_3 \dot\theta_3^2 \cos(\theta_2)\sin(\theta_3)^4 - L_2{L_3}^2 g m_4 \cos(\theta_3)\sin(\theta_2)\sin(\theta_3)^2 \\ & - {L_2}^2{L_3}^2 m_4 \dot\theta_2^2 \cos(\theta_2)^2\cos(\theta_3)\sin(\theta_3)^2 + {L_2}^2{L_3}^2 m_4 \dot\theta_2^2\cos(\theta_3)\sin(\theta_2)^2\sin(\theta_3)^2 \\ & - {L_2}^2{L_3}^2 m_4 \dot\theta_2\dot\theta_3\cos(\theta_3)^3\sin(\theta_2)^2 - {L_2}^2{L_{G3}}^2 m_3\dot\theta_2\dot\theta_3\cos(\theta_3)^3\sin(\theta_2)^2 \\ & + L_2{L_3}^3 m_4\dot\theta_3^2\cos(\theta_3)\sin(\theta_2)\sin(\theta_3)^3 - {L_2}^2{L_3}^2 m_4\dot\theta_2^2\cos(\theta_2)\sin(\theta_2)\sin(\theta_3)^3 \\ & + {L_2}^2{L_{G3}}^2 m_3\dot\theta_2^2\cos(\theta_2)\sin(\theta_2)\sin(\theta_3)^3 - L_2 L_3 L_{G3} g m_3 \cos(\theta_3)\sin(\theta_2)\sin(\theta_3)^2 \end{aligned}$$

$$
\begin{aligned}
&-{L_2}^2 L_3 L_{G3} m_3 \dot{\theta}_2^2 \cos(\theta_2)^2 \cos(\theta_3) \sin(\theta_3)^2 + {L_2}^2 L_3 L_{G3} m_3 \dot{\theta}_2^2 \cos(\theta_3) \sin(\theta_2)^2 \sin(\theta_3)^2 \\
&-{L_2}^2 {L_{G3}}^2 m_3 \dot{\theta}_2 \dot{\theta}_3 \cos(\theta_3) \sin(\theta_2)^2 \sin(\theta_3)^2 + {L_2}^2 {L_3}^2 m_4 \dot{\theta}_2^2 \cos(\theta_2) \cos(\theta_3)^2 \sin(\theta_2) \sin(\theta_3) \\
&+{L_2}^2 {L_{G3}}^2 m_3 \dot{\theta}_2^2 \cos(\theta_2) \cos(\theta_3)^2 \sin(\theta_2) \sin(\theta_3) - 2 {L_2}^2 L_3 L_{G3} m_3 \dot{\theta}_2^2 \cos(\theta_2) \sin(\theta_2) \sin(\theta_3)^3 \\
&+L_2 {L_3}^2 L_{G3} m_3 \dot{\theta}_3^2 \cos(\theta_3) \sin(\theta_2) \sin(\theta_3)^3 + {L_2}^2 L_3 L_{G3} m_3 \dot{\theta}_2 \dot{\theta}_3 \cos(\theta_3) \sin(\theta_2)^2 \sin(\theta_3)^2 \\
&+{L_2}^2 {L_3}^2 m_4 \dot{\theta}_2 \dot{\theta}_3 \cos(\theta_2) \cos(\theta_3)^2 \sin(\theta_2) \sin(\theta_3) \\
&+{L_2}^2 L_3 L_{G3} m_3 \dot{\theta}_2 \dot{\theta}_3 \cos(\theta_2) \cos(\theta_3)^2 \sin(\theta_2) \sin(\theta_3)\Big)
\end{aligned} \tag{A.2}
$$

References

[1] J. Padulo, G. Laffaye, A. Chaouachi, K. Chamari, Bench press exercise: the key points, J. Sports Med. Phys. Fitness 55 (6) (2015) 604–608.
[2] O. Gomo, R. Van Den Tillaar, The effects of grip width on sticking region in bench press, J. Sports Sci. 34 (3) (2016) 232–238, doi:10.1080/02640414.2015.1046395.
[3] E. Schick, J. Coburn, L. Brown, D. Judelson, A. Khamoui, T. Tran, B. Uribe, A comparison of muscle activation between a smith machine and free weight bench press, J. Strength Cond. Res. 24 (3) (2010) 779–784, doi:10.1519/JSC.0b013e3181cc2237.
[4] E. Iglesias, D. Boullosa, X. Dopico, E. Carballeira, Analysis of factors that influence the maximum number of repetitions in two upper-body resistance exercises: curl biceps and bench press, J. Strength Cond. Res. 24 (6) (2010) 1566–1572, doi:10.1519/JSC.0b013e3181d8eabe.
[5] S. De La Motte, T. Gribbin, P. Lisman, K. Murphy, P. Deuster, Systematic review of the association between physical fitness and musculoskeletal injury risk: part 2 - muscular endurance and muscular strength, J. Strength Cond. Res. 31 (11) (2017) 3218–3234, doi:10.1519/JSC.0000000000002174.
[6] R.D. Stevenson, A.G. Siddall, P.F. Turner, J.L. Bilzon, Physical employment standards for uk firefighters: minimum muscular strength and endurance requirement, J. Occup. Environ. Med. 59 (1) (2017) 74–79, doi:10.1097/JOM.0000000000000926.
[7] W.J. Kraemer, D.L. Hatfield, S.J. Fleck, Strength training, in: L.E. Brown (Ed.), Human Kinetics, 2007.
[8] R. Squadrone, R. Rodano, E. Preatoni, Comparison of velocity and power output data derived from an inertial based system and an optical encoder during squat lifts in a weight room setting, J. Sports Med. Phys. Fitness 52 (1) (2012) 40–46.
[9] D. Behm, K. Anderson, The role of instability with resistance training, J. Strength Cond. Res. 20 (3) (2006) 716–722.
[10] N. Madsen, T. McLaughlin, Kinematic factors influencing performance and injury risk in the bench press exercise, Med. Sci. Sports Exerc. 16 (4) (1984) 376–381.
[11] P. Cormie, G. Mccaulley, N. Triplett, J. Mcbride, Optimal loading for maximal power output during lower-body resistance exercises, Med. Sci. Sports Exerc. 39 (2) (2007) 340–349.
[12] D. García-Vallejo, A. Alcayde, J. López-Martínez, F. Montoya, Detection of communities within the multibody system dynamics network and analysis of their relations, Symmetry 11 (2019) 1525, doi:10.3390/sym11121525.
[13] M. Ackermann, W. Schiehlen, Dynamic analysis of human gait disorder and metabolical cost estimation, Arch. Appl. Mech. 75 (10–12) (2006) 569–594.
[14] R. Al Nazer, T. Rantalainen, A. Heinonen, H. Sievänen, A. Mikkola, Flexible multibody simulation approach in the analysis of tibial strain during walking, J. Biomech. 41 (2008) 1036–1043.
[15] M. Peasgood, J. McPhee, E. Kubica, Stabilization and energy optimization of a dynamic walking gait simulation, in: Proceedings of the ASME International Design Engineering Technical Conferences and Computers and Information in Engineering Conference - DETC2005, vol. 6 A, 2005, pp. 339–349.
[16] S. Rodrigo, J. Ambrosio, M. Da Silva, O. Penisi, Analysis of human gait based on multibody formulations and optimization tools, Mech. Based Des. Struct. Mach. 36 (4) (2008) 446–477.
[17] G. Bessonnet, P. Seguin, P. Sardain, A parametric optimization approach to walking pattern synthesis, Int. J. Rob. Res. 24 (7) (2005) 523–536.
[18] M. Ackermann, Dynamics and Energetics of Walking with Prostheses, Shaker-Verlag, Aachen, 2007.
[19] D. García-Vallejo, W. Schiehlen, 3D-Simulation of human walking by parameter optimization, Arch. Appl. Mech. 82 (2012) 533–556.
[20] D. García-Vallejo, J. Font-Llagunes, W. Schiehlen, Dynamical analysis and design of active orthoses for spinal cord injured subjects by aesthetic and energetic optimization, Nonlinear Dyn. 84 (2) (2016) 559–581.
[21] A. Falisse, G. Serrancolí, C. Dembia, J. Gillis, I. Jonkers, F. De Groote, Rapid predictive simulations with complex musculoskeletal models suggest that diverse healthy and pathological human gaits can emerge from similar control strategies, J. R. Soc. Interface 16 (157) (2019).
[22] A. Falisse, G. Serrancolí, C. Dembia, J. Gillis, F. DeGroote, Algorithmic differentiation improves the computational efficiency of OpenSim-based trajectory optimization of human movement, PLoS ONE 14 (10) (2019).
[23] G. Serrancolí, A. Falisse, C. Dembia, J. Vantilt, K. Tanghe, D. Lefeber, I. Jonkers, J. De Schutter, F. De Groote, Subject-exoskeleton contact model calibration leads to accurate interaction force predictions, IEEE Trans. Neural Syst. Rehabil. Eng. 27 (8) (2019) 1597–1605.
[24] A. Van Den Bogert, M. Hupperets, H. Schlarb, B. Krabbe, Predictive musculoskeletal simulation using optimal control: effects of added limb mass on energy cost and kinematics of walking and running, Proc. Inst. Mech.Eng. Part P 226 (2) (2012) 123–133.
[25] L. Sanchez-Medina, C. Perez, J. Gonzalez-Badillo, Importance of the propulsive phase in strength assessment, Int. J. Sports Med. 31 (2) (2010) 123–129, doi:10.1055/s-0029-1242815.
[26] J. Calatayud, J. Vinstrup, M. Jakobsen, E. Sundstrup, J. Carlos Colado, L. Andersen, Attentional focus and grip width influences on bench press resistance training, Percept. Mot. Skills 125 (2) (2018) 265–277, doi:10.1177/0031512517747773.
[27] J. Calatayud, J. Vinstrup, M. Jakobsen, E. Sundstrup, J. Colado, L. Andersen, Influence of different attentional focus on EMG amplitude and contraction duration during the bench press at different speeds, J. Sports Sci. 36 (10) (2018) 1162–1166, doi:10.1080/02640414.2017.1363403.
[28] D. Frost, J. Cronin, R. Newton, A biomechanical evaluation of resistance: fundamental concepts for training and sports performance, Sports Med. 40 (4) (2010) 303–326, doi:10.2165/11319420-000000000-00000.
[29] S. Sánchez-Salinas, C. Núñez Torres, J. López-Martínez, D. García-Vallejo, J. Muyor, Design and analysis of a constant-force bench press, Mech. Mach. Theory 142 (2019) 103612.
[30] B. Kim, A.D. Deshpande, Design of nonlinear rotational stiffness using a noncircular pulley-spring mechanism, J. Mech. Rob. 6 (4) (2014).
[31] A. Schepelmann, K.A. Geberth, H. Geyer, Compact nonlinear springs with user defined torque-deflection profiles for series elastic actuators, in: 2014 IEEE International Conference on Robotics and Automation (ICRA), IEEE, 2014, pp. 3411–3416.
[32] A. Rahmani, O. Rambaud, M. Bourdin, J.-P. Mariot, A virtual model of the bench press exercise, J. Biomech. 42 (11) (2009) 1610–1615, doi:10.1016/j.jbiomech.2009.04.036.
[33] A. Rahmani, B. Morel, P. Samozino, A Simple Method for Measuring Force, Velocity, Power and Force-Velocity Profile of Upper Limbs, Springer International Publishing, 2018, doi:10.1007/978-3-319-05633-3_7.
[34] D. Baker, Comparison of upper-body strength and power between professional and college-aged rugby league players., J. Strength Cond. Res. 15 (2001) 30–35.
[35] A. Saeterbakken, R. van den Tillaar, M. Fimland, A comparison of muscle activity and 1-RM strength of three chest-press exercises with different stability requirements, J. Sports Sci. 29 (5) (2011) 533–538.
[36] O. Rambaud, A. Rahmani, B. Moyen, M. Bourdin, Importance of uper-limb inertia in calculating concentric bench press foce, J. Strength Cond. Res. 22 (2) (2008) 383–389, doi:10.1123/ijspp.2016-0226.

[37] A. García-Ramos, S. Jaric, P. Padial, B. Feriche, Force-velocity relationship of upper body muscles: traditional versus ballistic bench press, J. Appl. Biomech. 32 (2) (2016) 178–185, doi:10.1123/jab.2015-0162.
[38] J. Muyor, D. Rodríguez-Ridao, I. Martín-Fuentes, J. Antequera-Vique, Evaluation and comparison of electromyographic activity in bench press with feet on the ground and active hip flexion, PLoS ONE 14 (6) (2019), doi:10.1371/journal.pone.0218209.
[39] J. González-Badillo, J. Yañez García, R. Mora-Custodio, D. Rodríguez-Rosell, Velocity loss as a variable for monitoring resistance exercise, Int. J. Sports Med. 38 (3) (2017) 217–225, doi:10.1055/s-0042-120324.
[40] G. Moras, S. Rodríguez-Jiménez, A. Busquets, J. Tous-Fajardo, M. Pozzo, I. Mujika, A metronome for controlling the mean velocity during the bench press exercise, J. Strength Cond. Res. 23 (3) (2009) 926–931, doi:10.1519/JSC.0b013e3181a0752d.
[41] R. Contini, Body segment parameters, part ii., Artif. Limbs 16 (1972) 1–19.
[42] D. Winter, Biomechanics and Motor Control of Human Movement, fourth ed., John Wiley & Sons, Inc., New York, 2009.
[43] J. Nocedal, S. Wright, Numerical Optimization, second ed., Springer Series in Operations Research, Springer Verlag, 2006.
[44] Y. Xiang, J. Arora, S. Rahmatalla, T. Marler, R. Bhatt, K. Abdel-Malek, Human lifting simulation using a multi-objective optimization approach, Multibody Syst. Dyn. 23 (4) (2010) 431–451, doi:10.1007/s11044-009-9186-y.
[45] F. Leboeuf, G. Bessonnet, P. Seguin, P. Lacouture, Energetic versus sthenic optimality criteria for gymnastic movement synthesis, Multibody Syst. Dyn. 16 (3) (2006) 213–236.
[46] A. Hill, The heat of shortening and the dynamic constants of muscle, Proc. R. Soc. London Ser. B 126 (1938) 136–195.
[47] M. Pandy, M. Pandy, F. Anderson, Optimal control of non-ballistic muscular movements: a constraint-based performance criterion for rising from a chair, J. Biomech. Eng. 117 (1) (1995) 15–26.
[48] M. Millard, A. Emonds, M. Harant, K. Mombaur, A reduced muscle model and planar musculoskeletal model fit for the simulation of whole-body movements, J. Biomech. 89 (2019) 11–20, doi:10.1016/j.jbiomech.2019.04.004.
[49] P. Gentil, J. Fisher, J. Steele, A review of the acute effects and long-term adaptations of single-and multi-joint exercises during resistance training, Sports Med. 47 (5) (2017) 843–855.
[50] P.W. Marshall, B.A. Murphy, Increased deltoid and abdominal muscle activity during swiss ball bench press, J. Strength Cond. Res. 20 (4) (2006) 745–750.
[51] Y.d.A.C. Campos, S.F.d. Silva, Comparison of electromyographic activity during the bench press and barbell pullover exercises, Motriz. J. Phys. Educ. 20 (2) (2014) 200–205.

Capítulo 5

Diseño y estudio experimental de una máquina de acondicionamiento muscular basada en un mecanismo de fuerza constante.

Diseño y Estudio Experimental de una Máquina de Acondicionamiento Muscular basada en un Mecanismo de Fuerza Constante.

Resumen

En el entrenamiento de la fuerza o la resistencia, se buscan patrones de movimiento de la carga y la activación que se adapten al objetivo del entrenamiento. Tradicionalmente, se emplean máquinas con masa móvil (pesas) como sistema de carga. Una característica de este tipo de máquinas es la aparición de fuerzas de inercia debidas a la aceleración de la masa móvil, lo que hace que la fuerza que ejerce el deportista pueda ser muy variable a lo largo del ejercicio.

En este trabajo se propone el empleo de un mecanismo de fuerza constante como sistema de carga en una máquina de acondicionamiento muscular tipo Smith. El propósito de este nuevo sistema es el de reducir las fuerzas de inercia y conseguir una curva de fuerza más constante. En primer lugar, se lleva a cabo la fabricación de sendas unidades de mecanismos de fuerza constante y su incorporacion a una máquina Smith. Para la caracterización del sistema se obtienen las curvas de fuerza-desplazamiento a velocidad constante. En segundo lugar, se llevan a cabo mediciones en el ejercicio de press de banca, realizado con el sistema tradicional de peso libre y con el nuevo sistema de carga propuesto. Los resultados muestran diferencias significativas en las curvas de fuerza para ambos sistemas de carga. Con el sistema de carga propuesto los picos de fuerza son menores y se reduce sustancialmente la fase de frenado.

Palabras clave: Máquina de acondicionamiento muscular, press de banca, mecanismo de fuerza constante, entrenamiento de la fuerza

1. Introducción

Las máquinas de acondicionamiento muscular son muy utilizadas en el entrenamiento de la fuerza y de la resistencia, y pueden encontrarse en la mayoría de los gimnasios y centros deportivos. Los ejercicios en las máquinas de musculación tienen como objetivo aumentar la fuerza muscular [1], mejorar la resistencia [2], la potencia muscular y la hipertrofia, o potenciar una característica concreta para un deporte específico [3]

Las máquinas de acondicionamiento muscular y su funcionalidad se caracteriza por sus diferentes diseños. Aparte de los tipos de ejercicios para los que están diseñadas, la característica más relevante de una máquina de acondicionamiento muscular es la naturaleza de la fuente de resistencia. Frost y col. [4] hicieron

una clasificación de las máquinas de acondicionamiento muscular basada en la fuente de la fuerza de resistencia, describiendo tres categorías diferentes: (1) resistencia isoinercial o de peso libre, en la que la fuerza de resistencia se debe a la masa en elevación y a la fuerza de la gravedad; (2) resistencia adaptativa, como las máquinas hidráulicas e isocinéticas, en las que se puede ejercer el máximo esfuerzo durante la fase concéntrica del ejercicio, pero a velocidad constante; y (3) resistencia variable. En este último grupo se incluyen los sistemas basados en levas, bandas elásticas y cadenas, y las máquinas neumáticas.

La cinemática del ejercicio, la cinética y la activación muscular son diferentes para cada tipo de fuente de resistencia, y deben elegirse en función del objetivo del entrenamiento. En este sentido, varios estudios han analizado y comparado el entrenamiento de resistencia con peso libre y de resistencia variable [5, 6, 7, 8, 9, 10, 11], o evaluaron el uso de la resistencia adaptativa en diferentes ejercicios [12, 13, 14, 15, 16, 17].

La resistencia isoinercial o de peso libre es el método más extendido para mejorar la fuerza y la capacidad de potencia [4]. La resistencia de peso libre también se conoce como de resistencia constante, donde el término "constante" puede deberse al uso de masas constantes (pesas), que no cambian a lo largo del ejercicio. Sin embargo, el uso de pesas implica fuerzas de inercia variables que son soportadas por el atleta. En la ejecución del ejercicio, se requiere una aceleración y un esfuerzo (fuerza) máximo al inicio del levantamiento, mientras que luego el esfuerzo neuromuscular disminuye [5], y se necesita una desaceleración al final de la fase concéntrica. Por tanto, en el movimiento concéntrico se pueden identificar dos fases: la propulsiva y la de frenado [18]. Durante la desaceleración el deportista cuenta con la ayuda de la aceleración debida al campo gravitatorio, por lo que en el ejercicio de peso libre se produce una disminución de la fuerza que este ejerce en la segunda parte de la fase concéntrica. De hecho, si la contribución de la aceleración de la gravedad a la frenada de la masa es insuficiente, el deportista llega incluso a ejercer fuerza en sentido contrario al del desplazamiento. Esta situación será más acusada cuando se ejecuta el ejercicio a velocidades altas.

La contribución de las fases de propulsión y frenado ha sido estudiada en el ejercicio de press de banca con peso libre [19], donde se evidenció la importancia de considerar estas fases en las evaluaciones de fuerza y potencia. Otros estudios señalan una menor actividad de la musculatura agonista y sinergista para una gran fase de frenado [20]. Frost y otros [21] compararon el ejercicio de press de banca con peso libre, en movimiento balístico, y utilizando una máquina de resistencia neumática [22]. Los resultados mostraron diferencias significativas en las curvas de velocidad, fuerza y potencia. Debido a las menores fuerzas de inercia, la resistencia neumática mostró una mayor fuerza y potencia durante el último periodo del 10-20 % de la fase concéntrica. Avrillon y col. [23] analizaron las resistencias de peso libre y neumáticas en el press de banca para movimientos balísticos. Además, Peltonen y col. [24] compararon la respuesta neuromuscular entre el peso libre y una máquina neumática, obteniendo como conclusión que la selección del dispositivo debe hacerse en función del objetivo del entrenamiento. Frost y col. [4] subrayan que un mayor conocimiento de las

propiedades biomecánicas que rigen cada tipo de resistencia, y/o de cómo pueden manipularse, proporcionará al investigador, al clínico y al profesional una apreciación mucho mayor de los beneficios y las limitaciones asociadas a cada modalidad de entrenamiento de resistencia.

Recientemente, los autores del presente trabajo propusieron un diseño conceptual de press de banca de fuerza constante [25]. En dicho trabajo se propone el uso de un mecanismo de fuerza constante como medio de carga en una máquina de acondicionamiento muscular. Los mecanismos de fuerza constante (CFM-Constant Force Mechanism) están diseñados para mantener un valor de fuerza constante a lo largo de un cierto rango de desplazamiento del mecanismo. Se pueden encontrar dos enfoques principales en el diseño de estos mecanismos [26]: mediante el uso de mecanismos flexibles (compliant mechanism), y mediante el uso de elementos elásticos junto con una transmisión no lineal. Por un lado, los mecanismos flexibles [27] se basan en miembros flexibles con formas y configuraciones particulares. Los CFM flexibles permiten una fuerza casi constante en un rango de desplazamiento limitado [28, 29, 30, 31]. Suelen tener un diseño compacto y se realizan principalmente en tamaño reducido para aplicaciones que requieren pequeños desplazamientos. Algunos trabajos recientes se han centrado en aumentar la carrera de estos mecanismos [32]. Por otro lado, los CFM que utilizan elementos elásticos (resortes) y transmisión no lineal pueden diseñarse para desplazamientos mayores y el valor de la fuerza constante puede modificarse fácilmente cambiando, añadiendo o quitando, resortes [33, 34, 35, 36, 37]. Por el contrario, el diseño es menos compacto y se ve afectado por las fuerzas de fricción.

Los mecanismos de fuerza constante se han diseñado para varias aplicaciones en robótica, por ejemplo, para la manipulación de objetos [38] o en la interacción con entornos desconocidos [39], en el diseño de pinzas de agarre para cirugía [40], en pinzas y micro pinzas [41, 42], en conectores de ajuste a presión [43], o para el equilibrio estático de la fuerza gravitacional [29, 44] entre otras aplicaciones.

En relación con las máquinas de musculación, se pueden encontrar algunas patentes que incluyen un mecanismo de fuerza constante como fuente de resistencia. Dirigida a entornos de baja gravedad, la Administración Nacional de Aeronáutica y del Espacio (NASA) registró una unidad de resistencia basada en la combinación de resortes y levas [45]. La patente nº 4231568 [46] también utiliza una disposición de resortes y levas para generar la fuerza de resistencia durante todo el ejercicio. Otras patentes se basan en el uso de múltiples resortes antagonistas paralelos [47, 48], en resortes de gas y transmisión no lineal [49], en cilindros de vacío [50], o en dispositivos neumáticos [22, 51].

A pesar del número de patentes registradas, que muestra el interés por el mecanismo de fuerza constante como unidad de resistencia para máquinas de musculación, no se ha encontrado en la literatura ninguna máquina comercial ni estudios experimentales sobre este tema.

En este trabajo, como continuación a la idea de concepto presentada en [25], se fabrica y evalúa experimentalmente un prototipo de máquina de acondicionamiento muscular de fuerza constante. En concreto, se proponen los siguientes objetivos:

(i) Fabricar e integrar un CFM en una máquina comercial tipo Smith y evaluar su comportamiento.

(ii) Comparar los patrones de fuerza en el ejercicio de press de banca, realizado con el nuevo sistema de carga propuesto y con el sistema tradicional de peso libre.

2. Diseño e instrumentación de una máquina tipo Smith de fuerza constante

La mayoría de las máquinas de musculación incluyen pilas de pesas u otros tipos de pesas guiadas como sistema de carga. Esta característica las hace adecuadas para la sustitución de las pesas por mecanismos de fuerza constante. En este trabajo se ha adaptado una máquina tipo Smith para incluir el mecanismo de fuerza constante como sistema de resistencia. En este apartado se describen las principales características mecánicas del diseño, así como los sensores que se han incorporado. La instrumentación se utiliza para la caracterización de la nueva máquina Smith de fuerza constante (CFSM - Constant Force Smith Machine) y para la medición del ejercicio de press de banca a realizar con la máquina.

2.1. Diseño mecánico

El concepto de CFM a implementar en la máquina Smith ha sido descrito y estudiado en trabajos anteriores presentados por los autores. En un primer trabajo [35], se abordó el diseño conceptual, la condición de fuerza constante, algunas consideraciones de diseño, y la influencia de la fricción de rodadura. Posteriormente, se validó experimentalmente un primer prototipo de reducidas dimensiones del CFM y se propuso un modelo 3D de un CFM para ser utilizado en una máquina tipo Smith [25, 37].

Aunque el principio de funcionamiento del CFM ha sido bien descrito en los trabajos referidos, para la claridad de este documento se ha considerado conveniente introducir brevemente el principio de funcionamiento del mismo, que puede explicarse a partir de la Figura 1. El CFM está diseñado de forma simétrica y consta de una leva fija, dos rodillos, un resorte que une ambos rodillos y dos tirantes unidos a los rodillos. Los tirantes se articulan en el plano de simetría del mecanismo, donde se aplica la fuerza exterior sobre el mecanismo. A partir de un análisis cuasi estático, la fuerza de accionamiento F dependerá de la rigidez del resorte K, de la pendiente del perfil de la leva β, del ángulo entre la dirección de la fuerza de accionamiento y el tirante α, y del coeficiente de fricción de rodadura μ_r. El valor de la fuerza de accionamiento puede obtenerse a partir de la Ec. [25].

$$F = 4K \underbrace{\Delta x \left(\frac{1 - \mu_r \tan\beta}{\tan\beta + \mu_r} - \tan\alpha \right)^{-1}}_{A}. \tag{1}$$

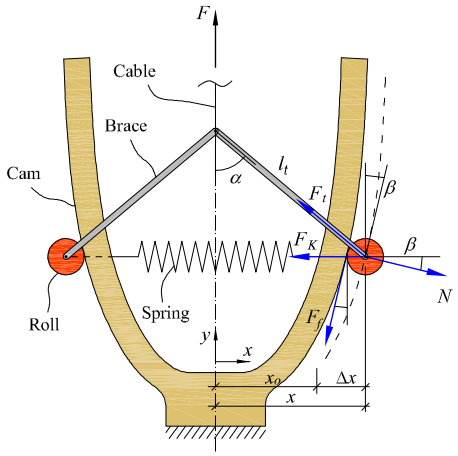

Figura 1: Diseño conceptual del CFM y diagrama de fuerzas para el rodillo derecho.

Para los resortes helicoidales, con rigidez constante K, la fuerza F se mantendrá constante si el término A de la Ec. (1) es constante, el cual depende del perfil de la leva. Los perfiles de leva que verifican que la fuerza se mantiene constante pueden obtenerse por integración numérica. Hay que tener en cuenta que la Ec. (1) se ha obtenido para el movimiento ascendente de los rodillos. En el caso de un desplazamiento descendente los signos que preceden al coeficiente de rozamiento cambian. Esto significa que no es posible obtener una fuerza constante para ambos desplazamientos con el mismo perfil de leva. En el presente trabajo se ha empleado un perfil de leva neutro ($\mu_r = 0$).

A continuación, se resumen las características de diseño del CFM implementado en la máquina tipo Smith. Se establecieron tres requisitos principales de diseño: (1) un desplazamiento de la barra de 0,70 m para cubrir la mayoría de los ejercicios a realizar con esta máquina de musculación; (2) una resistencia de fuerza de hasta 140 kp en intervalos de 10 kp y (3) reducir las masas móviles para minimizar las fuerzas de inercia.

El perfil de la leva y los resortes se han seleccionado para minimizar la influencia de la fricción en la respuesta de fuerza. Como se explica en la Ref. [35] es deseable un perfil de leva más abierto para reducir las fuerzas de fricción, sin embargo, está limitado por el alargamiento máximo admisible de los resortes. En este diseño se ha seleccionado como mejor opción resortes con una constante de rigidez teórica de 450 N/m y un alargamiento máximo de 270 mm.

Se han colocado dos CFM idénticos en ambos extremos de la barra guiada de la máquina Smith (Figura 2). Cada CFM puede disponer de entre 2 a 28 resortes en paralelo. Cada par de resortes da lugar a una fuerza de tracción de 5 kp, lo que significa que un CFM es capaz de ejercer una fuerza máxima de 70 kp N a intervalos de 5 kp. La figura 2(b) es un detalle de un CFM con 4 resortes. Además de la fuerza ejercida por los resortes, hay que tener en cuenta las masas móviles del conjunto en el valor de la fuerza resistente. Estos componentes son las

Tabla 1: Principales parámetros mecánicos del CFSM

Parámetro	Valor
Max. carga	140 kp
Intervalos de carga	10 kp
Max. desplazamiento	70 cm

masas móviles de los CFM, con 2,1 kg cada uno, y la masa de la barra horizontal guiada, con 5,70 kg. Además, cada pareja de resortes añade una masa de 0,22 kg.

La tabla 1 resume los principales parámetros mecánicos de la máquina.

2.2. Instrumentación y adquisición de datos

La máquina Smith ha sido instrumentada para medir la fuerza de resistencia y para comparar el ejercicio de press de banca realizado con el CFSM y con peso libre. Los sensores instalados en la máquina Smith se muestran en la Figura 3. La fuerza resistente se mide mediante una célula de carga tipo S (S Type Load Cell, 100kg, modelo CZL301C de Phidgets) situada entre la barra móvil y el gancho de un cabrestante, dispuesto convenientemente para elevar la barra. El desplazamiento vertical de la barra se mide con un encoder lineal de hilo de 2,5 m de Phidgets.

Se ha fabricado una plataforma de fuerza de bajo coste para medir la fuerza de reacción vertical del suelo durante la ejecución del ejercicio de press de banca. Esta plataforma de fuerza incluye cuatro células de compresión (Button Load Cell, 200kg, modelo CZL204E de Phidgets) y se sitúa bajo el banco en el ejercicio de press de banca. La salida de datos de las tarjetas de adquisición de las células de carga (PhidgetBridge 4-Input) y de la tarjeta del encoder (PhidgetEncoder HighSpeed 4-Input) se registran mediante código escrito en Phyton. Se ha empleado una frecuencia de muestreo de 125 Hz.

En el ejercicio de pres de banca, la duración y altura final de la barra en las sucesivas repeticiones resulta ligeramente diferente, por lo que el desplazamiento vertical de la barra se normaliza expresándolo en función del % de la fase concéntrica.

3. Evaluación experimental de la máquina tipo Smith de fuerza constante.

Las pruebas realizadas para la evaluación y caracterización del CFSM se han llevado a cabo con la ayuda de un cabrestante eléctrico. Este cabrestante se fija a la estructura de la máquina Smith en la viga superior (Figura 3) y se emplea para desplazar la barra móvil de la máquina a una velocidad constante de 8 m/min. La célula de carga tipo S está situada entre el gancho del polipasto y la barra para medir la fuerza de resistencia del CFSM (suma de la fuerza de los dos CFM más el peso de la barra). Se han tomado medidas de fuerza para

(a)

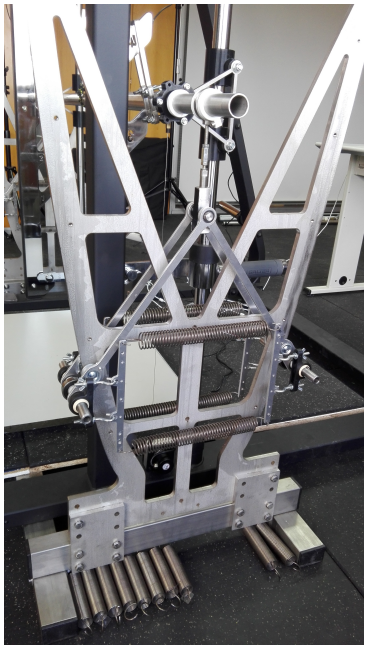

(b)

Figura 2: (a) La máquina Smith de fuerza constante y (b) detalle de un CFM acoplado a uno de los extremos de la barra móvil.

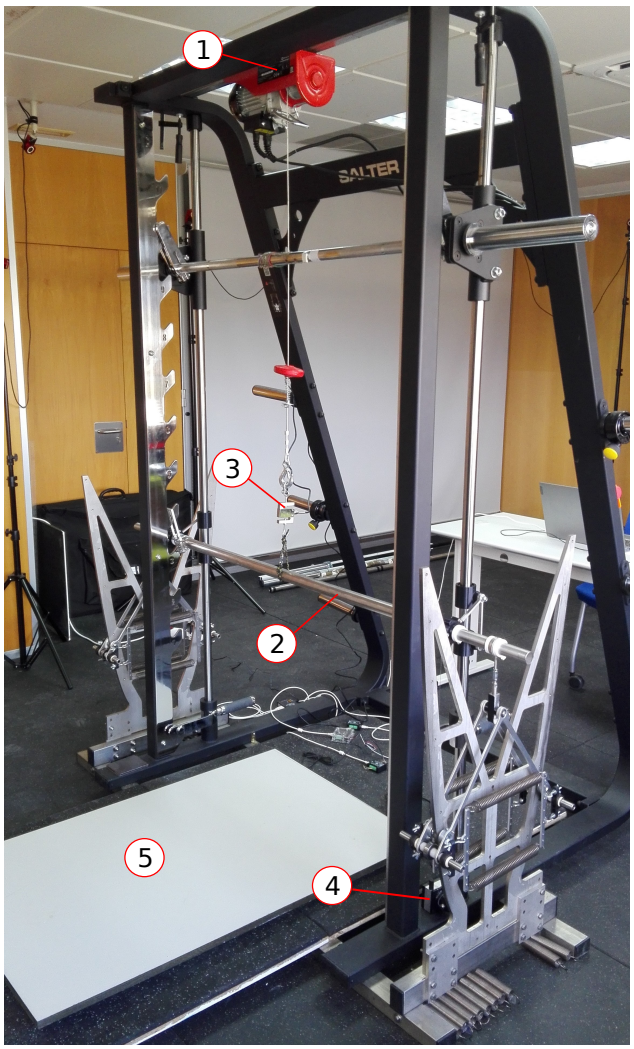

Figura 3: Sensorización de la máquina tipo Smith. Etiquetas: 1 cabrestante, 2 barra móvil, 3 célula de carga, 4 encoder de hilo, 5 plataforma de fuerza.

Tabla 2: Valores de fuerza del CFSM

	Fmax (N)	Fmin (N)	Fmedia (N)	SD (N)	SD (%)
0 resortes	97,56	76,29	87,92	3,30	3,75
8 resortes	309,03	272,08	291,45	6,59	2,26
16 resortes	545,34	451,86	490,04	14,26	2,91
24 resortes	756,97	638,05	688,72	18,07	2,62

distintos niveles de carga de la máquina, en concreto se ha ensayado con 4, 8 y 12 resortes por CFM (8, 16 y 24 resortes en total). Adicionalmente, también se ha medido la fuerza con los CFM sin ningún resorte. Las pruebas se han realizado comenzando con la barra en su posición inferior y elevándola una distancia de unos 70 cm. Posteriormente, se hace descender la barra hasta su posición inicial. Se han realizado tres repeticiones para cada nivel de carga.

En la Figura 4 se representan las curvas de fuerza obtenidas para los cuatro niveles de carga propuestos. Cada curva incluyen el tramo ascendente de la barra (mayor valor de la curva) y el tramo descendente (menor valor de la curva). Se muestra el valor medio de las tres repeticiones realizadas para cada ensayo, así como la dispersión de estos valores. Las curvas de fuerza muestran algunas fluctuaciones, debido probablemente a pequeñas desviaciones en el perfil de la leva fabricada, así como presencia de ruido debido principalmente a la rugosidad de la superficie de la leva, la cual ha sido obtenida mediante corte láser. Estos defectos y sus causas fueron estudiados en [37].

La Tabla 2 recoge los valores de fuerza máxima, fuerza mínima, fuerza media y desviación estándar en cada nivel de carga para la curva media. A partir de los resultados, se observa que el valor fuerza se mantiene sustancialmente constante en el desplazamiento efectuado, obteniéndose una desviación estándar en torno al 3 % para todos los niveles de carga. Los valores de fuerza media son los que se tomarán como referencia para identificar el nivel de carga para cada combinación de resortes. Puede comprobarse también que la adición de cada 4 resortes supone un incremento de la carga de unos 10,1 kp, valor que se aproxima a los 10 kp tomados en la fase de diseño.

4. Caso de estudio: el ejercicio de press de banca.

Uno de los ejercicios más utilizados para el entrenamiento de resistencia de la parte superior del cuerpo es el press de banca [52]. En esta sección se realiza un análisis comparativo del ejercicio de press de banca con peso libre (FW - free weight) y con el sistema de carga basado en mecanismos de fuerza constante.

El ejercicio de press de banca ha sido realizado por un voluntario de 70 kg de peso y 1,73 m de altura. Se le ha instruido al voluntario para que realice el ejercicio a la mayor velocidad que le sea posible (máxima potencia). Para cada máquina y nivel de carga, la serie ha consistido en tres repeticiones a máxima velocidad. Se ha llevado a cabo el ejercicio para dos niveles de carga. Para el primer nivel de carga se han empleado 8 resortes para el CFSM, lo que equivale

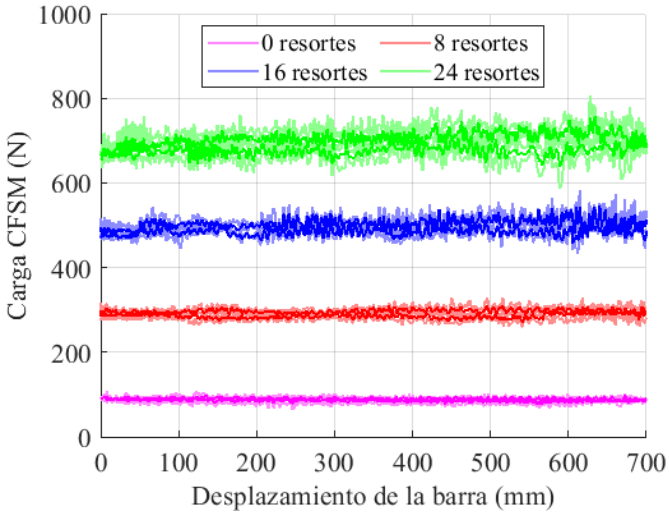

Figura 4: Curvas de fuerza-desplazamiento del CFSM para 8, 16, 24 resortes, y para ningún resorte. Para cada configuración se muestran tres repeticiones del desplazamiento ascendente y descendente de la barra.

a una carga estática de 291,5 N (ver Tabla 2), y pesas con un total de 30 kp (294,3 N). Para el segundo nivel de carga se han empleado 12 resortes para el CFSM, lo que equivale a una carga estática de 390,8 N, y pesas con un total de 40 kp (392,4 N). Estos dos niveles de carga se corresponden, aproximadamente, con el 50 % y el 65 % de la 1RM del voluntario (la 1RM es la máxima carga que puede levantar en una repetición).

Para el análisis comparativo, se han representado las curvas de fuerza en la fase concéntrica para cada caso (Figura 5). No se encuentran diferencias significativas en las curvas de fuerza entre ambos tipos de resistencia entre el 20 % y el 80 % de la fase concéntrica. Sin embargo, sí se aprecian diferencias significativas al inicio y al final de dicha fase. Al inicio del movimiento, se produce el pico máximo de fuerza que ejerce el deportista, siendo de 447 N y 578 N en el caso del CFSM para los niveles de carga del 50 % y 65 % de 1RM, respectivamente. En el caso de FW, los picos de fuerza registrados son de 561 N y 618 N. Los picos de fuerza son claramente superiores en el caso de entrenamiento con peso libre, llegando a ser hasta un 20 % superior en el caso del primer nivel de carga. Este momento de fuerza máxima corresponde con el inicio de la fase concéntrica, momento en que las masas adquieren la máxima aceleración.

Por otro lado, cuando se alcanza el 80 % de la fase concéntrica, se incia la fase de frenado, cayendo el valor de la fuerza rápidamente. Para el CFSM, la caída en la curva de fuerza es menos pronunciada, siendo esto debido a la menor masa móvil y fuerzas de inercia. Aun así, los valores de fuerza descienden hasta valores cercanos a cero para el primer nivel de carga, y hasta valores por debajo de los

100 N para el segundo nivel de carga. Esta caída es bastante más significativa para el caso de peso libre. Cabe resaltar que en peso libre se obtienen valores de fuerza negativos pasado el 90 % de la fase concéntrica, lo cual indica que el deportista debe ejercer fuerza en sentido contrario al del movimiento para frenar la masa. Estos valores negativos de fuerza llegan a alcanzar valores notablemente altos, llegando hasta los -300 N y -164 N para el primer y segundo nivel de carga, respectivamente.

En cuanto a los valores obtenidos entre el 20 %-80 % de la fase concéntrica, donde el valor de la fuerza se mantiene sensiblemente estable, los valores medios obtenidos para el primer nivel de carga son de 310 N y 340 N para el CFM y el FW, respectivamente; siendo para el segundo nivel de carga de 404 N y 417 N. Así, en este intervalo del movimiento, la fuerza ejercida por el usuario resulta ligeramente superior en el caso de peso libre.

5. Conclusiones

En este trabajo se ha llevado a cabo la fabricación e implementación de un mecanismo de fuerza constante como sistema de carga en una máquina comercial tipo Smith. Se han fabricado dos mecanismos de fuerza constante idénticos para acoplarlos en sendos extremos de la barra móvil de la máquina de Smith. A continuación, se han realizado ensayos a la máquina de acondicionamiento muscular propuesta. La evaluación experimental ha mostrado que los valores de carga se mantienen sensiblemente constantes a lo largo de todo el desplazamiento de la barra.

La máquina de Smith se ha utilizado para realizar ensayos ejecutando el ejercicio de press de banca. Se han obtenido las curvas de fuerza en la fase concéntrica del ejercicio con dos sistemas de carga diferentes: peso libre y CFM. Las curvas muestran diferencias significativas al inicio y al final de la fase concéntrica. Para el caso de peso libre, al inicio de ejercicio se produce un pico de fuerza significativamente mayor que para el caso de CFM. La mayor diferencia obtenida entre los dos sistemas de carga se produce durante la fase de frenado, al final de la fase concéntrica, donde en peso libre la caída en el valor de la fuerza es muy superior al del CFM, llegando a aplicar fuerza en sentido contrario al del movimiento. Por lo tanto, los resultados obtenidos confirman que la curva de fuerza se mantiene más estable con el nuevo sistema de carga propuesto, siendo este el objetivo de su implementación.

Agradecimientos

Este trabajo ha sido parcialmente financiado por el Programa Operativo FEDER 2014-2020 y la Consejería de Transformación Económica, Industria, Conocimiento y Universidades de la Junta de Andalucía bajo el proyecto UAL2020-CTS-A2100.

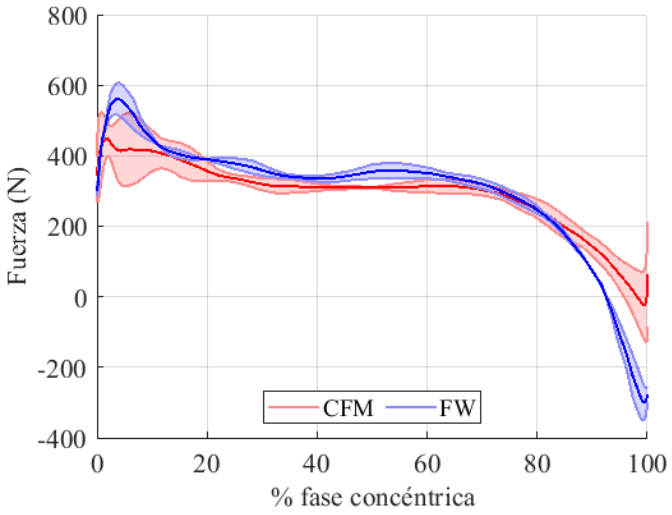

(a)

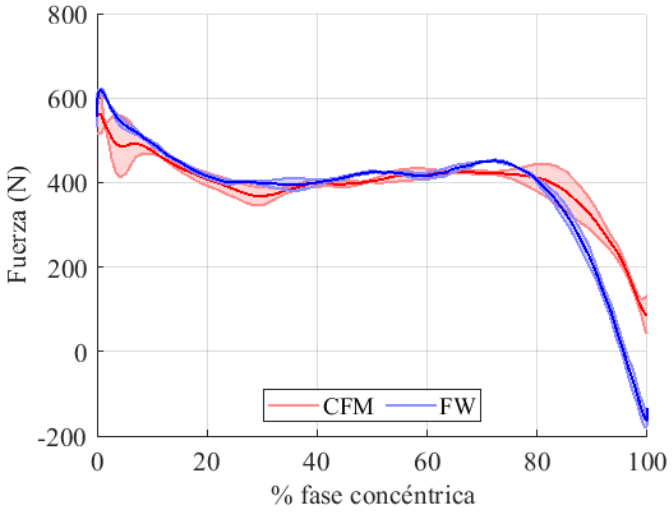

(b)

Figura 5: Curvas de fuerza en función del % de la fase concéntrica del desplazamiento medidas por la plataforma de fuerza durante el ejercicio de press de banca, para peso libre (FW) y para el mecanismo de fuerza constante (CFM). (a) Primer nivel de carga (50 % de 1RM). (b) Segundo nivel de carga (65 % de 1RM). La zona sombreada representa la desviación de las repeticiones con respecto al valor medio (línea resaltada).

Referencias

[1] S. Fleck, W. Kraemer, Designing Resistance Training Programs, 4th Edition, Human Kinetics, 2004.

[2] P. Sorace, T. LaFontaine, Resistance training muscle power: Design programs that work!, ACSM's Health and Fitness Journal 9 (2) (2005) 6–12.

[3] D. Murray, S. Bera, L. Brown, B. Findley, Strength assesment, in: Brown LE, editor. Strength Training. Champaign, IL: Human Kinetics, 2007, pp. 97–112.

[4] D. Frost, J. Cronin, R. Newton, A biomechanical evaluation of resistance: Fundamental concepts for training and sports performance, Sports Medicine 40 (4) (2010) 303–326. doi:10.2165/11319420-000000000-00000.

[5] A. Saeterbakken, V. Andersen, R. Van Den Tillaar, Comparison of kinematics and muscle activation in free-weight back squat with and without elastic bands, Journal of Strength and Conditioning Research 30 (4) (2016) 945–952. doi:10.1519/JSC.0000000000001178.

[6] R. Häberle, F. Schellenberg, R. List, M. Plüss, W. Taylor, S. Lorenzetti, Comparison of the kinematics and kinetics of shoulder exercises performed with constant and elastic resistance, BMC Sports Science, Medicine and Rehabilitation 10 (1). doi:10.1186/s13102-018-0111-7.

[7] S. Walker, H. Peltonen, J. Avela, K. Häkkinen, Kinetic and electromyographic analysis of single repetition constant and variable resistance leg press actions, Journal of Electromyography and Kinesiology 21 (2) (2011) 262–269. doi:10.1016/j.jelekin.2010.12.004.

[8] S. Walker, H. Peltonen, J. Avela, K. Häkkinen, Neuromuscular fatigue in young and older men using constant or variable resistance, European Journal of Applied Physiology 113 (4) (2013) 1069–1079. doi:10.1007/s00421-012-2526-2.

[9] S. Walker, J. Hulmi, M. Wernbom, K. Nyman, W. Kraemer, J. Ahtiainen, K. Häkkinen, Variable resistance training promotes greater fatigue resistance but not hypertrophy versus constant resistance training, European Journal of Applied Physiology 113 (9) (2013) 2233–2244. doi:10.1007/s00421-013-2653-4.

[10] V. Andersen, M. Fimland, M. Kolnes, A. Saeterbakken, Elastic bands in combination with free weights in strength training: Neuromuscular effects, Journal of Strength and Conditioning Research 29 (10) (2015) 2932–2940. doi:10.1519/JSC.0000000000000950.

[11] V. Andersen, M. Fimland, M. Kolnes, S. Jensen, M. Laume, A. Saeterbakken, Electromyographic comparison of squats using constant or variable resistance, Journal of Strength and Conditioning Research 30 (12) (2016) 3456–3463. doi:10.1519/JSC.0000000000001451.

[12] J. Ataee, M. Koozehchian, R. Kreider, L. Zuo, Effectiveness of accommodation and constant resistance training on maximal strength and power in trained athletes, PeerJ 2014 (1). doi:10.7717/peerj.441.

[13] R. Nijem, J. Coburn, L. Brown, S. Lynn, A. Ciccone, Electromyographic and force plate analysis of the deadlift performed with and without chains, Journal of Strength and Conditioning Research 30 (5) (2016) 1177–1182. doi:10.1519/JSC.0000000000001351.

[14] P. Swinton, A. D. Stewart, J. Keogh, I. Agouris, R. Lloyd, Kinematic and kinetic analysis of maximal velocity deadlifts performed with and without the inclusion of chain resistance, Journal of Strength and Conditioning Research 25 (11) (2011) 3163–3174. doi:10.1519/JSC.0b013e318212e389.

[15] K. Neelly, J. Terry, M. Morris, A mechanical comparison of linear and double-looped hung supplemental heavy chain resistance to the back squat: A case study, Journal of Strength and Conditioning Research 24 (1) (2010) 278–281. doi:10.1519/JSC.0b013e3181b2977a.

[16] D. Baker, R. Newton, Effect of kinetically altering a repetition via the use of chain resistance on velocity during the bench press, Journal of Strength and Conditioning Research 23 (7) (2009) 1941–1946. doi:10.1519/JSC.0b013e3181b3dd09.

[17] J. Bernentg, C. Coker, D. Briggs, The biomechanical and perceptual influence of chain resistance on the performance of the olympic clean, Journal of Strength and Conditioning Research 22 (2) (2008) 390–395.

[18] B. Jidovtseff, J.-L. Croisier, N. Scimar, C. Demoulin, D. Maquet, J.-M. Crielaard, The ability of isoinertial assessment to monitor specific training effects, Journal of Sports Medicine and Physical Fitness 48 (1) (2008) 55–64.

[19] L. Sánchez-Medina, C. Pérez, J. González-Badillo, Importance of the propulsive phase in strength assessment, International Journal of Sports Medicine 31 (2) (2010) 123–129. doi:10.1055/s-0029-1242815.

[20] R. Newton, W. Kraemer, K. Häkkinen, B. Humphries, A. Murphy, Kinematics, kinetics, and muscle activation during explosive upper body movements, Journal of Applied Biomechanics 12 (1) (1996) 31–43. doi:10.1123/jab.12.1.31.

[21] D. Frost, J. Cronin, R. Newton, A comparison of the kinematics, kinetics and muscle activity between pneumatic and free weight resistance, European Journal of Applied Physiology 104 (6) (2008) 937–956. doi:10.1007/s00421-008-0821-8.

[22] D. Keiser, Pneumatic exercising device, US Patent 4,257,593 (Mar. 24 1981).

[23] S. Avrillon, B. Jidovtseff, F. Hug, G. Guilhem, Influence of isoinertial-pneumatic mixed resistances on force-velocity relationship, International Journal of Sports Physiology and Performance 12 (3) (2017) 385–392. doi:10.1123/ijspp.2016-0226.

[24] H. Peltonen, K. Häkkinen, J. Avela, Neuromuscular responses to different resistance loading protocols using pneumatic and weight stack devices, Journal of Electromyography and Kinesiology 23 (1) (2013) 118–124. doi:10.1016/j.jelekin.2012.08.017.

[25] S. Sanchez-Salinas, C. Nunez-Torres, J. Lopez-Martinez, D. Garcia-Vallejo, J. M. Muyor, Design and analysis of a constant-force bench press, Mechanism and Machine Theory 142 (2019) 103612. doi:10.1016/j.mechmachtheory.2019.103612.

[26] P. Wang, Q. Xu, Design and modeling of constant-force mechanisms: A survey, Mechanism and Machine Theory 119 (2018) 1–21. doi:10.1016/j.mechmachtheory.2017.08.017.

[27] L. Howell, Compliant Mechanisms, John Wiley Sons, New York, 2001.

[28] J. Gallego, J. Herder, Classification for literature on compliant mechanisms: A design methodology based approach, in: Proceedings of the ASME International Design Engineering Technical Conferences and Computers and Information in Engineering Conference 2009, DETC2009, Vol. 7 PART A, 2010, pp. 289–297.

[29] K. Tolman, E. Merriam, L. Howell, Compliant constant-force linear-motion mechanism, Mechanism and Machine Theory 106 (2016) 68–79. doi:10.1016/j.mechmachtheory.2016.08.009.

[30] P. Wang, S. Yang, Q. Xu, Design and optimization of a new compliant rotary positioning stage with constant output torque, International Journal of Precision Engineering and Manufacturing 19 (12) (2018) 1843–1850. doi:10.1007/s12541-018-0213-x.

[31] G. Hao, A framework of designing compliant mechanisms with nonlinear stiffness characteristics, Microsystem Technologies 24 (4) (2018) 1795–1802.

[32] F. Ma, G. Chen, H. Wang, Large-stroke constant-force mechanisms utilizing second buckling mode of flexible beams: Evaluation metrics and design approach, Journal of Mechanical Design 142 (10) (2020) 103303. doi:10.1115/1.4046242.

[33] H. Bidgoly, M. Ahmadabadi, M. Zakerzadeh, Design and modeling of a compact rotational nonlinear spring, in: IEEE International Conference on Intelligent Robots and Systems, Vol. 2016-November, 2016, pp. 4356–4361.

[34] Y. Liu, D.-P. Yu, J. Yao, Design of an adjustable cam based constant force mechanism, Mechanism and Machine Theory 103 (2016) 85–97. doi:10.1016/j.mechmachtheory.2016.04.014.

[35] J. López-Martínez, D. García-Vallejo, F. Arrabal-Campos, J. García-Manrique, Design of three new cam-based constant-force mechanisms, Journal of Mechanical Design, Transactions of the ASME 140 (8). doi:10.1115/1.4040174.

[36] M. Li, W. Cheng, Design and experimental validation of a large- displacement constant-force mechanism, Journal of Mechanisms and Robotics 10 (5). doi:10.1115/1.4040437.

[37] S. Sánchez-Salinas, A. García-Agúndez, J. López-Martínez, D. García-Vallejo, Experimental validation of a constant-force mechanism and analysis of its performance with a calibrated multibody model, Mechanism and Machine Theory 173 (2022) 104819.

[38] C.-C. Lan, J.-Y. Wang, Design of adjustable constant-force forceps for robot-assisted surgical manipulation, in: Proceedings - IEEE International Conference on Robotics and Automation, 2011, pp. 386–391.

[39] Y.-H. Chen, C.-C. Lan, An adjustable constant-force mechanism for adaptive end-effector operations, Journal of Mechanical Design, Transactions of the ASME 134 (3).

[40] A. Lamers, J. Gallego Sánchez, J. Herder, Design of a statically balanced fully compliant grasper, Mechanism and Machine Theory 92 (2015) 230–239. doi:10.1016/j.mechmachtheory.2015.05.014.

[41] X. Zhang, Q. Xu, Design and testing of a novel 2-dof compound constant-force parallel gripper, Precision Engineering 56 (2019) 53–61. doi:10.1016/j.precisioneng.2018.09.004.

[42] G. Hao, J. Mullins, K. Cronin, Simplified modelling and development of a bi-directionally adjustable constant-force compliant gripper, Proceedings of the Institution of Mechanical Engineers, Part C: Journal of Mechanical Engineering Science 231 (11) (2017) 2110–2123. doi:10.1177/0954406216628557.

[43] Y.-H. Chen, C.-C. Lan, Design of a constant-force snap-fit mechanism for minimal mating uncertainty, Mechanism and Machine Theory 55 (2012) 34–50. doi:10.1016/j.mechmachtheory.2012.04.006.

[44] R. Nathan, A constant force generation mechanism, Journal of Mechanical Design, Transactions of the ASME 107 (4) (1985) 508–512. doi:10.1115/1.3260755.

[45] D. Smith, Resistive exercise device, US Patent 6,958,032 (Oct. 25 2005).

[46] R. Riley, D. Carey, Exercise machine with spring-cam arrangement for equalizing the force required through the exercise stroke, US Patent 4,231,568 (Nov. 4 1980).

[47] D. Hoecht, M. Ross, F. Bohm, Constant resistance exercising apparatus and system, US Patent 2005/0181915 A1 (Aug. 18 2005).

[48] P. Colosky, T. Ruttley, Gravity-independent constant force resistive exercise unit, US Patent 6,685,602 (Feb. 3 2004).

[49] N. Funk, J. Funk, Portable exercise device providing constant force output, US Patent 9,358,420 (Jun. 7 2016).

[50] J. Raboin, J. Niebuhr, S. Cruz, C. D. Lamoreaux, Advance resistive exercise device, US Patent 7,462,141 (Dec. 9 2008).

[51] R. Wilmarth, Pneumatic exercising device, US Patent 4,397,462 (Aug. 9 1983).

[52] J. Padulo, G. Laffaye, A. Chaouachi, K. Chamari, Bench press exercise: The key points, Journal of Sports Medicine and Physical Fitness 55 (6) (2015) 604–608.

Capítulo 6

Síntesis y Conclusiones

6.1. Conclusiones generales

En esta tesis se ha diseñado un sistema de carga para una máquina de Smith en la que la resistencia la proporcionan mecanismos de fuerza constante. Los mecanismos utilizados se basan en el uso de resortes y levas para conseguir la característica de fuerza constante. Se ha realizado un análisis comparativo del ejercicio de press de banca, en su ejecución tradicional, basada en el levantamiento de pesas y con el uso del mecanismo de fuerza constante como sistema de carga. Los resultados obtenidos muestran diferencias significativas en la fuerza que debe ejercer el deportista durante la realización del ejercicio. En concreto, la menor masa del sistema de carga propuesto permite mantener una curva de fuerza más estable, con una menor caída en la fase de frenado.

La presente Tesis Doctoral se presenta por la modalidad de compendio de publicaciones y ha sido desarrollada en el periodo comprendido entre 2018 y 2022. Los objetivos planteados se han llevado a cabo con éxito, y ello, se ha plasmado en las publicaciones científicas derivadas de la tesis [79, 80, 81].

6.1.1. Publicación científica 1: Validación experimental de un mecanismo de fuerza constante y análisis de su rendimiento con un modelo multicuerpo calibrado

El prototipo del mecanismo de fuerza constante fabricado presenta un buen rendimiento en cuanto a la consecución de su característica principal de fuerza constante. El diseño del mecanismo, basado en resortes y levas, permite conseguir grandes carreras y un nivel de fuerza modificable con faci-

lidad. Los principales factores que afectan a la curva ideal de fuerza constante son la fricción entre los elementos rodantes y el proceso de fabricación de la leva. Las fuerzas de fricción provocan inevitablemente bucles de histéresis. A pesar de esta histéresis, identificando el valor del coeficiente de rozamiento de rodadura, el perfil de la leva puede diseñarse para una fuerza constante más precisa en uno de los dos sentidos de desplazamiento. Las irregularidades de la superficie de la leva debidas al proceso de fabricación por corte láser provocan ruido en la curva de fuerza. Sin embargo, si es necesario, estas irregularidades podrían evitarse con una fabricación mediante fresado CNC. También se hacen presentes algunas fluctuaciones en la curva de fuerza obtenida en los resultados experimentales, las cuales están también causadas por imprecisión en la fabricación de la leva. Se ha desarrollado un modelo multicuerpo del CFM y se ha validado con los resultados experimentales presentados en este artículo. Así, utilizando el modelo multicuerpo del CFM, se pudieron extraer conclusiones relevantes sobre la influencia de los efectos inerciales, errores de funcionamiento y un posible error de fabricación. De este modo, se pudo concluir que, reduciendo el tiempo de ejecución, pueden surgir variaciones significativas de la fuerza necesaria para seguir un perfil cicloidal de movimiento impuesto. Las simulaciones también han revelado la influencia significativa de los posibles errores de fabricación, como una desviación lineal de los perfiles de la leva. Por lo tanto, el control de la calidad del perfil de la leva adquiere una gran importancia. Además, la simulación mostró que pueden surgir variaciones significativas de la fuerza de entrada como consecuencia de una desviación en la trayectoria del rodillo sobre la leva. Por lo tanto, es de vital importancia cuidar la inclinación de la fuerza de entrada durante la carrera del mecanismo para que esto no ocurra. Por último, el modelo multicuerpo será útil en el diseño de futuros CFM.

6.1.2. Publicación científica 2: Diseño y análisis de un press de banca de fuerza constante

Este trabajo propone un nuevo diseño de press de banca basado en el uso de un mecanismo de fuerza constante y se compara con uno de resistencia isoinercial mediante simulaciones matemáticas. Debido a la baja inercia de las partes móviles del mecanismo de fuerza constante, el press de banca propuesto es capaz de mantener una fuerza de resistencia casi constante, y que puede adaptarse a diferentes valores añadiendo o quitando resortes dispuestos en paralelo. Se ha fabricado y evaluado un prototipo a escala del mecanismo de fuerza constante para validar su funcionamiento. Se ha desarrollado un modelo matemático del ejercicio de press de banca que incluye

el brazo, el antebrazo y la mano. Guiando adecuadamente el modelo con un movimiento registrado mediante ensayos, puede utilizarse para evaluar las curvas de fuerza, momentos articulares y potencia muscular. Partiendo de mediciones del ejercicio de press de banca realizadas en el laboratorio, se ha analizado el ejercicio mediante dinámica inversa. Los resultados de diez repeticiones del ejercicio de press de banca se han analizado desde un punto de vista estadístico, mostrando los valores medios y las desviaciones estándar. Los resultados muestran que el press de banca con fuerza constante presenta diferencias cualitativas en las fuerzas verticales en el hombro y la muñeca, el momento neto en el hombro y las curvas de potencia muscular en comparación con la resistencia isoinercial tradicional (peso libre). Debido a la baja inercia de las masas en movimiento del dispositivo de resistencia de fuerza constante, las curvas de fuerza muestran patrones mucho más constantes que las de la resistencia isoinercial, y evita la fase de frenado que suele producirse en las ejecuciones rápidas y explosivas. Prácticamente, se eliminan los grandes valores pico en las curvas de fuerza y momento al principio de la fase concéntrica. Además, se reduce la potencia máxima requerida. En general, se obtienen patrones de curva más suaves y una menor dispersión entre las repeticiones del ejercicio para la resistencia de fuerza constante. Esto podría tener ventajas en el entrenamiento de fuerza y resistencia, disminuyendo el riesgo de lesiones, o en la fisioterapia deportiva, en la recuperación de patologías musculoesqueléticas. Estas hipótesis deberán ser analizadas en futuros trabajos.

6.1.3. Publicación científica 3: Diseño de trayectorias y pares mediante optimización paramétrica para el ejercicio de press de banca en una máquina Smith

Este trabajo presenta una metodología para el diseño de trayectorias y pares mediante optimización para el ejercicio de press de banca. En particular, esta metodología tiene como objetivo comprender la realización adecuada del ejercicio de press de banca en condiciones de entrenamiento para ganar resistencia o para realizar el ejercicio de la manera más segura, es decir, evitando las sobrecargas. El problema de control óptimo se formula como un problema de optimización no lineal con restricciones. Las variables de diseño son la trayectoria y los pares articulares en los nodos temporales. La solución debe cumplir una serie de restricciones cinemáticas y dinámicas en un conjunto de puntos de colocación, los llamados puntos de control. En este estudio se formulan dos funciones de coste diferentes. Una se basa en el es-

fuerzo dinámico y la otra en la potencia mecánica desarrollada. El marco de optimización descrito anteriormente se utiliza para estudiar el rendimiento del press de banca desde el punto de vista de un sujeto que entrena para ganar resistencia o para evitar sobrecargas de par articular. Para ello, se han probado y comparado los dos criterios generando trayectorias y pares articulares mediante optimización siguiendo un movimiento de referencia del press de banca obtenido en el laboratorio. Hay que destacar que la combinación de valores utilizada para los factores de peso juega un papel importante en la solución obtenida. Por lo tanto, las trayectorias y los historiales de par muscular obtenidos por optimización deben interpretarse como óptimos para la combinación particular de pesos utilizada. Se encuentra que la minimización del esfuerzo dinámico conduce a trayectorias que se ejecutan con valores mayores del par del codo, lo que podría no ser una distribución realista de los pares articulares según la literatura. Hay que tener en cuenta que el modelo de press de banca utilizado no incluye propiedades musculares, y que los resultados obtenidos pueden variar al incorporar modelos musculares realistas.

A diferencia del criterio de esfuerzo dinámico, el criterio de potencia mecánica al cuadrado proporciona resultados que se ajustan a trayectorias y a distribuciones del par articular más realistas. En concreto, el movimiento predicho se asemeja razonablemente bien al movimiento del voluntario obtenido en las pruebas. Esto sugiere que el sujeto realiza el ejercicio de forma eficiente en cuanto a su coste energético. En este caso, la metodología propuesta es útil para predecir el rendimiento de los ejercicios de fuerza realizados en condiciones de mejora de la resistencia. En este trabajo se ha estudiado el efecto de la carga levantada y el tiempo de duración del ejercicio. La variación de la carga da lugar a unos historiales de par articular significativamente diferentes, en los que, como se ha explicado anteriormente, los criterios de esfuerzo dinámico proporcionan valores mayores para el par del codo, lo que lleva a su nivel máximo el par alcanzable en el codo. El análisis de la influencia de los diferentes criterios posibles de obtención de pares articulares, como el esfuerzo dinámico o el criterio de potencia mecánica, mediante la realización de simulaciones, permite estudiar aspectos de coordinación de las actividades humanas y muestra una potencial aplicación de este enfoque al diseño de terapias de rehabilitación y al diseño de programas de entrenamiento. Los resultados de la optimización ofrecen información relevante en la planificación del entrenamiento deportivo, así como en la prescripción del ejercicio físico, ya que proporcionan un perfil de velocidad adecuado para disminuir el esfuerzo realizado, lo que se traduce en una disminución de la fatiga de los grupos musculares considerados, y ofrecen información sobre el trabajo muscular durante la carrera de ejercicio.

6.1.4. Aportación científica 4: Diseño y estudio experimental de una máquina de acondicionamiento muscular basada en un mecanismo de fuerza constante.

En este trabajo se ha llevado a cabo la fabricación e implementación de un mecanismo de fuerza constante como sistema de carga en una máquina comercial tipo Smith. Se han fabricado dos mecanismos de fuerza constante idénticos para acoplarlos en sendos extremos de la barra móvil de la máquina de Smith. A continuación, se han realizado ensayos a la máquina de acondicionamiento muscular propuesta. La evaluación experimental ha mostrado que los valores de carga se mantienen sensiblemente constantes a lo largo de todo el desplazamiento de la barra.

La máquina de Smith se ha utilizado para estudiar el ejercicio de press de banca. Se han obtenido las curvas de fuerza en la fase concéntrica del ejercicio con dos sistemas de carga diferentes: peso libre y CFM. Las curvas muestran diferencias significativas al inicio y al final de la fase concéntrica. Para el caso de peso libre, al inicio de ejercicio se produce un pico de fuerza significativamente mayor que para el caso de CFM. La mayor diferencia obtenida entre los dos sistemas de carga se produce durante la fase de frenado, al final de la fase concéntrica, donde para el peso libre la caída en el valor de la fuerza es muy superior que para el CFM, llegando a aplicar fuerza en sentido contrario al del movimiento. Por lo tanto, los resultados obtenidos confirman que la curva de fuerza se mantiene más estable con el nuevo sistema de carga propuesto, siendo este el objetivo de su implementación.

6.2. Trabajos futuros

Actualmente, están en curso diversas ampliaciones relacionadas con la línea de investigación de esta tesis, enfocadas a comparar los dos sistemas de carga, peso libre y resistencia de fuerza constante propuesta, de forma más exhaustiva. Además de comparar las curvas de fuerza vertical, se realizarán estudios para comparar los patrones de movimiento, la actividad electromiográfica y las fuerzas musculares durante la ejecución del ejercicio. Para el estudio de las fuerzas a nivel muscular se mejorará el modelo matemático propuesto mediante la implementación de un modelo musculo-esquelético.

Otra línea de trabajo de interés es el análisis de sensibilidad en un modelo completo del ejercicio de press de banca para ver la influencia de la asimetría natural del cuerpo humano.

Un trabajo más extenso consistirá en la realización de estudios con volun-

tarios para evaluar las ventajas en el entrenamiento de la fuerza y resistencia con máquinas de acondicionamiento muscular que usen como medio de carga mecanismos de fuerza constante, las cuales podrían disminuir el riesgo de lesiones, o en la fisioterapia deportiva en la recuperación de patologías musculoesqueléticas. En esta línea, el sistema de carga desarrollado será aplicable a cualquier ejercicio que se pueda realizar en la máquina Smith adaptada, como puede ser el ejercicio de sentadillas. De igual forma, el sistema de carga podría ser incorporado a cualquier otra máquina de acondicionamiento muscular que disponga de pesas guiadas, como es el caso de las máquinas multifunción de poleas.

Bibliografía

Bibliografía

[1] M. Ackermann. *Dynamics and energetics of walking with prostheses.* Aachen: Shaker-Verlag, 2007.

[2] M. Ackermann y W. Schiehlen. "Dynamic Analysis of Human Gait Disorder and Metabolical Cost Estimation". En: *Arch. Appl. Mech.* 75.10-12 (2006), págs. 569-594.

[3] R. Al-Nazer y col. "Flexible multibody simulation approach in the analysis of tibial strain during walking". En: *Journal of Biomechanics* 41 (2008), págs. 1036-1043.

[4] L. L. Andersen y col. "Muscle activation and perceived loading during rehabilitation exercises: comparison of dumbbells and elastic resistance". En: *Physical Therapy* 90.4 (2010), págs. 538-549.

[5] V. Andersen y col. "Elastic bands in combination with free weights in strength training: Neuromuscular effects". En: *Journal of Strength and Conditioning Research* 29.10 (2015), págs. 2932-2940.

[6] V. Andersen y col. "Electromyographic comparison of squats using constant or variable resistance". En: *Journal of Strength and Conditioning Research* 30.12 (2016), págs. 3456-3463.

[7] J. Ataee y col. "Effectiveness of accommodation and constant resistance training on maximal strength and power in trained athletes". En: *PeerJ* 2014.1 (2014).

[8] S. Avrillon y col. "Influence of isoinertial-pneumatic mixed resistances on force-velocity relationship". En: *International Journal of Sports Physiology and Performance* 12.3 (2017), págs. 385-392.

[9] D.G. Baker y R.U. Newton. "Effect of kinetically altering a repetition via the use of chain resistance on velocity during the bench press". En: *Journal of Strength and Conditioning Research* 23.7 (2009), págs. 1941-1946.

[10] D.G. Behm y K.G. Anderson. "The role of instability with resistance training". En: *Journal of Strength and Conditioning Research* 20.3 (2006), págs. 716-722.

[11] J.M. Bernentg, C.A Coker y D. Briggs. "The biomechanical and perceptual influence of chain resistance on the performance of the olympic clean". En: *Journal of Strength and Conditioning Research* 22.2 (2008), págs. 390-395.

[12] G. Bessonnet, P. Seguin y P. Sardain. "A parametric optimization approach to walking pattern synthesis". En: *The International Journal of Robotics Research* 24.7 (2005), págs. 523-536.

[13] H.J. Bidgoly, M.N. Ahmadabadi y M.R. Zakerzadeh. "Design and modeling of a compact rotational nonlinear spring". En: *IEEE International Conference on Intelligent Robots and Systems*. Vol. 2016-November. 2016, págs. 4356-4361.

[14] P. Bilancia y G. Berselli. "Design and testing of a monolithic compliant constant force mechanism". En: *Smart Materials and Structures* 29.4 (2020), pág. 044001.

[15] C. Boyle y col. "Dynamic modeling of compliant constant-force compression mechanisms". En: *Mechanism and Machine Theory* 38.12 (2003), págs. 1469-1487.

[16] Y.-H. Chen y C.-C. Lan. "An adjustable constant-force mechanism for adaptive end-effector operations". En: *Journal of Mechanical Design, Transactions of the ASME* 134.3 (2012).

[17] P.E. Colosky y T.M. Ruttley. *Gravity-independent constant force resistive exercise unit*. US Patent 6,685,602. 2004.

[18] G. Dalleau y col. "The influence of variable resistance moment arm on knee extensor performance." En: *Journal of Sports Sciences,* 28.6 (2010), págs. 657-665.

[19] B. Ding, X. Li e Y. Li. "FEA-based optimization and experimental verification of a typical flexure-based constant force module". En: *Sensors and Actuators A: Physical* 332 (2021), pág. 113083.

[20] E.F. Duval. *Dual pulley constant force mechanism*. US Patent 7,677,540. 2010.

[21] W. E. Ebben y R. L. Jensen. "Electromyographic and kinetic analysis of traditional, chain, and elastic band squats." En: *Journal of Strength and Conditioning Research* 16.4 (2002), págs. 547-550.

[22] G. Endo y col. "A passive weight compensation mechanism with a non-circular pulley and a spring". En: *Proceedings - IEEE International Conference on Robotics and Automation*. 2010, págs. 3843-3848.

[23] A. Falisse y col. "Algorithmic differentiation improves the computational efficiency of OpenSim-based trajectory optimization of human movement". En: *PLoS ONE* 14.10 (2019).

[24] A. Falisse y col. "Rapid predictive simulations with complex musculoskeletal models suggest that diverse healthy and pathological human gaits can emerge from similar control strategies". En: *Journal of the Royal Society Interface* 16.157 (2019).

[25] D. M. Frost, J. B. Cronin y R. U. Newton. "A comparison of the kinematics, kinetics and muscle activity between pneumatic and free weight resistance". En: *European journal of applied physiology* 104.6 (2008), págs. 937-956.

[26] D.M. Frost, J. Cronin y R.U. Newton. "A biomechanical evaluation of resistance: Fundamental concepts for training and sports performance". En: *Sports Medicine* 40.4 (2010), págs. 303-326.

[27] N.W. Funk y J.H. Funk. *Portable exercise device providing constant force output*. US Patent 9,358,420. 2016.

[28] J.A. Gallego y J. Herder. "Classification for literature on compliant mechanisms: A design methodology based approach". En: *Proceedings of the ASME International Design Engineering Technical Conferences and Computers and Information in Engineering Conference 2009, DETC2009*. Vol. 7 PART A. 2010, págs. 289-297.

[29] I. Gandhi y H. Zhou. "Synthesizing Constant Torque Compliant Mechanisms Using Precompressed Beams". En: *Journal of Mechanical Design* 141.1 (2019), pág. 014501.

[30] D. García-Vallejo, J.M. Font-Llagunes y W. Schiehlen. "Dynamical analysis and design of active orthoses for spinal cord injured subjects by aesthetic and energetic optimization". En: *Nonlinear Dynamics* 84.2 (2016), págs. 559-581.

[31] D. García-Vallejo y W. Schiehlen. "3D-Simulation of human walking by parameter optimization". En: *Archive of Applied Mechanics* 82 (2012), págs. 533-556.

[32] D. García-Vallejo y col. "Detection of Communities within the Multibody System Dynamics Network and Analysis of Their Relations". En: *Symmetry* 11 (2019).

[33] R. Häberle y col. "Comparison of the kinematics and kinetics of shoulder exercises performed with constant and elastic resistance". En: *BMC Sports Science, Medicine and Rehabilitation* 10.1 (2018).

[34] D. Hoecht, M.P. Ross y F. Bohm. *Constant resistance exercising apparatus and system.* US Patent 2005/0181915 A1. 2005.

[35] L.L. Howell. *Compliant Mechanisms.* John Wiley Sons, New York, 2001.

[36] L.L. Howell y S.P. Magleby. *Substantially constant-force exercise machine.* US Patent 7,060,012. 2006.

[37] M. A. Israetel y col. "Kinetic and kinematic differences between squats performed with and without elastic bands." En: *Journal of Strength and ConditioningResearch* 24.1 (2010), págs. 190-194.

[38] B. Jidovtseff y col. "The ability of isoinertial assessment to monitor specific training effects." En: *Journal of sports medicine and physical fitness,* 48.1 (2008), págs. 55-64.

[39] D.L. Keiser. *Pneumatic exercising device.* US Patent 4,257,593. 1981.

[40] G. Keung y C. Chen. "Novel design of an adjustable constant force mechanism based on cam and spring". En: *IFToMM World Congress on Mechanism and Machine Science.* Springer. 2019, págs. 1481-1490.

[41] W. J. Kraemer, N. D. Duncan y J. S. Volek. "Resistance training and elite athletes: adaptations and program considerations." En: *Journal of Orthopaedic Sports Physical Therapy* 28.2 (1998), págs. 110-119.

[42] Y.-L. Kuo y C.-C. Lan. "A Two-Dimensional Adjustable Constant-Force Mechanism". En: *Journal of Mechanical Design* 142.6 (2020).

[43] A.J. Lamers, J.A. Gallego-Sánchez y J.L. Herder. "Design of a statically balanced fully compliant grasper". En: *Mechanism and Machine Theory* 92 (2015), págs. 230-239.

[44] C.-C. Lan y J.-Y. Wang. "Design of adjustable constant-force forceps for robot-assisted surgical manipulation". En: *Proceedings - IEEE International Conference on Robotics and Automation.* 2011, págs. 386-391.

[45] C.-C. Lan, S.-A. Yang e Y.-S. Wu. "Design and experiment of a compact quasi-zero-stiffness isolator capable of a wide range of loads". En: *Journal of Sound and Vibration* 333.20 (2014), págs. 4843-4858.

[46] M. Li y W. Cheng. "Design and experimental validation of a large-displacement constant-force mechanism". En: *Journal of Mechanisms and Robotics* 10.5 (2018), pág. 051007.

[47] C.H. Liu, F.M. Chung e Y.P. Ho. "Topology Optimization for Design of a 3D-Printed Constant-Force Compliant Finger". En: *IEEE/ASME Transactions on Mechatronics* (2021).

[48] X. Liu, X. Huang y H. Hua. "On the characteristics of a quasi-zero stiffness isolator using Euler buckled beam as negative stiffness corrector". En: *Journal of Sound and Vibration* 332.14 (2013), págs. 3359-3376.

[49] Y. Liu, Z. Li y S. Bai. "Design of a Reconfigurable Novel Constant-Force Mechanism for Assistive Exoskeletons". En: *IFToMM Symposium on Mechanism Design for Robotics*. Springer. 2021, págs. 122-131.

[50] Y. Liu, D.-P. Yu y J. Yao. "Design of an adjustable cam based constant force mechanism". En: *Mechanism and Machine Theory* 103 (2016), págs. 85-97.

[51] Y. Liu, Y. Zhang y Q. Xu. "Design and Control of a Novel Compliant Constant-Force Gripper Based on Buckled Fixed-Guided Beams". En: *IEEE/ASME Transactions on Mechatronics* 22.1 (2017), págs. 476-486.

[52] J. López-Martinez y col. "Estudio de nuevos mecanismos de fuerza constante". En: *13º Congreso Iberoamericano de Ingeniería Mecánica. Lisboa, Portugal, Oct. 23-26* (201), págs. 1-9.

[53] J. López-Martínez y col. "Design of three new cam-based constant-force mechanisms". En: *Journal of Mechanical Design, Transactions of the ASME* 140.8 (2018).

[54] F. Ma, G. Chen y H. Wang. "Large-Stroke Constant-Force Mechanisms Utilizing Second Buckling Mode of Flexible Beams: Evaluation Metrics and Design Approach". En: *Journal of Mechanical Design* 142.10 (2020), pág. 103303.

[55] N. Madsen y T. McLaughlin. "Kinematic factors influencing performance and injury risk in the bench press exercise". En: *Medicine and Science in Sports and Exercise* 16.4 (1984), págs. 376-381.

[56] J.C. Meaders y C.A. Mattson. "Optimization of near-constant force springs subject to mating uncertainty". En: *Structural and Multidisciplinary Optimization* 41.1 (2010), págs. 1-15.

[57] K.R. Neelly, J.G. Terry y M.J. Morris. "A mechanical comparison of linear and double-looped hung supplemental heavy chain resistance to the back squat: A case study". En: *Journal of Strength and Conditioning Research* 24.1 (2010), págs. 278-281.

[58] R.U. Newton y col. "Kinematics, kinetics, and muscle activation during explosive upper body movements". En: *Journal of Applied Biomechanics* 12.1 (1996), págs. 31-43.

[59] R.M. Nijem y col. "Electromyographic and force plate analysis of the deadlift performed with and without chains". En: *Journal of Strength and Conditioning Research* 30.5 (2016), págs. 1177-1182.

[60] J. Padulo y col. "Bench press exercise: The key points". En: *Journal of Sports Medicine and Physical Fitness* 55.6 (2015), págs. 604-608.

[61] M. Peasgood, J. McPhee y E. Kubica. "Stabilization and energy optimization of a dynamic walking gait simulation". En: *Proceedings of the ASME International Design Engineering Technical Conferences and Computers and Information in Engineering Conference - DETC2005*. Vol. 6 A. 2005, págs. 339-349.

[62] H. Peltonen, K. Häkkinen y J. Avela. "Neuromuscular responses to different resistance loading protocols using pneumatic and weight stack devices". En: *Journal of Electromyography and Kinesiology* 23.1 (2013), págs. 118-124.

[63] H.-T. Pham y D.-A. Wang. "A constant-force bistable mechanism for force regulation and overload protection". En: *Mechanism and Machine Theory* 46.7 (2011), págs. 899-909.

[64] H.N. Prakashah y H. Zhou. "Synthesis of constant torque compliant mechanisms". En: *Journal of Mechanisms and Robotics* 8.6 (2016).

[65] J.L. Raboin y col. *Advance resistive exercise device*. US Patent 7,462,141. 2008.

[66] A. Rahmani y col. "A virtual model of the bench press exercise". En: *Journal of Biomechanics* 42.11 (2009), págs. 1610-1615.

[67] R.Q. Riley y D.L. Carey. *Exercise machine with spring-cam arrangement for equalizing the force required through the exercise stroke*. US Patent 4,231,568. 1980.

[68] S.E. Rodrigo y col. "Analysys of human gait based on multibody formulations and optimization tools". En: *Mechanics Based Design of Structures and Machines* 36.4 (2008), págs. 446-477.

[69] A.H. Saeterbakken, V. Andersen y R. Van Den Tillaar. "Comparison of Kinematics and Muscle Activation in Free-Weight Back Squat with and Without Elastic Bands". En: *Journal of Strength and Conditioning Research* 30.4 (2016), págs. 945-952.

[70] L. Sánchez-Medina, C.E. Pérez y J.J. González-Badillo. "Importance of the propulsive phase in strength assessment". En: *International Journal of Sports Medicine* 31.2 (2010), págs. 123-129.

[71] A. Schepelmann, K.A. Geberth y H. Geyer. "Compact nonlinear springs with user defined torque-deflection profiles for series elastic actuators". En: *Proceedings - IEEE International Conference on Robotics and Automation*. 2014, págs. 3411-3416.

[72] N. Schmit y M. Okada. "Synthesis of a non-circular cable spool to realize a nonlinear rotational spring". En: *IEEE International Conference on Intelligent Robots and Systems*. 2011, págs. 762-767.

[73] G. Serrancolí y col. "Subject-Exoskeleton Contact Model Calibration Leads to Accurate Interaction Force Predictions". En: *IEEE transactions on neural systems and rehabilitation engineering : a publication of the IEEE Engineering in Medicine and Biology Society* 27.8 (2019), págs. 1597-1605.

[74] D.C. Smith. *Resistive exercise device*. National Aeronautics and Space Administration (NASA), Washington, DC, US Patent 6,958,032. 2005.

[75] R. Squadrone, R. Rodano y E. Preatoni. "Comparison of velocity and power output data derived from an inertial based system and an optical encoder during squat lifts in a weight room setting". En: *Journal of Sports Medicine and Physical Fitness* 52.1 (2012), págs. 40-46.

[76] E.L. Starostin. "Calculating a cam profile for a constant-force mechanism". En: *Soviet machine science* 4 (1987), págs. 69-76.

[77] E Sundstrup y col. "Evaluation of elastic bands for lower extremity resistance training in adults with and without musculoskeletal pain." En: *Scandinavian Journal of Medicine Science in Sports* 24.5 (2014), e353-e359.

[78] P.A. Swinton y col. "Kinematic and kinetic analysis of maximal velocity deadlifts performed with and without the inclusion of chain resistance". En: *Journal of Strength and Conditioning Research* 25.11 (2011), págs. 3163-3174.

[79] S. Sánchez-Salinas y col. "Design and analysis of a constant-force bench press". En: *Mechanism and Machine Theory* 142 (2019).

[80] S. Sánchez-Salinas y col. "Design of trajectories and torques by parameter optimization for the bench press exercise on a Smith machine". En: *Mechanism and Machine Theory* 155 (2021).

[81] S. Sánchez-Salinas y col. "Experimental validation of a constant-force mechanism and analysis of its performance with a calibrated multibody model". En: *Mechanism and Machine Theory* 173 (2022).

[82] Y. Tian y col. "A novel compliant mechanism based system to calibrate spring constant of AFM cantilevers". En: *Sensors and Actuators A: Physical* 309 (2020), pág. 112027.

[83] Y. Tian y col. "Design of a flexure-based mechanism possessing low stiffness and constant force". En: *Review of Scientific Instruments* 90.10 (2019), pág. 105005.

[84] K.A. Tolman, E.G. Merriam y L.L. Howell. "Compliant constant-force linear-motion mechanism". En: *Mechanism and Machine Theory* 106 (2016), págs. 68-79.

[85] W. Van De Sande, A. Ali y G. Radaelli. "Design and Evaluation of a Passive Constant Force Mechanism for a Cardiac Ablation Catheter". En: *Journal of Medical Devices* 15.2 (2021), pág. 021003.

[86] A.J. Van Den Bogert y col. "Predictive musculoskeletal simulation using optimal control: Effects of added limb mass on energy cost and kinematics of walking and running". En: *Proceedings of the Institution of Mechanical Engineers, Part P: Journal of Sports Engineering and Technology* 226.2 (2012), págs. 123-133.

[87] R. Van Den Tillaar. "The effects of grip width on sticking region in bench press." En: *Journal of Sports Sciences* 34.3 (2016), págs. 232-238.

[88] S. Walker y col. "Kinetic and electromyographic analysis of single repetition constant and variable resistance leg press actions". En: *Journal of Electromyography and Kinesiology* 21.2 (2011), págs. 262-269.

[89] S. Walker y col. "Neuromuscular fatigue in young and older men using constant or variable resistance". En: *European Journal of Applied Physiology* 113.4 (2013), págs. 1069-1079.

[90] S. Walker y col. "Variable resistance training promotes greater fatigue resistance but not hypertrophy versus constant resistance training". En: *European Journal of Applied Physiology* 113.9 (2013), págs. 2233-2244.

[91] H. Wang y col. "Analysis of Muscle Activity Utilizing Bench Presses in the AnyBody Simulation Modelling System". En: 5 (2016), págs. 1-7.

[92] P. Wang y Q. Xu. "Design and modeling of constant-force mechanisms: A survey". En: *Mechanism and Machine Theory* 119 (2018), págs. 1-21.

[93] P. Wang y Q. Xu. "Design and Testing of a Flexure-Based Constant-Force Stage for Biological Cell Micromanipulation". En: *IEEE Transactions on Automation Science and Engineering* (2017).

[94] P. Wang y Q. Xu. "Design of a flexure-based constant-force XY precision positioning stage". En: *Mechanism and Machine Theory* 108 (2017), págs. 1-13.

[95] B.L. Weight y col. "Configuration selection, modeling, and preliminary testing in support of constant force electrical connectors". En: *Journal of Electronic Packaging, Transactions of the ASME* 129.3 (2007), págs. 236-246.

[96] R.F. Wilmarth. *Pneumatic exercising device*. US Patent 4,397,462. 1983.

[97] Q. Xie, S. Liu y H. Jiang. "Design of a passive constant-force mechanism based on a five-bar mechanism". En: *Mechanism and Machine Theory* 143 (2020), pág. 103662.

[98] T. Ye y col. "A novel two-stage constant force compliant microgripper". En: *Journal of Mechanical Design* 143.5 (2021), pág. 053302.